FIBREGY

Development, engineering, production and life cycle management of improved FIBRE-based material solutions for the structure and functional components of large offshore wind enerGY and tidal power platforms

D6.1 (WP6): Middle scale test on dry coatings and connections

Responsible Partner: CORSO

Contributor(s): CORSO, INEGI, IXBLUE, CIMNE, ULIM, TSI

DOCUMENT INFORMATION TABLE

CONTRACT NUMBER:	952966	
PROJECT ACRONYM:	Fibregy	
PROJECT COORDINATOR:	Borja Servan Camas	
DOCUMENT RESPONSIBLE	Corso Magenta	CORSO
DELIVERABLE TYPE:	Report	
DOCUMENT TITLE:	Middle scale test on dry coatings and connections	
DOCUMENT ID:	D6.1	
DISSEMINATION LEVEL:	PU: Public	
FILENAME:	FIBREGY_D6.1_Middle scale test on dry coatings and connections	
STATUS:	First version	

Authoring & Review

PREPARED / REVIEWED BY				
Name	Role	Partner	Date	Comments
Olivia Chan taw	Creator Redactor 1	CORSO	14/04/2023	Initial redaction Chapters 2, 3.1
João Cardoso	Contributor	INEGI	27/04/2023	Initial redaction Chapter 3
Natacha Goutay	Reviewer 1	CORSO	27/04/2023	All
João Manuel Cardoso	Reviewer 2	INEGI	27/04/2023	All
Anthony Comer	Reviewer 3	ULIM	27/04/2023	Chapters 2.1, 3.1
Akshay Hejjaji	Reviewer 4	ULIM	27/04/2023	Chapters 2.1, 3.1
Gursahib S.Bhatia	Reviewer 5	ULIM	27/04/2023	Chapters 2.1, 3.1

EXECUTIVE SUMMARY

This deliverable D6.1 is the continuation of the study, at a more representative scale, of the coating and the connections done at coupon level in the WP2 of this FibreGY project. The subjects can be treated separately.

Regarding the dry coatings, three axes are developed.

The first one is the quantification of the impact of the presence of a coating on the composite material. This is done by mechanical bending at 0° and 90°. It shows that a coating, applied by liquid process or by dry process by vacuum infusion impacted the mechanical response of the composite at different level. Furthermore, same characterisation shows not all dry coatings protect well the materials against environmental actions.

Second, real expositions in sea environment are performed. The issue of coatings exposed to the weather is good. Dry coating performs good, as well as liquid paint. Immersion in the sea demonstrated that dry coating is not a good candidate to work as an antifouling actor.

The combination of those two first study demonstrates that, after aging, even if the coatings look good, that not means that the composite material has not be damaged.

Finally, trials to integrate RFID sensors and optic fibres at the backing of the dry coating turn well. The concept is feasible but the final application has to be validated.

Regarding the assessment of FRP connection technologies for offshore structures, which relates to subtask 6.1.2, a connection (bolted composite joint) at subcomponent level was designed, manufactured, and tested. Static and fatigue tests were performed at ambient temperature to assess its behaviour under a dynamic loading scenario. Several conclusions were drawn, which can further help validate and develop numerical and predictive models for offshore structures made of FRP. The work conducted and reported here follows the building block approach, contributing to a deeper understanding of connection performance at a more realistic level. This complements the work performed during WP2 (experimental testing) and WP4 (development of predictive models).

TABLE OF CONTENTS

LIST OF FIGURES

![FIBREGY]

This project has received funding from the European Union's Horizon 2020 research and innovation programme under grant agreement No 952966.

LIST OF TABLES

LIST OF ANNEXES

1. INTRODUCTION

It has been demonstrated through durability tests in the D2.3 "Environmental protection of composites" that in terms of protection, dry coating performed as well or better than traditional liquid paint. Those evaluations have been made on adhesion to the substrate, water protection and colour evolution. What's more, other tests were carried out to see if the coating protected well the substrate by evaluating the mechanical properties after UV aging. The outcome of the test campaign is that there is a mechanical response evolution between a non-aged / non-coated sample and an UV-aged / coated sample.

As a reminder, the use of dry coatings in the manufacturing process permits to save time. Indeed, it erases the paint process by giving an already painted substrate at the demoulding stage of the infusion process. Its use remains very interesting.

To have a more representative understanding of the role of the coating on the protection of the composites, middle scale tests have to be completed.

The first study has the objective to better understand the impact of the coating on the mechanical properties. The analysis of a non-aged / coated sample will be address as well as the examination of a salt spray-aged / coated sample. That way, it will be evaluated the impact of the coating on the composite matrix before aging and the protection giving the coating when exposed to different environments.

The second investigation is to access the performance of the coating in realistic sea conditions. Liquid and dry coating painted samples will be exposed in real life measuring their durability against weathering exposure. Same samples will be immersed in real sea water to obtain their protection against fouling.

Finally, as the incorporation of sensors at the backing of the dry coatings remains very interesting to be an alternative to the classical solutions and no solutions have been found in the framework of D2.5 "Multifunctional materials for Structural Health Monitoring (SHM) Diagnosis and Structural Performance Assessment", two options will be here described (RFID sensors and optical fibre).

Regarding the middle-scale tests on connections, the third chapter will detail the tests carried out on connections, particularly a middle-scale subcomponent, which has undergone static and dynamic (fatigue) loadings. The purpose of this was to proceed with the validation using the building block approach (Figure 1), which started at WP2 using coupon static and fatigue testing, at T2.3 and T2.4, respectively. Numerical models were developed through WP3 and WP4 which have allowed us to validate and correlate the results from the physical tests. When the numerical models are well-matured and the finite element analysis is predictive, these simulations can replace some physical tests. This is particularly important for the larger scales where the cost of physical/experimental testing different configurations is almost prohibitive. Therefore, the objective of these tests is to deepen the knowledge of the different attributes and phenomena occurring at the subcomponent level and use that info as an important input for further developing the predictive models, particularly under fatigue loadings.
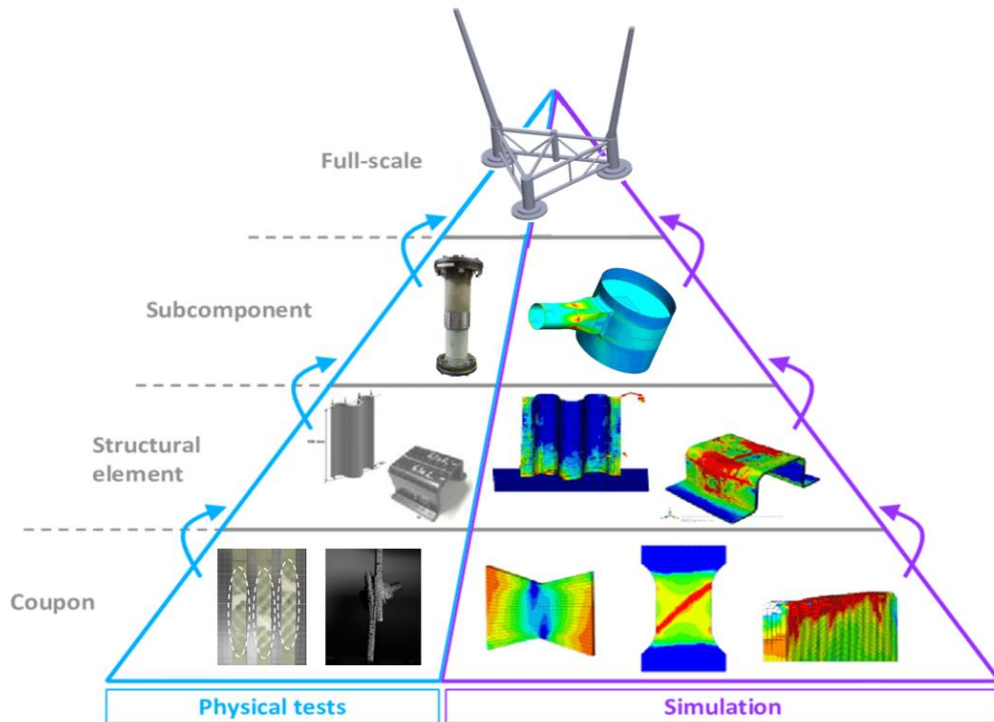
Figure 1 – Building block approach

To sum up the information portrayed in the pyramid in Figure 1, the idea of the building block approach is to build the knowledge on the material and structural behaviours step by step, starting from the fundamental stage at the coupon level up to the full scale (i.e. the full wind turbine or even the full platform). Simulations based on finite element methods are used at different stages of the pyramid, being an important companion of the physical tests and whose results can be correlated in both ways. The simpler geometries, at the bottom of the pyramid, were tested in higher numbers and with fewer costs than the upper elements, which due to their complexity could only be physically tested a few. This approach is very well known when designing composite structures for the aerospace industry [1].

The first subchapter of Chapter 3 will address the manufacturing and testing of larger joints bonded with the reversible adhesive, in order to evaluate their service performance and "end of life" dismantling capacity, while in Subchapter 3.2, it will be exposed the process of defining the subcomponent to be tested, the fatigue tests plan and fatigue concepts, the test methods and finally the results and their analysis.

2. MIDDLE SCALE TEST ON DRY COATINGS

The performance of the dry coating compared to a traditional liquid paint was evaluated in the framework of D2.3 "Environmental protection of composites" [2]. A better understanding of the behaviour of the coating facing different type of environment exposition is described in this chapter.

2.1. Influence of the protection of composite by dry coating on mechanical resistance against aging (laboratory scale)

A coating has two functions: decorate and protect. Its second action is even more important knowing the composite aging. Indeed, epoxy resin is sensitive to UV. To evaluate the protection given by the coating and access if a dry coating behaves similar to a standard liquid paint, durability tests are simulated by two laboratory tests. The first test is the exposition to ultra violet (UV): it simulated the sun ray's impact. The second test is an exposition to a corrosive atmosphere (salt spray test) as can be found on wind turbine platforms.

After the aging, mechanical properties of the composite can be tested and compared to the initial stage.

2.1.1. Sample description

Following the previous description, samples produced with dry coating and others painted by liquid paint were manufactured. The manufacturing process, resins and non-crimp fibre fabric were consistent with those reported in D2.1 "Catalogue of optimum FRP solutions for different applications in OWTP platforms".

Coating	Composite Resin	Fibres
Dry coating A: Hempathane 55210	Thermoset Infugreen	
Dry coating B: Alexit 471	Thermoplastic Elium	
Dry coating C: Alexit 411-77	Thermoset Infugreen	Glass Fibre - H2026 - U-E-1182g/m²-1270mm
	Thermoplastic Elium	
Liquid paint: Hempathane 55210	Thermoset Infugreen	
	Thermoplastic Elium	

Table 1 – Sample composition (coating, resin, fibres)

To compared dry coating performance to traditional liquid paint, coupons were produced by vacuum assisted liquid resin infusion with and without the dry coating inside the composite mould. For coupons infused without the dry coating, they are painted after the process by spray gun.

The principle of the resin infusion process with integrated dry coating is represented in the figure below. The dry coating is intended to be used at the bottom of composite mould when doing infusion. The dry coating is located as an extra layer during the fabric layup, as the coating will protect the structure, it is placed directly in contact with the mould, and then dry-reinforcement fibre is laid up on the top followed by a layer of peel ply layer consequently. The vacuum bag will seal and create the vacuum atmosphere required for the process of vacuum assisted liquid resin infusion.
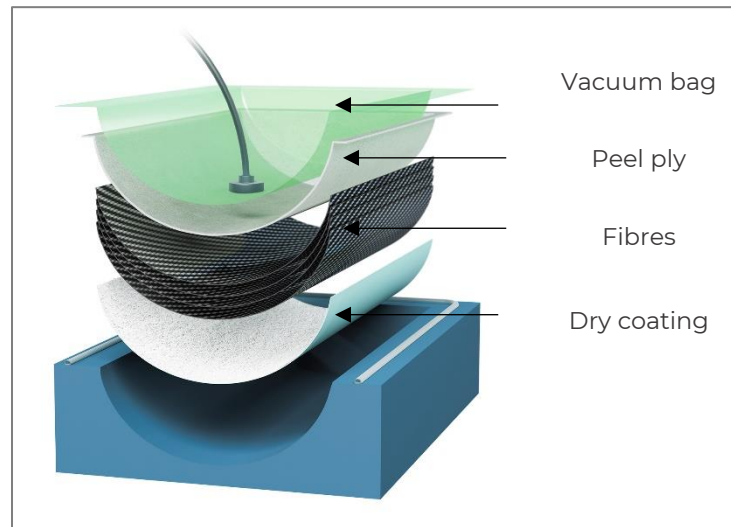
Figure 2 – Use of dry coating in vacuum infusion process principle

The parameters used for the vacuum infusion are given in the next table. Specific manufacturing details are stated in D2.1 "Catalogue of optimum FRP solutions for different applications in OWTP platforms".

Resin	Infugreen 810	Elium 188X0
Curing agent	SD8824	BP-40-SAQ
Ratio	100/22	100/3
Thickness	~3.4mm	~3.4mm
Fabric	Glass Fibre - H2026 - U-E-1182g/m²-1270mm	Glass Fibre - H2026 - U-E-1182g/m²-1270mm
Lay up	[0]2s (4 Layers)	[0]2s (4 Layers)
Curing temperature	60°C	60°C
Curing time	16h	24h

Table 2 – Vacuum infusion parameters

For the samples infused without the dry coating, the liquid paint scheme is:

Layer	Paint	Thickness	Application method	Drying
1: Primer	Hempadur 15579	~100 μm	Spray gun	24hours
2: Topcoat	Hempathane 55210	~30 μm	Spray gun	24 hours
3: Topcoat	Hempathane 55210	~30 μm	Spray gun	24 hours

Table 3 – Liquid paint process

(Side prepared and painted: smooth (in contact with the mould), surface preparation: sanding)

Pictures of the samples is available in Annex 1.

2.1.2. Test description

Different configurations have been tested following the next map:
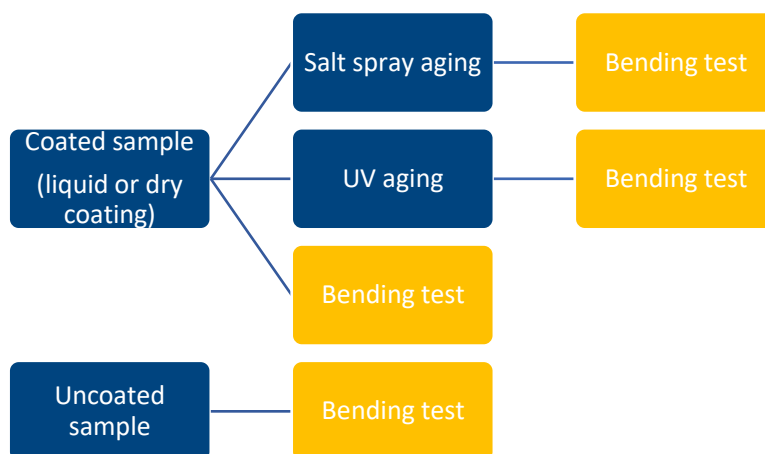
Figure 3 – Test matrix

To have reference values, bending tests on uncoated and coated/unaged samples have been performed. Mechanical characterisation has also been performed on aged samples.

2.1.2.1.   Aging

Neutral salt spray test (ISO 7253)

This test is based on the standard ISO 7253:1996 - Paints and varnishes — Determination of resistance to neutral salt spray (fog).

The neutral salt spray test is a common test to evaluate paints applied on metallic substrate to resist to corrosion. Samples with scribes created in the coated are exposed in a chamber at 35°C where saline solution is sprayed on the samples (NaCl at 50g/L, pH between 6,5 and 7,2). The duration of exposition is 1 month.

Exposition to UV (ISO 11507)

This test is based on the standard ISO 11507:2007 - Paints and varnishes — Exposure of coatings to artificial weathering — Exposure to fluorescent UV lamps and water.

Exposition to UV is a way to simulate the aging of the coatings. To perform this, samples are exposed to UV lamps, which are representatives to UV sun rays, and condensation which is representative of atmospheric humidity.

For the framework of this project, method A of the ISO 11507 standard was used and fluorescent tubes UVB 313 were employed for the light source. The duration of exposition is 1 month.

2.1.2.2.   Bending

Flexure samples were tested in a three-point-bending loading mode in accordance with ISO 14125. Samples were measured using a vernier callipers and a micrometre for the thickness. The lay-up, and nominal dimensions and span-to-thickness ratio are summarised in the next table. For 0° samples, the fibres are predominantly aligned with the length of the test specimen. For 90° samples, the fibres are predominantly aligned with the width of the test specimens. Samples were stored in polyester bags under ambient conditions prior to testing. The samples were tested on a Tinius Olsen electro-mechanical straining frame with load cell of 10 kN rating for Flexural 0° and 1 kN for Flexural 90° specimens. LVDT (Linear Variable Differential Transformer: A displacement transducer) was used to record the deflection of the central region of the specimen for Flexural 0° specimens. In the case of Flexural 90° specimens, the cross-head stroke was recorded to obtain the deflection of the specimen. For all the Salt Spray, all Un-aged and two cases of UV aged samples, the LVDT was used for 90° specimens as well. The tests were conducted under displacement control with a displacement rate of 1 mm/min. The roller diameters at the load nose and support points were 10 mm and 4 mm respectively. The next figure depicts a flexural sample being tested under 3-point loading. Data reduction was performed for the calculations of the required properties. The following results were

extracted from the Flexure 0° and 90° test data, viz. Flexural Strength (σ_F), Flexural Modulus (E_F) and Flexural strain (ε_f) at failure. The strain to failure is the strain at which a first sign of load drop is observed in the mechanical response curves.

The calculations were performed using the following formulae,

(1)
$$Flexural\ Strength\ (\sigma_F) = \frac{3 \times F \times L}{2 \times b \times h^2}$$

(2)
$$Flexural\ Strain\ (\varepsilon_f) = \frac{6 \times s \times h}{L^2}$$

(3)
$$Flexural\ Modulus\ (E_F) = \frac{(\sigma_F'' - \sigma_F')}{(\varepsilon_f'' - \varepsilon_f')}$$

Where, F is the applied load, L is the span, b is the sample width, h is the sample thickness, s is the deflection, σ_F'' is the stress at which strain is 0.0025 and σ_F' is the stress at which strain is 0.0005. The strength/load at failure and the strain at failure are reported at the point of initiation of the failure in the specimen. In the flexural stress vs strain plots, the failure initiation point corresponds to the first load drop observed in the curve. However, for the representation of overall material response, the complete curves have been plotted beyond the point of first load drop.

Material	Minimum number of samples	Lay-up	Thickness excluding coating (mm)	Width (mm)	Span (mm)	Span-to-thickness ratio
Elium / Glass fibres	3	[0]₂ₛ	3	15	60	20
	3	[90]₂ₛ	3	15	60	20
Infugreen / Glass fibres	3	[0]₂ₛ	3	15	60	20
	3	[90]₂ₛ	3	15	60	20

Table 4 – Flexure test sample lay-up and nominal dimensions

Details is given in Annex 2
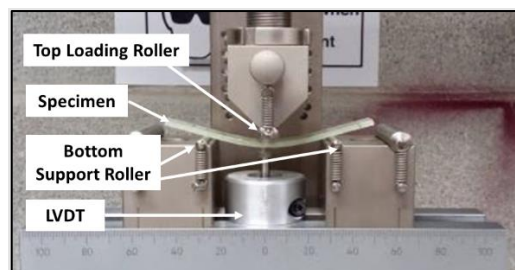
Figure 4 – Flexure test sample under 3-pt bend loading configuration

Below, 4 definitions are defined:

- Flexural Stress: stress on the surface of the material under the load nose on either the tension or compression side.

- Flexural Strength: largest flexural stress capable of being supported by the material. In the current work, the flexural strength is taken as the first load drop in the stress-strain curve.

- Strain: change in length divided by original length measured on the surface of the sample under the load nose on the tension side.

- Flexural Modulus: flexural stiffness of the material.

For the framework of the project, the samples were tested with the coating at the top, as seen in the next figure. In 0° samples the material strength is mainly controlled by the material located directly under the load nose. If ageing had a damaging effect on the coating and the material, then a reduction in the flexural strength and/or modulus will be seen.
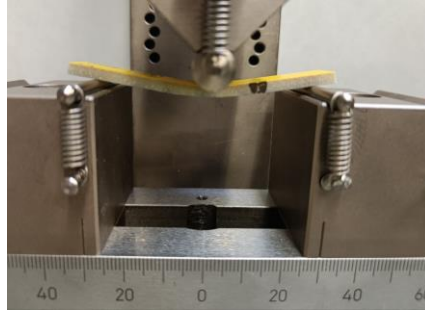
Figure 5 – Flexure test with coated sample

All the configurations tested are summarized in the following respective table for 0° and 90°. The interpretation of each result will be demonstrated in the following chapters.

Sr. No.	Material (0°)	Un-aged		Salt Spray Aged		UV-aged	
		Strength (MPa)	Modulus (GPa)	Strength (MPa)	Modulus (GPa)	Strength (MPa)	Modulus (GPa)
1.	Laminate- Glass Fibre- InfuGreen Coating- HEMP/55210 Dry	1065.8 (24.5)	32.4 (0.5)	813.3 (39.4)	28.5 (1.3)	872.2 (90.5)	25.9 (1.6)
2.	Laminate: Glass Fibre- Elium Coating: ALEXIT/471 Dry	1222.4 (29.3)	34.4 (1.0)	1062.8 (16.7)	32.0 (1.4)	1080.5 (41.7)	29.5 (2.0)
3.	Laminate: Glass Fibre- InfuGreen Coating- ALEXIT/411-77	973.2 (85.0)	29.4 (1.2)	940.1 (72.4)	29.5 (1.0)	934.3 (63.2)	30.2 (0.6)
4.	Laminate: Glass Fibre- Elium Coating: ALEXIT/411-77	1105.9 (37.9)	30.9 (0.9)	914.1 (30.6)	29.2 (1.1)	978.9 (99.7)	26.6 (5.1)
5.	Laminate- Glass Fibre- InfuGreen Coating- HEMP/55210 Liquid Paint	852.9 (139.0)	30.7 (1.2)	838.7 (27.4)	29.8 (1.7)	929.5 (47.8)	28.8 (1.6)
6.	Laminate: Glass Fibre- Elium Coating: HEMP/55210 Liquid Paint	1087.3 (35.2)	34.6 (0.7)	1054.5 (76.5)	35.6 (0.5)	1142.3 (36.8)	32.2 (1.5)
7.	Laminate: Glass Fibre- Elium Coating: No Coating	939.5 (51.3)	30.3 (1.8)	-	-	-	-
8.	Laminate: Glass Fibre- InfuGreen Coating: No Coating	1075 (61.8)	39.3 (1.8)	-	-	-	-

Table 5 – 0° Bending results summary

Note-Standard deviation in parenthesis.

Sr. No.	Material (90°)	Un-aged		Salt Spray Aged		UV-aged	
		Strength (MPa)	Modulus (GPa)	Strength (MPa)	Modulus (GPa)	Strength (MPa)	Modulus (GPa)
1.	Laminate- Glass Fibre-InfuGreen Coating- HEMP/55210 Dry	60.8 (2.7)	11.2 (0.3)	34.7 (0.5)	9.7 (0.1)	56.3 (4.3)	9.2 (0.5)
2.	Laminate: Glass Fibre-Elium Coating: ALEXIT/471 Dry	53.9 (7.3)	11.3 (0.6)	24.6 (1.5)	8.8 (0.9)	38.0 (1.4)	9.6 (0.5)
3.	Laminate: Glass Fibre-InfuGreen Coating- ALEXIT/411-77	56.5 (2.4)	10.7 (0.3)	33.9 (5.9)	9.9 (0.6)	55.7 (1.9)	10.3 (0.4)
4.	Laminate: Glass Fibre-Elium Coating: ALEXIT/411-77	49.0 (3.25)	10.8 (0.1)	38.3 (1.1)	10.0 (0.1)	49.5 (9.8)	10.4 (0.1)
5.	Laminate- Glass Fibre-InfuGreen Coating- HEMP/55210 Liquid Paint	60.8 (5.4)	9.9 (0.4)	36.7 (1.3)	9.5 (0.4)	62.0 (3.5)	10.1 (0.2)
6.	Laminate: Glass Fibre-Elium Coating: HEMP/55210 Liquid Paint	39.0 (7.3)	10.0 (0.3)	41.9 (5.9)	10.1 (1.2)	40.1 (4.5)	9.6 (0.3)
7.	Laminate: Glass Fibre-Elium Coating: No Coating	70.6 (4.4)	11.1 (0.8)	-	-	-	-
8.	Laminate: Glass Fibre-InfuGreen Coating: No Coating	58.4 (2.2)	9.1 (0.4)	-	-	-	-

Table 6 – 90° Bending results summary

Note-Standard deviation in parenthesis.

2.1.3. Result

2.1.3.1. Reminder of the results of UV aged coated sample

In the framework of D2.3 "Environmental protection of composites", the characterisation of the impact of aging on the composite and the coating protection performance were only operated by comparing two types of samples:

- Reference sample which are uncoated coupons.
- UV aged coated sample. In this category the samples were painted by dry coating directly during the vacuum infusion process or after the manufacturing by liquid paint.

Two types of composite resin have also been studied: Infugreen and Elium.

The main conclusions are:

- No difference on the protection level of one type of coatings (dry or liquid) has been demonstrated.
- A difference can be seen between the reference (non-aged / no coated) and UV aged coated sample.
  - o UV aged -coated Infugreen (liquid or dry) sample performed less compared to the reference (results based on flexural 0°).
  - o UV aged coated Elium samples performed less than the reference but also responded differently (bilinear behaviour) representative to a structural change in the structure (results base on flexural 90°).

The mechanical response and values where difference can be seen are reminded below.

Reference	UV aged Dry coating	UV aged Liquid paint
Figure 6 – Flexural stress vs flexural strain plots for 0°, Infugreen control (no coating)	Figure 7 – Flexural stress vs flexural strain plots for 0°, UV aged Dry coating Hempathane 55210/Infugreen	Figure 8 – Flexural stress vs flexural strain plots for 0°, UV aged Liquid paint Hempathane 55210/Infugreen
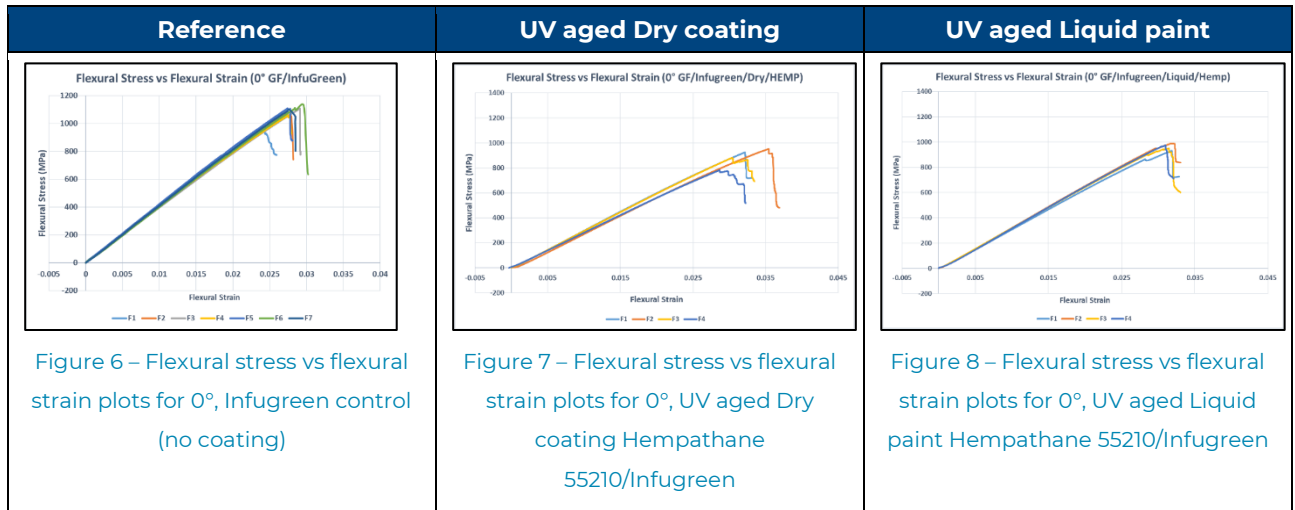
Table 7 – Flexural 0° response on Infugreen Reference and UV aged

Composite Resin	Coating	Number of samples	Load at Failure (kN))	Failure Strength (MPa)	Flexural Modulus, E_f (GPa)	Strain-at-failure (%)
Infugreen	Control (no coating)	7	1.759 (0.108)	1075 (61.8)	39.3 (1.8)	2.75 (0.17)
	Dry coating Hempathane 55210	4	1.777 (0.146)	872.2 (90.5)	25.9 (1.6)	3.27 (0.20)
	Liquid Hempathane 55210	4	1.678 (0.087)	929.5 (47.8)	28.8 (1.6)	2.97 (0.11)

Table 8 – Flexural 0° results on Infugreen Reference and UV aged

Reference	UV aged Dry coating	UV aged Liquid paint
Figure 9 – Flexural stress vs flexural strain plots for 90°, Elium control (no coating)	Figure 10 – Flexural stress vs flexural strain plots for 90°, UV aged Dry coating Alexit 471/Elium	Figure 11 – Flexural stress vs flexural strain plots for 90°, UV aged Liquid paint Hempathane 55210/Elium
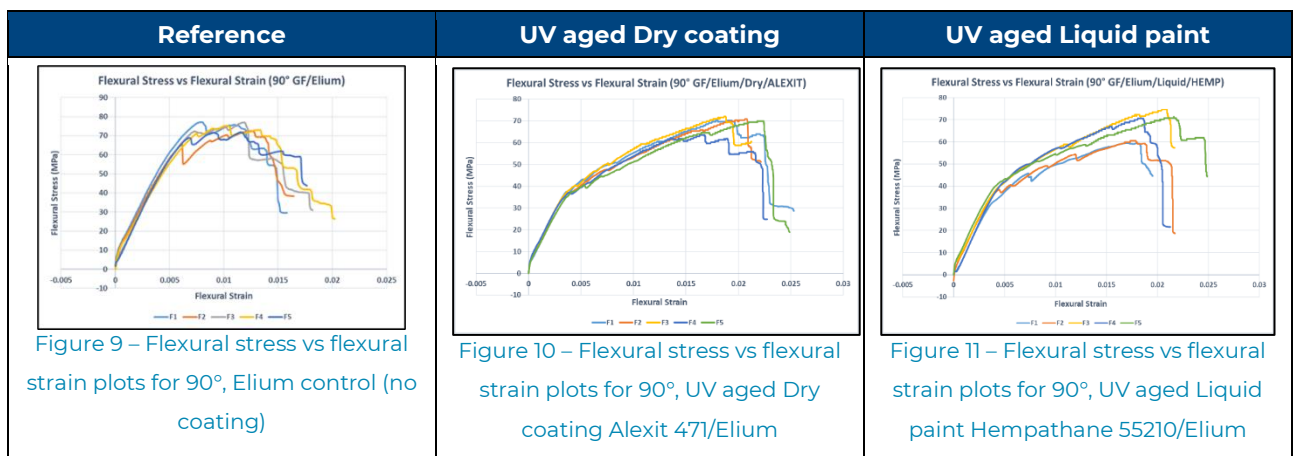
Table 9 – Flexural 90° response on Elium Reference and UV aged

Composite Resin	Coating	Number of samples	Load at Failure (kN))	Failure Strength (MPa)	Flexural Modulus, E_f (GPa)	Strain-at-failure (%)	Max Load (kN)	Max Strength (MPa)	Strain at Max Load (%)
Elium	Control (no coating)	5	0.117 (0.007)	70.6 (4.4)	11.1 (0.8)	0.72 (0.07)	-	-	-
	Dry coating Alexit 471	5	0.069 (0.003)	38.0 (1.4)	9.6 (0.5)	0.40 (0.03)	0.125 (0.006)	69.4 (3.4)	1.96 (0.21)
	Liquid Hempathane 55210	5	0.067 (0.008)	40.1 (4.5)	9.6 (0.3)	0.48 (0.07)	0.113 (0.012)	67.3 (6.9)	1.92 (0.19)

Note-Standard deviation in parenthesis.

Table 10 - Flexural 90° results on Elium Reference and UV aged

From previous statements, it can be assumed that UV impacted the composite performance as a result of the poor protection of the coating (dry or liquid). Even though it is not expecting the coating to have any significant impact on the flexural strength and modulus of the composite, the coating may impact the composite at the initial stage (before aging). What is more, the coating may be performant against another type of aging. This will be address in the next subchapter.

2.1.3.2. Influence of the coating (dry or liquid) on the mechanical properties (before aging)

First, the impact of the presence of the coating in the composite matrix is studied in this chapter.

The next figures show the results after 0° and 90° bending of unaged coated and unaged **un**coated sample on Infugreen first then Elium.

After, comparative tables are made to evaluated better the impact of the coating. All raw data and graphs will be address in Annex 2.

Composite resin: Infugreen
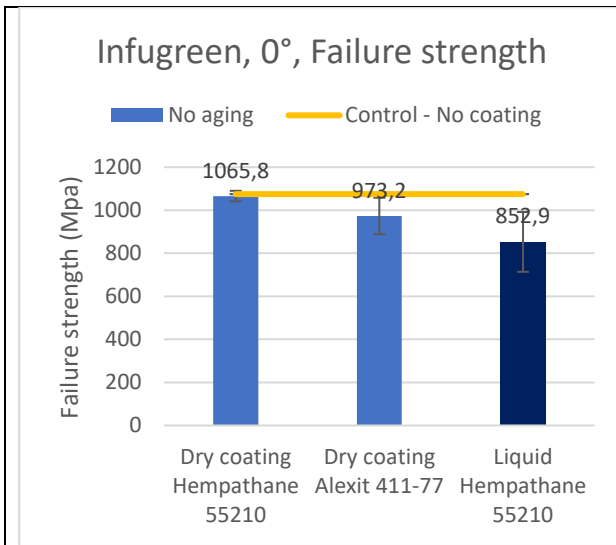
Figure 12 – Failure strength 0°, Infugreen, with or without coating
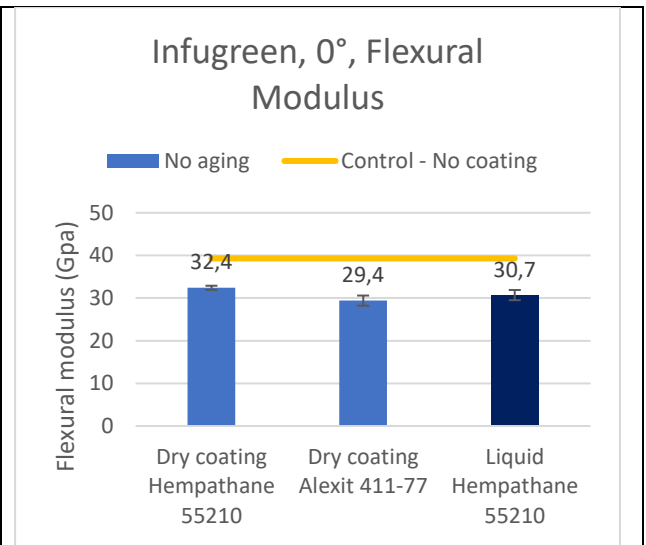
Figure 13 – Flexural modulus 0°, Infugreen, with or without coating
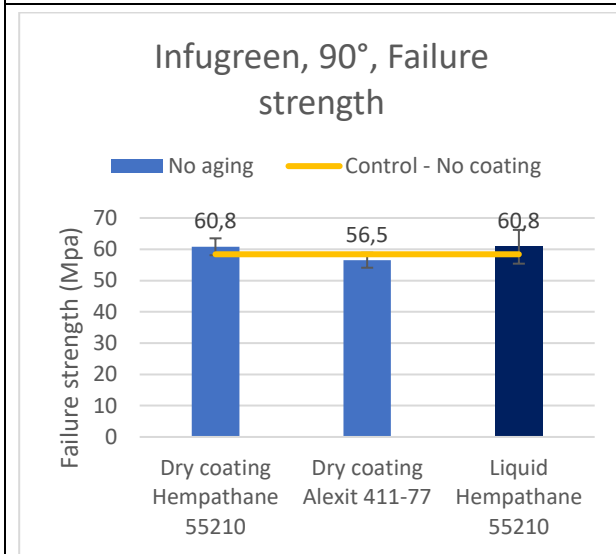
Figure 14 - Failure strength 90°, Infugreen, with or without coating
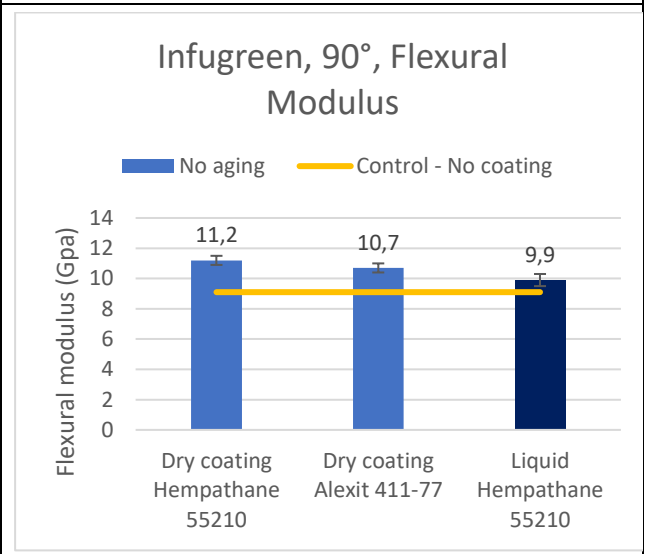
Figure 15 - Flexural modulus 90°, Infugreen, with or without coating

Table 11 – Bending test, Infugreen, with or without coating

Infugreen	0°, failure strengh	0°, flexural modulus	90°, failure strengh	90°, flexural modulus
Dry coating	=*	<	=	>
Liquid paint	<	<	=	=

Table 12 – Comparison response, Infugreen, with or without coating

*the dry coating response on this parameter is … than the reference response

Composite resin: Elium

Figure 16 - Failure strength 0°, Elium, with or without coating

Figure 17 - Flexural modulus 0°, Elium, with or without coating

Figure 18 – Failure strength 90°, Elium, with or without coating

Figure 19 - Flexural modulus 90°, Elium, with or without coating
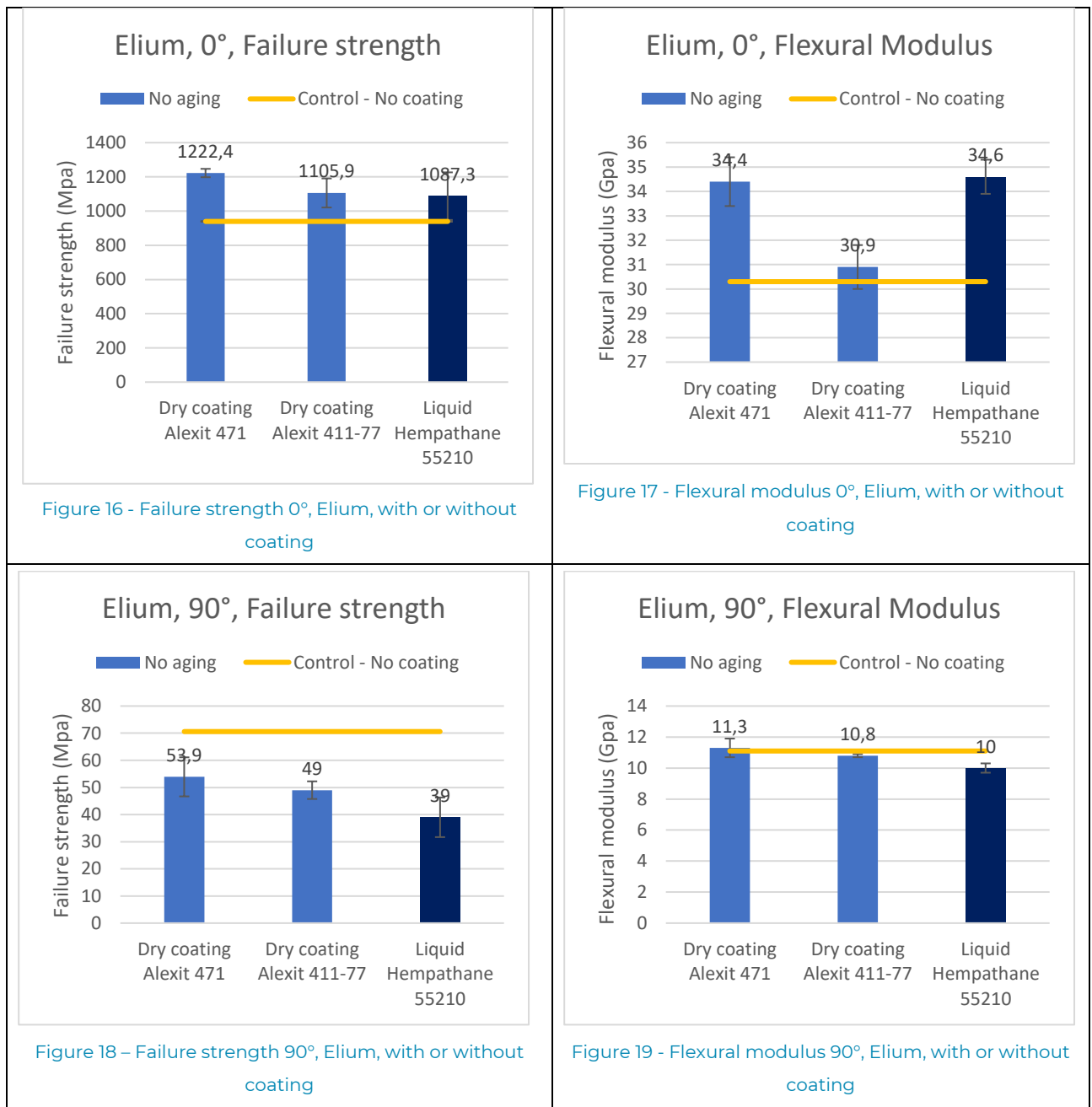
Table 13 – Bending test, Elium, with or without coating

Elium	0°, failure strengh	0°, flexural modulus	90°, failure strengh	90°, flexural modulus
Dry coating	>*	=	<	=
Liquid paint	>	>	<	=

Table 14 – Comparison response, Elium, with or without coating

*the dry coating response on this parameter is … than the reference response

For both composite resin Infugreen and Elium, the coated (dry or liquid) do not behaves the same as the control uncoated sample.

On Infugreen, the values of both coated samples (dry and liquid) are similar than the reference. We can assume that there is no huge impact on the properties. However, we can notice two different behaviour for the flexural modulus: the addition of the coating had decreased it when testing in bending 0° but increased for the bending 90°.

On Elium the results are different. The dry coating Alexit 471 and the liquid paint Hempathane 55210 increased a lot the flexural modulus of the matrix when doing 0° bending. But on the other hand, all coatings decreased the flexural strength (90°).

To conclude, the coating has an impact on the mechanical properties on the composite. This impact depends of the type of coating: dry or liquid and on the composite type. It cannot be said that the addition of the coating increase or decrease the mechanical of the properties as each parameters had a opposite evolution.

2.1.3.3.   Impact of the type of aging on the composite properties and comparison of the protection performance between the dry coating and the liquid paint

The previous chapter described the fact that coatings have an impact on the mechanical properties of the composite even before aging. This impact may stay constant after aging, which will mean that the coating protected well the composite. This will be study in this chapter by comparing the performance of coated samples before and after aging.

2.1.3.3.1.   Case of UV exposure

The next figures show the results after 0° and 90° bending of **un**aged coated and **UV** aged coated sample on Infugreen first then Elium.

After, comparative tables are made to evaluated better the impact of the coating. All raw data and graphs will be address in Annex 2.

Composite resin: Infugreen

Figure 20 – Failure strength 0°, Infugreen, UV aged/non-aged

Figure 21 – Flexural Modulus 0°, Infugreen, UV aged/non-aged

Figure 22 - Failure strength 90°, Infugreen, UV aged/non-aged

Figure 23 - Flexural Modulus 90°, Infugreen, UV aged/non-aged
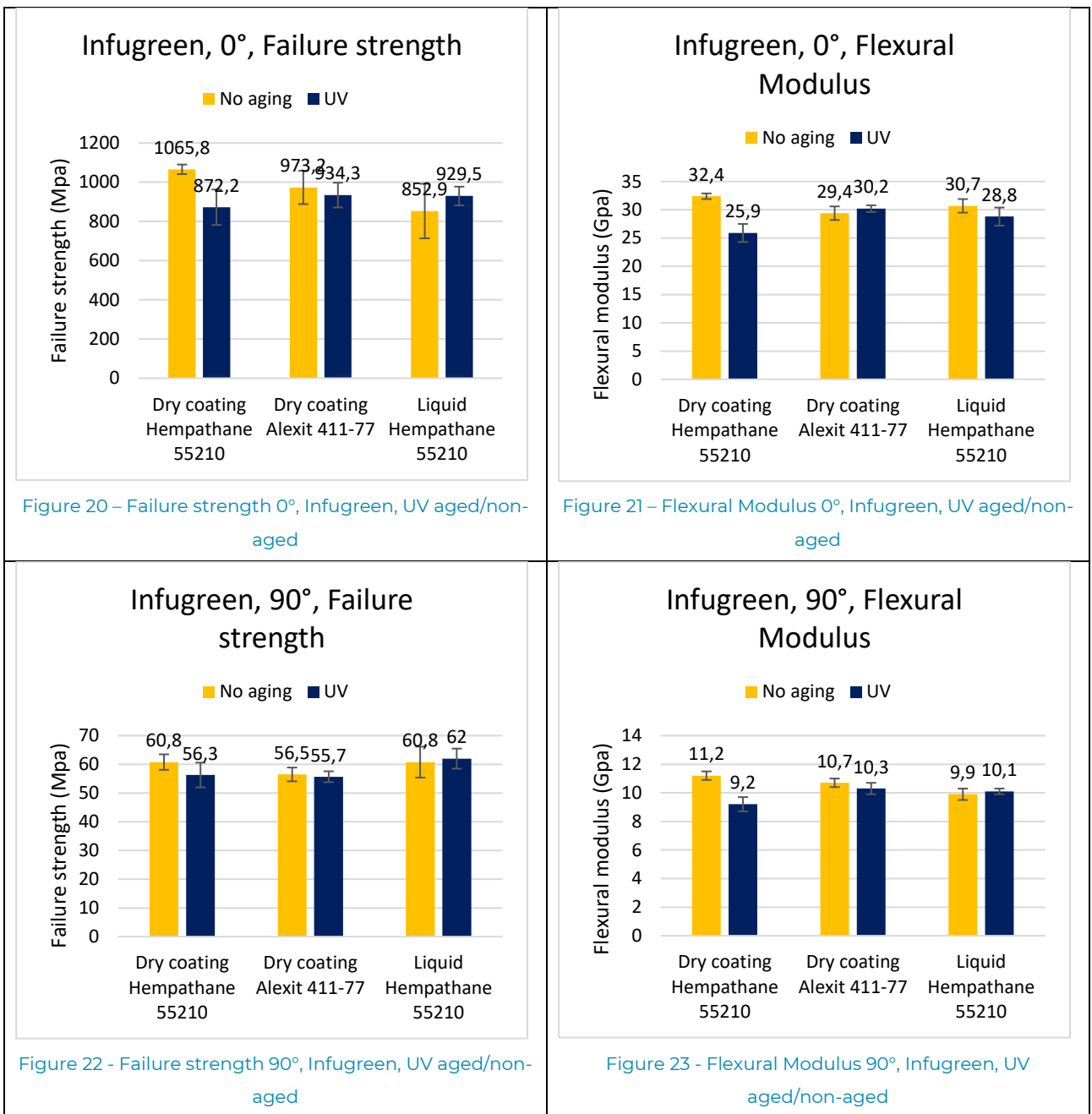
Table 15 – Bending test, Infugreen, UV aged/non-aged

Infugreen, UV	0°, failure strengh	0°, flexural modulus	90°, failure strengh	90°, flexural modulus
Dry coating Hempathane 55210	<*	<	=	<
Dry coating Alexit 411-77	=	=	=	=
Liquid paint Hempathane 55210	=	=	=	=

Table 16 – Comparison response, Infugreen, UV aged/non-aged

*the aged coating sample response on this parameter is … than the non-aged coating sample response

Composite resin: Elium

Elium, 0°, Failure strength

No aging ■ **UV**

	Dry coating Alexit 471	Dry coating Alexit 411-77	Liquid Hempathane 55210
No aging	1222,4	1105,9	1087,3
UV	1080,5	978,9	1142,3
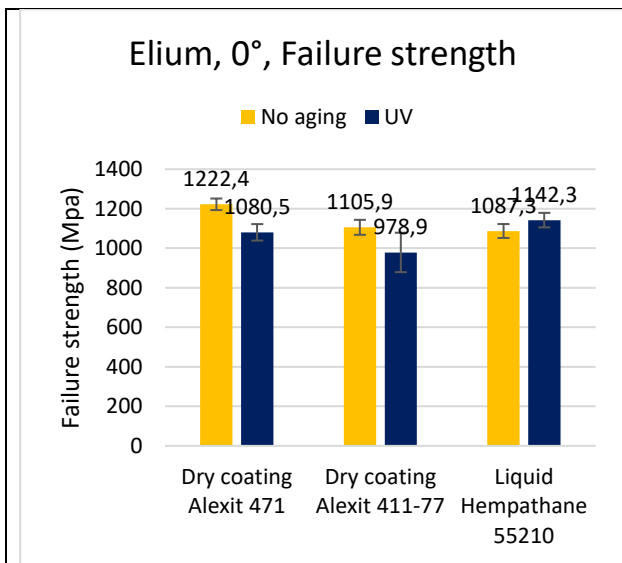
Figure 24 - Failure strength 0°, Elium, UV aged/non-aged

Elium, 0°, Flexural Modulus

No aging ■ **UV**

	Dry coating Alexit 471	Dry coating Alexit 411-77	Liquid Hempathane 55210
No aging	34,4	30,9	34,6
UV	29,5	26,6	32,2
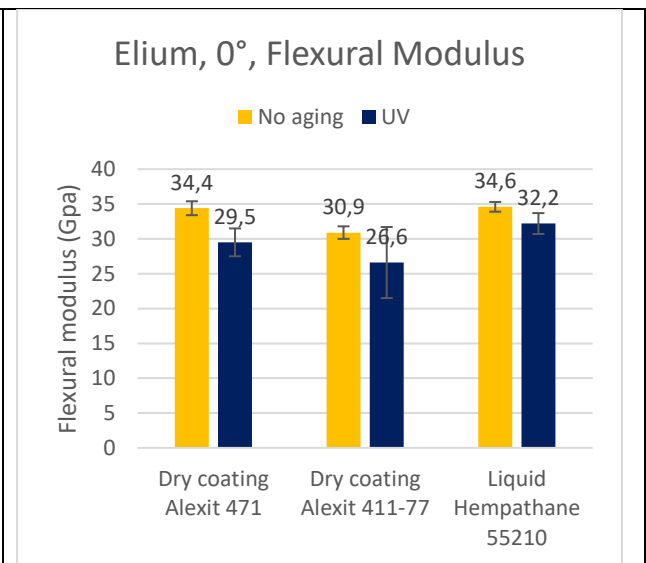
Figure 25 - Flexural modulus 0°, Elium, UV aged/non-aged

Elium, 90°, Failure strength

No aging ■ **UV**

	Dry coating Alexit 471	Dry coating Alexit 411-77	Liquid Hempathane 55210
No aging	53,9	49	39
UV	38	49,5	40,1
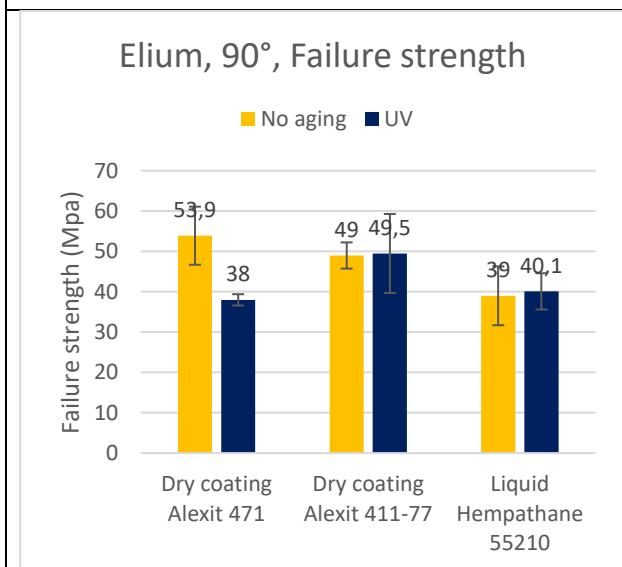
Figure 26 – Failure strength 90°, Elium, UV aged/non-aged

Elium, 90°, Flexural modulus

No aging ■ **UV**

	Dry coating Alexit 471	Dry coating Alexit 411-77	Liquid Hempathane 55210
No aging	11,3	10,8	10
UV	9,6	10,4	9,6
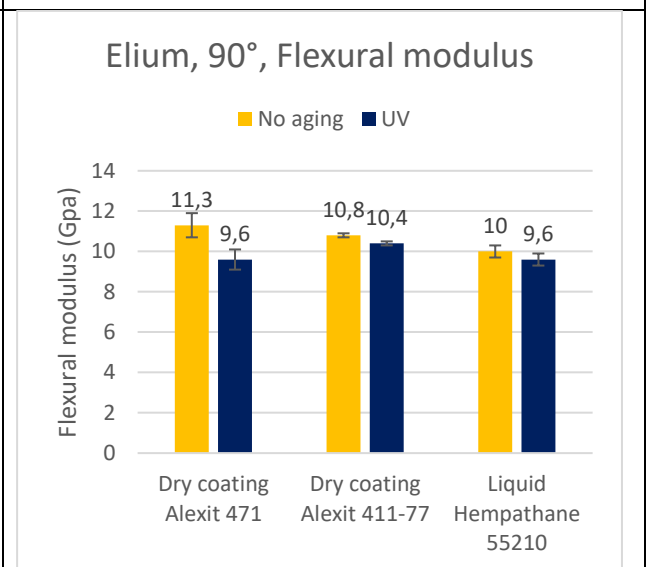
Figure 27 – Flexural modulus 90°, Elium, UV aged/non-aged

Table 17 – Bending test, Elium, UV aged/non-aged

Elium, UV	0°, failure strength	0°, flexural modulus	90°, failure strength	90°, flexural modulus
Dry coating Alexit 471	<*	<	<	<
Dry coating Alexit 411-77	=	=	=	=
Liquid paint Hempathane 55210	=	=	=	=

Table 18 – Comparison response, Elium, UV aged/non-aged

*the aged coating sample response on this parameter is … than the non-aged coating sample response

Bases on Table 16 and Table 18, it appears clearly that a decrease of the properties for dry coated samples happened after UV exposure. The remark is valid for dry coating Hempathane 55210 on Infugreen and dry coating Alexit 471 on Elium. The common point between those 2 paints is their colour: yellow.

It is very interesting to notice also that the same coating Hempathane 55210 but in liquid form protected well the composite. This may be explained by the fact that a primer was used the liquid paint process. This primer may not only be used to increase the adhesion of the coating on the substrate but also act as a barrier against UV.

The protection brought by the dry coating on UV depends on the paint type: it works with Alexit 411-77 but not with Hempathane 55210 or Alexit 471. In the case of resin Infugreen, liquid Hempathane 55210 protected better than the dry coating.

Against UV, the protection brought by the dry coatings depends on the coating reference that was transformed. In some case, the use of a primer seems mandatory.

2.1.3.3.2. Case of corrosion exposure

The methodology will be the same as before.

The next figures show the results after 0° and 90° bending of **un**aged coated and **salt spray** aged coated sample on Infugreen first then Elium.

After, comparative tables are made to evaluated better the impact of the coating. All raw data and graphs will be address in Annex 2.

Composite resin: Infugreen

Figure 28 - Failure strength 0°, Infugreen, Salt spray aged/non-aged

Figure 29 – Flexural modulus 0°, Infugreen, Salt spray aged/non-aged

Figure 30 – Failure strength 90°, Infugreen, Salt spray aged/non-aged

Figure 31 – Flexural modulus 90°, Infugreen, Salt spray aged/non-aged
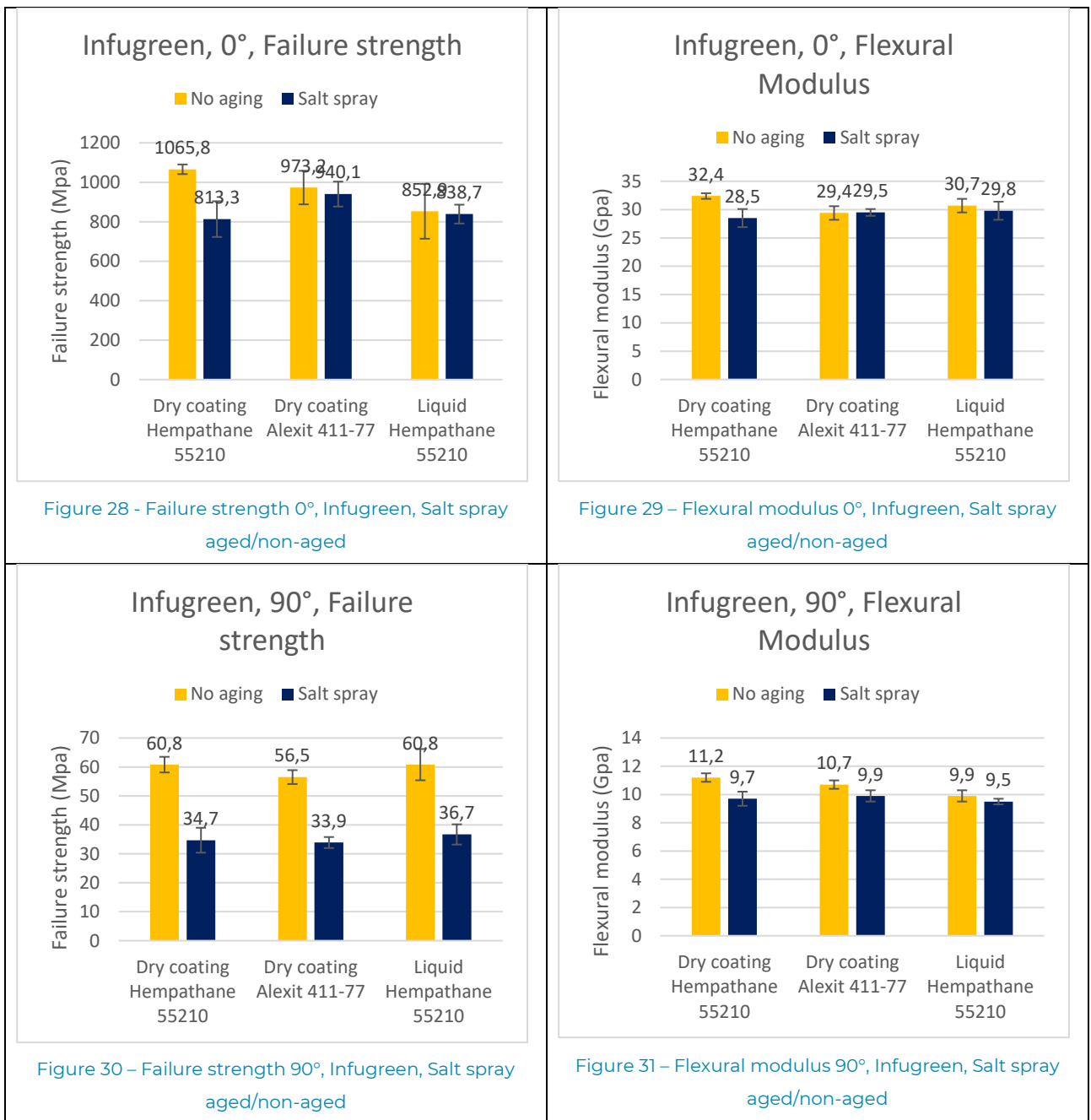
Table 19 – Bending test, Infugreen, Salt spray aged/non-aged

Infugreen, Salt spray	0°, failure strengh	0°, flexural modulus	90°, failure strengh	90°, flexural modulus
Dry coating Hempathane 55210	<*	<	<	<
Dry coating Alexit 411-77	=	=	<	=
Liquid paint Hempathane 55210	=	=	<	=

Table 20 – Comparison response, Infugreen, Salt spray aged/non-aged

*the aged coating sample response on this parameter is … than the non-aged coating sample response

FIBREGY

This project has received funding from the European Union's Horizon 2020 research and innovation programme under grant agreement No 952966.

Composite resin: Elium

Figure 32 - Failure strength 0°, Elium, Salt spray aged/non-aged

Figure 33 – Flexural modulus 0°, Elium, Salt spray aged/non-aged

Figure 34 - Failure strength 90°, Elium, Salt spray aged/non-aged

Figure 35 - Flexural modulus 90°, Elium, Salt spray aged/non-aged
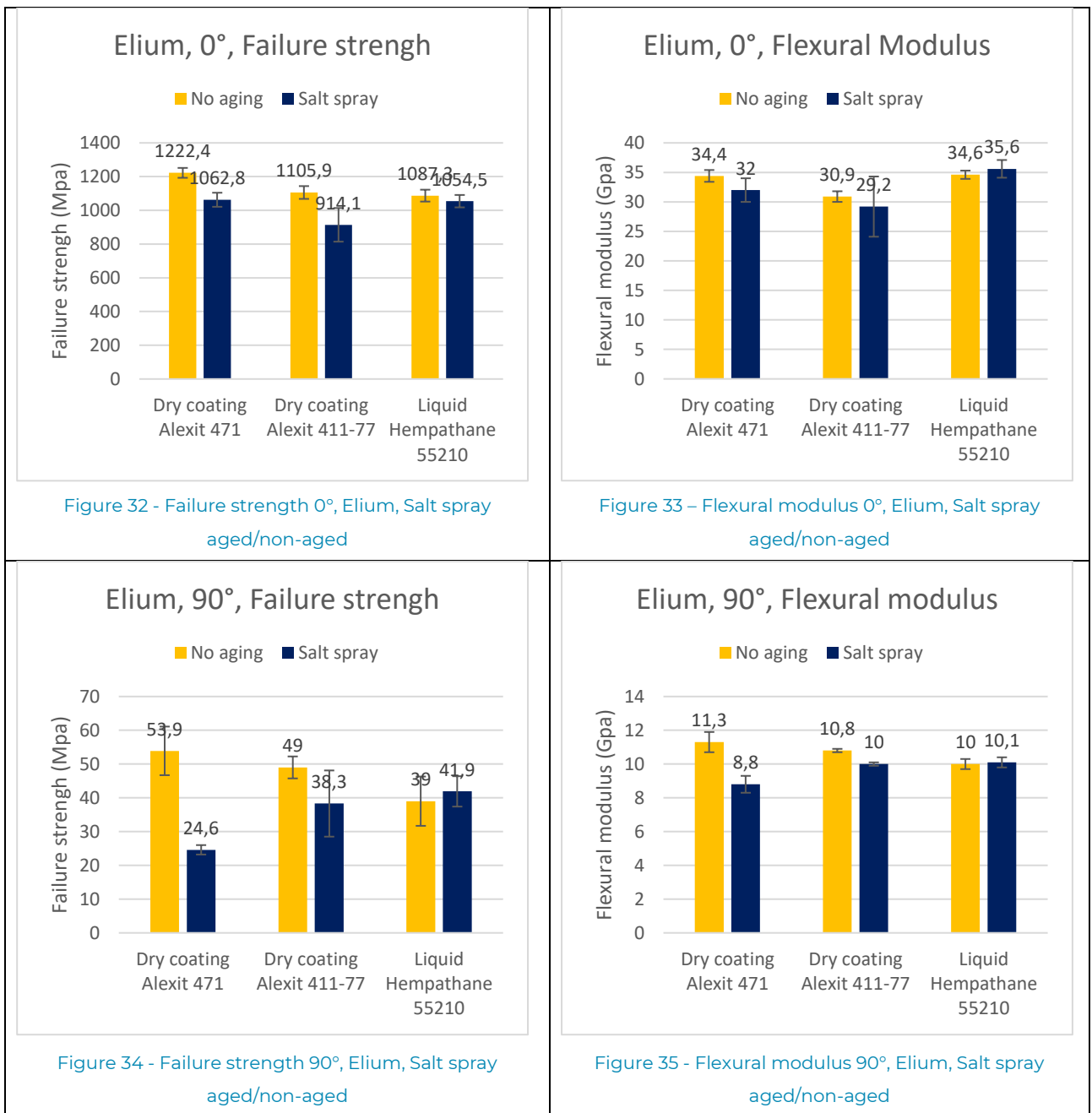
Table 21 – Bending test, Elium, Salt spray aged/non-aged

Elium, Salt spray	0°, failure strengh	0°, flexural modulus	90°, failure strengh	90°, flexural modulus
Dry coating Alexit 471	<*	=	<	<
Dry coating Alexit 411-77	<	=	=	<
Liquid paint Hempathane 55210	=	=	=	=

Table 22 -Comparison response, Elium, Salt spray aged/non-aged

*the aged coating sample response on this parameter is ... than the non-aged coating sample response

The response is similar to the UV. The dry coating Hempathane 55210 and Alexit 471 didn't protect the composite materials against the artificial corrosion atmosphere as all parameters had lower values compared to non-aged coupons.

What is more, none of the coatings dry or liquid have been efficient to protect Infugreen for the 90° failure strength as the lost in performance is about 40% (Figure 30).

For this exposure, none of the coatings protected well the composite resin Infugreen. For Elium, only the liquid paint permits to maintain all the mechanical properties after aging.

Against corrosion, Infugreen seems to be sensitive to it and none of the selected coatings succeed to protect it whereas liquid paint Hempathane 55210 seems to be a good candidate to protect the acrylic resin Elium.

2.1.4. Conclusion

Even though the coating appears negligeable in a laminate composite because of its thickness (compared to the fibres for example), this study showed that coatings have an impact on the mechanical properties on the composite. This impact depends of the type of coating: dry or liquid and on the composite type. However, it cannot be said that the addition of the coating increase or decrease the mechanical of the properties.

The protection brought by a coating, which can be in its liquid or dry coating form depends on the chosen reference and its composition.

Taking into account, both aging exposure (UV and corrosion by salt spray), the liquid paint Hempathane 55210 appears to be the best candidate to protect Elium and Infugreen against UV and a corrosive atmosphere. The fact that a primer was used in the painting process may explained this. However, this solution is not 100% suitable as a lack of performance was observed comparing the salt pray aged coupons to the non-aged one.

However, the interpretation of the results has to be put in parallel with the shape of the response curve as sometimes bilinear responses are obtained. This phenomenon, meaning a change in the composite behaviour, can be accepted depending of the requirements. What is more, the result are very dependant to the thickness of the samples (see equations), so a minor difference in the thickness can apply a bigger difference in the mechanical response.

2.2. Durability and protection of the coating against real sea environment

To have a better representation of the coating performance in real life, middle scale tests are done after the tests done at a laboratory scale (D.2.3). The aim of this study is to evaluate the behaviour of the coating, especially to compare dry coating with liquid paint, in a real environment. To evaluate this, coated samples will be exposed in a marine environment to access the durability against the weather and a corrosive environment. Other samples are immersed in the sea water to see the performance of the coating and its texture to resistance to fouling.

The exposition duration was fixed for 9 months: from July 2022 to April 2023 to cover one summer and one winter period which are the most severe conditions.

2.2.1. Sample description

To respond to the objectives described before, the following matrix is done.

Test	Coating				
	Dry coating			Liquid	
	Hempathane 55210				Protis
	Reference	Texture 1: Sharklet	Texture 2: High smooth	Reference	Antifouling paint
9 months Real sea immersion	3	3	3	3	3
9 months Emerged weathering exposition	3	/	/	3	/

Table 23 – Sample matrix for real sea environment

For the immersion, 5 types of samples are created. 3 of them are produced with the same dry coating Hempathane 55210 but with 3 different textures. 2 of the samples are painted with liquid paint: the liquid Hempathane 52210 and an antifouling black paint.

Because of the toxicity of the traditional liquid antifouling paint and the difficult to use the fouling release paints, the technology of the dry coating is investigated to have a paint system resistant to fouling. Thiis can be practicable as the surface of the dry coating can be controlled. Indeed, textures can be created at the surface of the dry coating. Two interesting textures have been found on the D2.3 "Environmental protection of composites" which are:

- The Sharklet texture: this patented texture is used for antimicrobial growth. [3]
- Have a very smooth surface, so a low surface energy to prevent fouling.

As the presence of the texture and an antifouling paint are only necessary for the assessment of the fouling, none of those will be evaluate for the emerged weathering exposition.

Manufacturing of the samples

Ixblue manufactured the samples with the following parameters: laminates were infused with and without and dry coating.

Resin	Infugreen 810
Curing agent	SD8824
Ratio	100/22
Thickness	~5mm
Fabric	Glass Fibre - H2026 - U-E-1182g/m²-1270mm
Lay up	[0]2s (4 Layers)
Curing temperature	Ambient
Curing time	24h

Table 24 – Manufacturing parameters

After the infusion, the samples infused without dry coating were painted with the reference paint Hempathane 55210 and an antifouling paint with the next schema.

Layer	Paint	Thickness	Application method	Drying
1: Primer	Hempadur 15579	~150 µm	Roller	24hours
2: Topcoat	Hempathane 55210	~50 µm	Roller	24 hours

Table 25 – Paint layers for liquid Hempathane 55210

Layer	Paint	Thickness	Application method	Drying
1: Primer	Epoxyguard IM409	~450 µm	Roller	24hours
2: Undercoat	Undercoat 215+	~100 µm	Roller	24 hours
3: Antifouling	Protis	~150 µm	Roller	24 hours

Table 26 – Paint layers for liquid antifouling paint

The resin Infugreen was chosen because it will be used for the demonstrator, it is important to keep the most parameters identical when doing preliminary tests. The paint Hempathane was chosen to be transform into dry coating as it was already tested in D2.3 "Environmental protection of composites" and because it is the paint used in the metal structure W2Power.

Examples of the samples are shown below.

Coating				
Dry coating			Liquid	
Hempathane 55210				Protis
Reference	Texture 1: Sharklet	Texture 2: High smooth	Reference	Antifouling paint
Figure 36 – Dry coating Hempathane 55210 sample	Figure 37 – Dry coating Hempathane 55210 – Texture Sharklet sample	Figure 38 – Dry coating Hempathane 55210 – Texture high smooth sample	Figure 39 – Liquid Hempathane 55210 sample	Figure 40 – Liquid antifouling paint sample

Table 27 – Samples for real sea environment after painting (dry coating or liquid)

2.2.2. Evaluation of the dry coating protection against real weathering exposition

To evaluate the impact of the environment on the coating, the following inspection will be performed:

- The visual aspect of the coating (degree of blistering or presence of delamination of the coating)
- Gloss measurement
- Colour measurement
- Resistance to water absorption after the exposition.

2.2.2.1. Weathering exposition principle

The samples are exposed to a marine environment. They are held on exposure frame at 0.75m above the water level and with an angle of 45° to the horizontal plane to fulfil the requirements of ISO 8565. The frame is located so that test objects are neither protected nor shaded by nearby objects and that no water runs off.

The conditions that the coating will meet are: rain, ultraviolet rays of the sun, high humidity, freeze, hail, impact, high salinity. This environment was already simulated at a laboratory scale in D2.3 "Environmental protection of composites". In this real condition test, the resistance of the coating is evaluated in a more complex way.

The samples are inspected after 1, 3, 6 and 9 months in order to evaluate:

- The gloss evolution
- The colour evolution
- The degree of blistering
- The degree of chalking
- The degree of delamination (around a scribe).

The exposure began the 11th of July.

As a reminder, only Hempathane 55210 dry coating and Hempathane 55210 liquid paint will be compared.

2.2.2.2.   Impact on the adhesion

2.2.2.2.1.   General visual aspect

At each inspection, the samples, dry coated or liquid coated, show:

- No blistering
- No chalking (by using tape method)
- No delamination around the scribe done at the beginning of the exposure.

In the next table, a comparison between before and after exposure is made. Small comment on the difference of colours on the pictures (they seem different due to difference of ambient light and the lack of use of a colour box). The evolution of colour will be assessed with a spectro colorimeter.
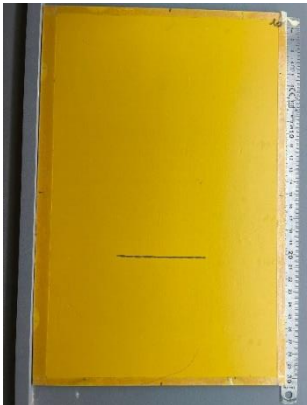
Hempathane 55210 Coating form	Before exposure	After 9 months exposure
Dry coating	Figure 41 – Dry coating Hempathane 55210 before exposure	Figure 42 – Dry coating Hempathane 55210 after 9 months exposure
Liquid	Figure 43 – Liquid Hempathane 55210 before exposure	Figure 44 – Liquid Hempathane 55210 after 9 months exposure

Table 28 – Comparison of the coating dry and liquid before and after weathering exposition

In general, the Hempathane 55210 dry coating is aging the same as the liquid paint

2.2.2.2.2. Adhesion evaluation description

The adhesin can be evaluated through a pull off test. It is based on the standard ISO 4624:2016 Paints and varnishes — Pull-off test for adhesion.

The pull-off test consists of measuring the tensile stress necessary to break the weakest interface of the sample. It is a qualitative test by the detection of the weakest interface but also a quantitative test by the quantification of the tensile stress needed to break this interface.

To achieve this, a dolly is glued to the coating surface. After curing of the adhesive, an instrument pulls the dolly and measure the strength to break the interface between the coating and the substrate. To do that, the choice of the adhesive is important. Indeed, the adhesion between the adhesive and the dolly and the adhesive and the coating surface must be higher than the adhesion at the interface which is evaluated (mostly the interface coating/substrate).

The mains steps to perform the test are:

- Sand the dolly and the coating to activate both surfaces. Then dust and degrease.

- Glue the dolly to the surface (apply a homogenous thickness of glue on the dolly and remove any excess). Let it cured according to technical data sheet information.

Figure 45 – Pull-off preparation

- Pull the dolly with the dedicated instrument, report the force value and analyse the weakest interface.
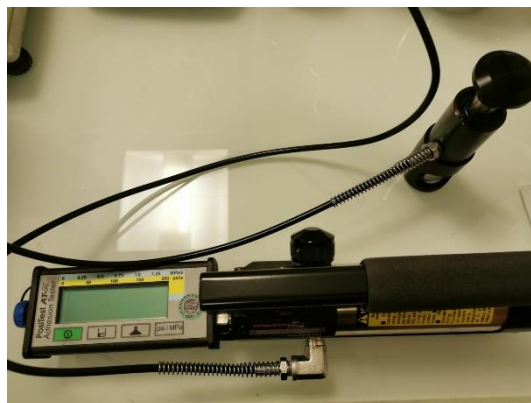
Figure 46 – Example of pull-off instrument
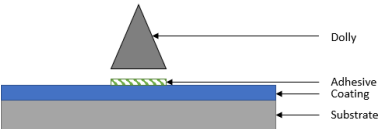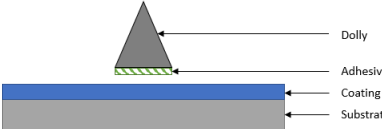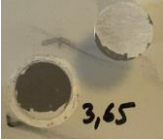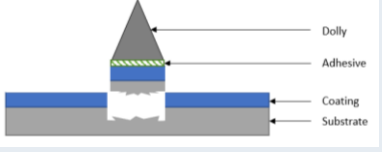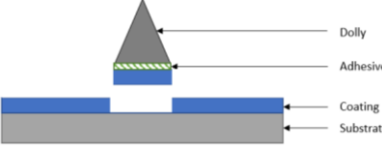
For analysing of the results (value and interface), three terms are defined:

- Esubstrate = Substrate cohesion energy

- Einterface = Adhesion energy between the coating and the substrate
- Ecoating = Coating cohesion energy

Keeping in mind that the interface coating/substrate Einterface is to evaluate, several cases can occur, each one will be described below.

The interface adhesion performance can be classified as: case 2 > case 4 > case 3, where case 2 is the best scenario.

Cases	Weakest interface	Illustration	Visual	Interpretation
1	At both interfaces of the adhesive used for gluing the dolly: Dolly/ Adhesive Adhesive/ Coating	Figure 47 – Adhesive/Dolly failure Figure 48 – Adhesive/Coating failure	Figure 49 – Dolly/Adhesive failure example Figure 50 – Adhesive/Coating failure example	1. Wrong adhesive choice: adhesive/dolly or adhesive/coating adhesion lower than Einterface. 2. Lack in test preparation: not enough amount of adhesive or not enough activation by sanding. → Repeat the test by solving issues below or →Einterface> adhesive/dolly or adhesive/coating adhesion.
2	Inside the substrate	Figure 51 – Inside the substrate failure	Figure 52 – Inside the substrate failure example	Einterface>Esubtrate and Ecoating>Esubstrate → This can be read as the best result: the adhesion coating/substrate is higher than the substrate cohesion so the coating performed well in terms of adhesion and cohesion
3	Coating/su bstrate	Figure 53 – Coating/Substrate failure	Figure 54 – Coating/Substra te failure example	Einterface<Esubtrate Einterface<Ecoating Good adhesive choice and test preparation. → Values obtained by the instruments are representative of the interface examined. → Poor adhesion on the substrate.
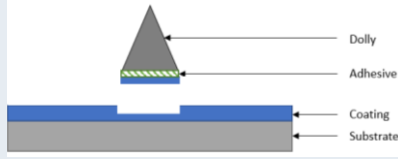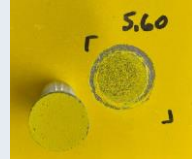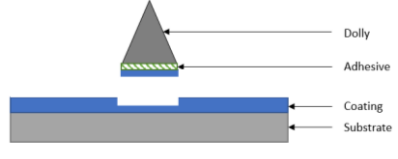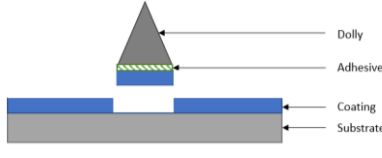
4	Between coating layers (if relevant)	 Figure 55 – Between coating layers failure	 Figure 56 – Between coating layers failure example	$E_{interface} > E_{coating}$ $E_{subtrate} > E_{coating}$ → Cohesion of coating can be improved.

Table 29 – Pull-off result interpretation

2.2.2.2.3. Results

The characterisation at coupon level done in D2.3 "Environmental protection of composites" showed by the next results of adhesion of both liquid and dry coating that dry coating adheres better that liquid paint.

Coating	Adhesion by pull off (MPa)	Weakest interface	Pictures
Dry coating Hempathane 55210	3.98 +/- 1.15	Between coating layers Figure 55 – Between coating layers failure	 Figure 57 – Dry coating Hempathane 55210/Infugreen pull-off result
Liquid paint Hempathane 55210	5.59 +/- 0.13	Coating (primer)/substrate Figure 53 – Coating/Substrate failure	 Figure 58 – Liquid paint Hempathane 55210/Infugreen pull-off result

To see if dry coating adheres better than liquid paint, pull off are performed on the aged coupons, the results are shown in the next table.
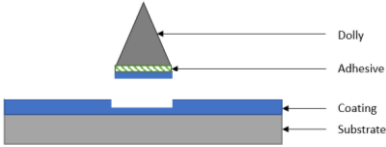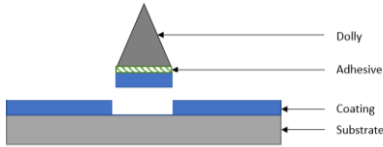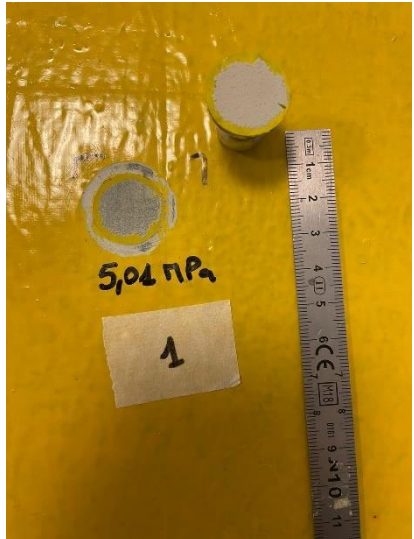
Coating	Adhesion by pull off (MPa) after exposition	Weakest interface	Pictures
Dry coating Hempathane 55210	4.52 +/- 0.86	Between coating layers Figure 55 – Between coating layers failure	 Figure 59 – Dry coating failure after weathering exposition
Liquid paint Hempathane 55210	4.79 +/- 0.24	Coating (primer)/substrate Figure 53 – Coating/Substrate failure	 Figure 60 – Liquid paint failure after weathering exposition

Table 30 – Pull off results after 9 months weathering exposition

The adhesion level and failure of the coating after exposition are at the same level as before. The liquid paint breaks at the interface between the coating and the substrate: it is the lowest interface of the system. This interface substrate/coating when the dry coating is used, is stronger as the failure occurred in the paint layers.

Taking into account the failure response, the dry coating adheres better than liquid paint on composite. Moreover, both coatings behave he same in terms of adhesion: the exposition to weathering conditions did not damage this property.

2.2.2.3.   Impact on the colour

2.2.2.3.1.   Colour evaluation description (ISO 7724-3)

The colorimetry is science and techniques allowing to define and measure colour and colour difference. In the system called CIE L*a*b*, one colour can be defined with three parameters: L, a, and b corresponding to point coordinates belonging to colour space. "L" represents the lightness, "a" a position between red and green, "b" a position between yellow and blue. This can be illustrated as follow. [4-5]
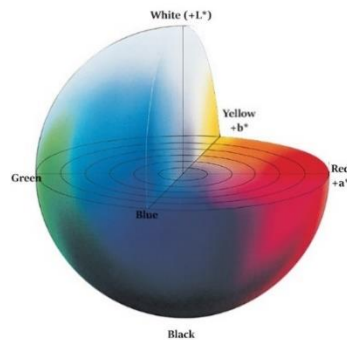
Figure 61 – CIE L*a*b* colour space

In practical, the material used to measure the value is called a spectro-colorimeter. Its operating mode is described in the next figure.
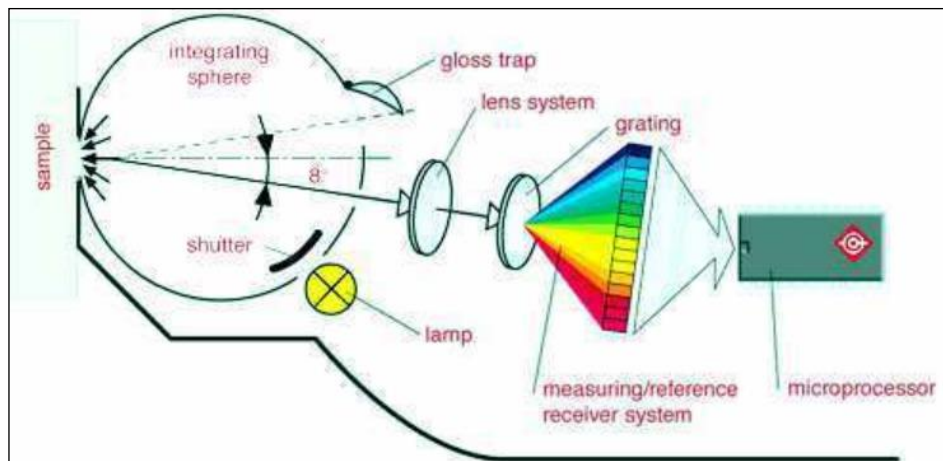
Figure 62 – Spectro-colorimeter principle

When working on the difference between two colours (colour (1) and colour (2)), the following calculation is made:

$$\Delta E = \sqrt{\left(L(2) - L(1)\right)^2 + \left(a(2) - a(1)\right)^2 + \left(b(2) - b(1)\right)^2}$$

It is commonly considered that a ΔE<1 means that the difference between two colours cannot be seen by human eyes. This statement will be selected in this project to evaluate colour changing after aging.

2.2.2.3.2. Results

In the next figure, it can be seen that both dry coating and liquid colour evolved during the exposure. The dry coating follow the line evolution of the liquid paint.

Colour evolution during a 9 months weathering exposition
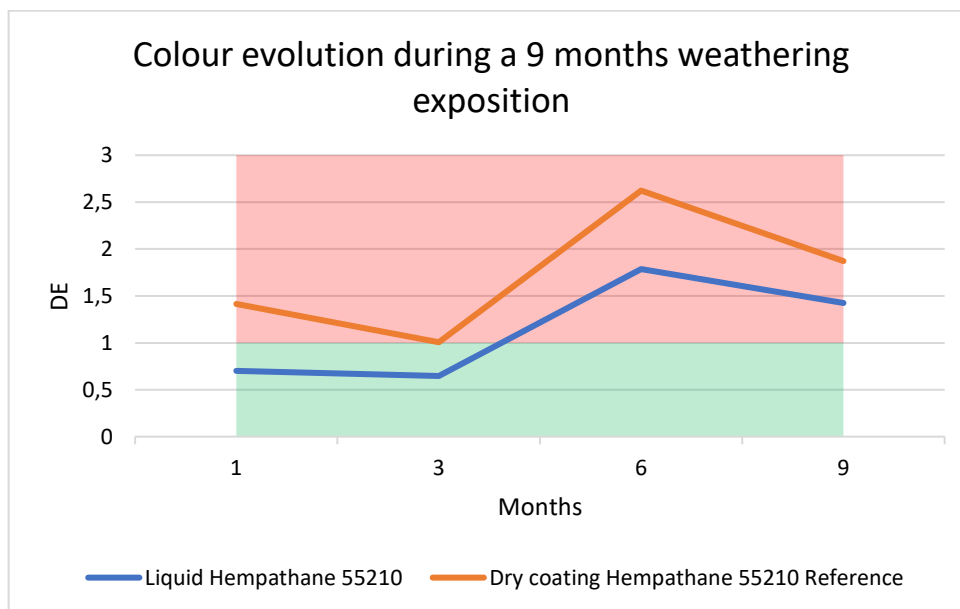
Figure 63 – Colour evolution of coatings during 9 months of weathering exposition

In conclusion, the dry coating performs as well as the liquid paint in colour.

2.2.2.4. Impact on the gloss

2.2.2.4.1. Gloss evaluation description (ISO 2813)

The gloss of a coating is its property to reflect the light. Coatings are classified in three categories: high, semi or low gloss surfaces.

To evaluate this parameter, gloss meters are used. A light source illuminates the coating with a specific angle: 20°, 60°, 85° for respectively high, semi and low gloss (when there is no specification, 60° is used). Then the quantity of light reflected by the coating is measured and transformed into a gloss value between 0 (for low gloss) and 100 (for high gloss) GU (gloss unit) as illustrated below.
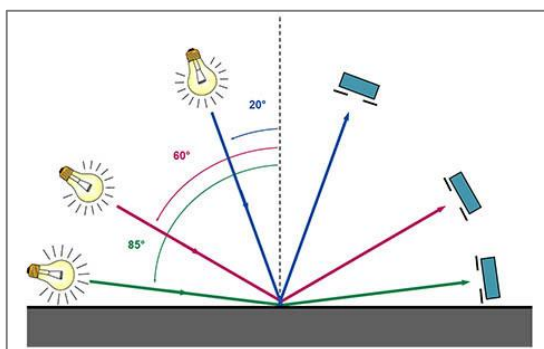
Figure 64 : Gloss measurement principle

2.2.2.4.2.

Results

In the next figure, it can be seen that both dry coating and liquid paint gloss evolved during the exposure. However, the gloss of the dry coating in time is more stable.
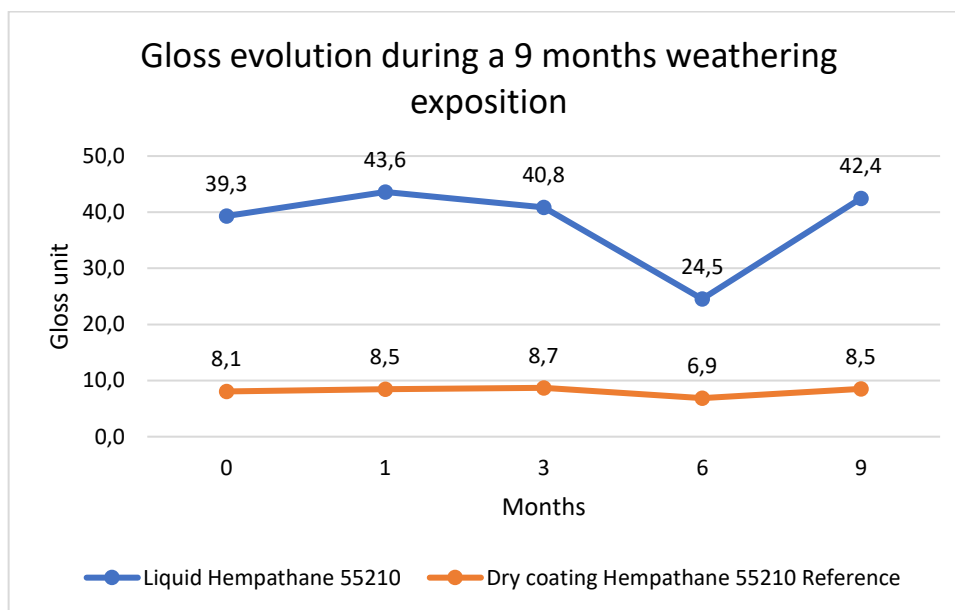
Figure 65 – Gloss evolution of coatings during 9 months of weathering exposition

In terms of gloss evaluation, a paint transforms into dry coating have a better stability than the same paint applied by liquid process.

2.2.2.5.   Protection against water uptake

2.2.2.5.1.   Evaluation of the water absorption

This evaluation permits to know if the material is sensitive to water. The percentage of water absorbed by the material is obtained by the measure of the mass before (m(before)) and after (m(after)) exposure and it is calculated with:

$$\% \; mass \; evolution = \frac{m(after) - m(before)}{m(before)} * 100$$

In this study, this calculation will permit to access if the coating protected well the composite substrate by creating a barrier to the water (humidity, rain).

2.2.2.5.2.   Results

The mass evolution is about 0.2% for both coating type: liquid and dry coating. The mass increase is inferior to 1% so the coating protected well the composite.

Dry coating protected the composite against water as well as liquid paint.

![FIBREGY]

This project has received funding from the European Union's Horizon 2020 research and innovation programme under grant agreement No 952966.

2.2.2.6.

Conclusion

The paint that has been transform into dry coating behaves the same as liquid paint in terms of general aging, colour evolution, gloss evolution and mass evolution. However, dry coating adheres better to the composite even after exposure to severe environmental conditions.

2.2.3. Evaluation of the dry coating and its texture against real sea immersion

2.2.3.1. Real sea immersion principle

2.2.3.2. Durability of the dry coating against fouling resistance

If the behaviour of the coating is important to follow above the water line, its performance in the water is also significant. Samples, different by their texture, their coating type (standard or antifouling) and their coating form (liquid or dry) are immersed in the sea water. The aim is to determine if dry coating with controlled texture is able to resist to fouling (phenomenon only under the sea).

The painted samples are mounted onto an aluminium frame. In this frame, the panels are distributed to minimise effect of exposure at different depth of immersion on the results.

The samples are inspected after 1, 3, 6 and 9 months in order to evaluate the general aspect and the fouling resistance.

The exposure began the 11th of July.
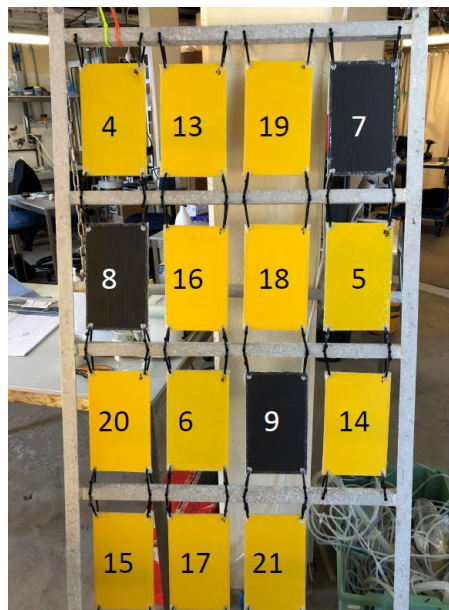
Figure 66 – Samples for real sea immersion on the frame before the launch*

*:

4-5-6: Liquid Hempathane 55210

7-8-9: Liquid Antifouling paint (black)

13-14-15: Dry coating Hempathane 55210 Reference

16-17-18: Dry coating Hempathane 55210 Texture 1 Sharklet

19-20-21: Dry coating Hempathane 55210 Texture 2 High Smooth

![FIBREGY]

This project has received funding from the European Union's Horizon 2020 research and innovation programme under grant agreement No 952966.

2.2.3.2.1.

Antifouling resistance evaluation

The methodology to evaluate the fouling resistance of a material by visual inspection is by:

- Determinate the presence of specific type of microorganisms: slide, algae, tubeworms, barnacle and Bryozoa.
- Evaluate their quantity using a scale where 0 represent the absence of the organism and 4 for a severe presence.

From this, a weighted average called damage can be calculated depending on the impact of each organism.

2.2.3.2.2.   Results

The following figures represented the calculated damage by each type of coating. After, pictures at each inspection are shown.
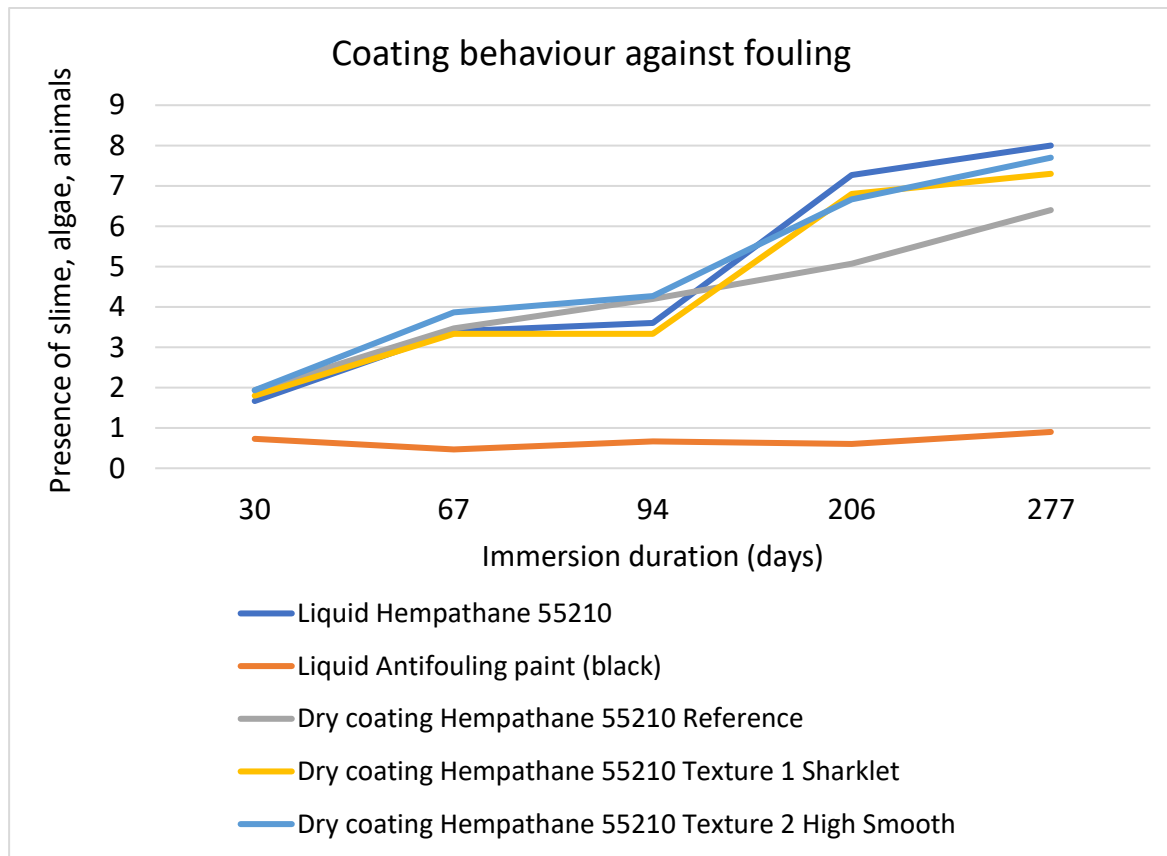
Figure 67 – Coatings behaviour against fouling during 9 months of immersion

Duration	30 days	94 days
Pictures	Figure 68 – Samples after 30 days of immersion	Figure 69 – Samples after 94 days of immersion
Duration	208 days	277 days
Pictures	Figure 70 – Samples after 208 days of immersion	Figure 71 – Samples after 277 days of immersion

Table 31 – Overview of the characterisation of the samples at each inspection

The damage graph representing the presence of microorganism on the coating and the pictures demonstrate that the coating Hempathane 55210 cannot act as the fouling coating whatever its way of application or texture.

2.2.3.3. Durability of the dry coating against water uptake

As the presence of the fouling is very important, the mass that must be measured will be the reflect of the mass of the microorganisms and not the water that can be in the material. For that reason, the parameters is no longer something interesting to follow.

2.2.3.4. Conclusion

As expected, a standard/non-antifouling liquid paint, like Hempathane 55210, does not an action against fouling. The dry coating using the same paint and with a regular texture does not act as an antifouling either. For the textured dry coatings, smooth or rough, do not prevent the microorganism to hang to the coating. This study does not validate the use of textured dry coatings in replacement of traditional antifouling paint.

2.2.4. Conclusion on the exposition to the real sea environment

On the one hand, when above the sea, dry coating behaves as liquid paint. The results have confirmed the trials done in D2.3 "Environmental protection of composites". The manufacturing by infusion with the dry coating at the bottom of the mould does not have an impact on the protection performance of the coating. The advantages offer by the technology is saving time on the manufacturing process and permit to have a better adhesion to the composite substrate. This can be possible by   a mechanic and chemical anchoring between the resin (which is curing) and the glass fibres back of the dry coating. This allows a good durability of the coating.

On the other hand, under the sea, the technology of the dry coating and the fact that a texture can be applied on it not allow a resistance to fouling.

In other words, the dry coating shall be use for not immersed part.

2.3. Incorporation of monitoring sensors at the backing of the dry coating

To follow the integration of the composite parts in the existing W2Power structure, the case of the sensors already embedded at the backing of the dry coating was studied in the framework of the deliverable D2.5 "Multifunctional materials for Structural Health Monitoring (SHM) Diagnosis and Structural Performance Assessment".

Accelerometers and strain gauges were selected. However, because of thickness constraint, they could not be integrated directly at the backing of the dry coating. Indeed, the dry coating has a maximum thickness of 500 μm so it can only tolerate sensors less thick and the selected sensors had a minimum thickness of 3 mm. The solution founded at this stage was to put the sensors at the interface between the composite and the dry coating.

To go further with this work, the opportunity to evaluate two other types of sensors, that complied with the thickness criteria, appears: RFID sensor (tag) and optical fibres. For each sensor, the feasibility of manufacturing dry coatings integrating them will be carried out. A particular attention will also be done on the workability of the sensor after its integration.

2.3.1. Identification of new sensor type and feasibility

2.3.1.1. RFID sensors

RFID means Radio-Frequency IDentification. It uses electromagnetic fields and it is widely used in the retail industry to perform inventories. Three elements compose this system of transmission and reception of waves: a transponder, a receiver and a transmitter.

The RFID sensor, called also RFID tag acts as the receiver and the transmitter of the signal. It is composed of a microchip, an antenna and a substrate as follow:
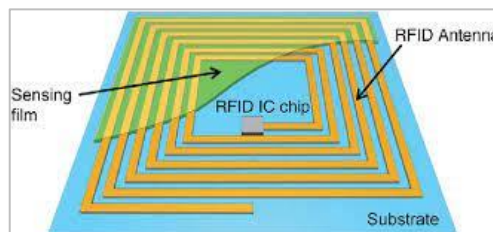
Figure 72 – RFID tag composition

New improvement specific to the chip permits not only to identify tags but also collect data sush as temperature, humidity, strain, etc. This technology can be interesting in the tracking of the behaviour of the composite in the W2Power structure.

Dry coating manufacturing

The sample of rfid sensor that will be tested has the following characteristics:

Dimensions	Substrate	Chip
Length (mm)	85	4
Width (mm)	35	4
Thickness (mm)	0.07	0.35

Table 32 – Dimensions of the RFID tag

The following sample of dry coating with embedded tag was produced.

Figure 73 – Dry coating with RFID sensor, paint side

Figure 74 – Dry coating with RFID sensor, back side

The tag is visible from the paint or the back side. Seeing it from the paint side can be useful to identify its location and make easier its detection when collecting data is necessary.

Detection of the sensor

To detect the tag, readers are used: they send a signal, if the sensor is operational, it sends back a signal to the reader.

In our case, a reader from the brand Denso was employed and the tag responds: it was detected. The process of embedding the RFID sensor at the backing of the dry coating did not damage it.

2.3.1.2.   Optical fibre

Optical fibres are flexible, in general transparent, fibres composed of glass or plastic. They are widely used in communication to transmit data by the transmission of light. It is also used as sensors to obtain information about the strain, temperature and/or pressure of a system.

Due to their very thin thickness, it appears as a good candidate for a sensor that can be embedded at the backing of the dry coating.

2 samples of optical fibres were provided by TSI. Their characteristics are presented in the next table.

Nature	Colour	Thickness
Acrylic	Transparent	250 µm
Polyamide	Yellow	130 – 135 µm

Table 33 – Optical fibre characteristics

Dry coating manufacturing

One important criterion has to be respected when working with optical fibre: leave about 20 cm out of the coating to permit to connect materials to collect the data.

The following samples of dry coating with embedded optical fibre were produced.
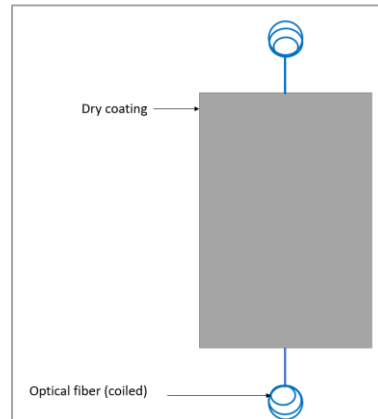
Figure 75 – Dry coating with embedded optical fibre, schema

Figure 76 – Dry coating with acrylic optical fibre, paint side

Figure 77 – Dry coating with acrylic optical fibre, back side

Figure 78 – Dry coating with polyamide optical fibre, paint side

Figure 79 – Dry coating with polyamide optical fibre, back side

Both optical fibres integrate well in the dry coating. From the paint (front) side, no demarcation line is observed. From the back point of view, the optical fibre is visible but this can be solved by the fact that this side will not be exposed as it will be the side inside the composite piece.

Detection of the sensor

Acrylic Fibre Optic Sensors (FOS): The sample is difficult to manipulate. Therefore, the FOS can be easily broken during the transportation & measurements. This can be explained by the fact that this FOS is delivered without a protection on it. As a conclusion, it can be said that this type of embedding process is not recommended for further work.

Polyamide FOS: In this case the FOS have a protection, the sample is easy to manipulate. The light (red) went through the fibre optic fibres easily, which is an indicator that the sensor operates correctly. Pictures described this are showed below. As a conclusion, it is noticed this type of embedding process is a good technical solution for further work.
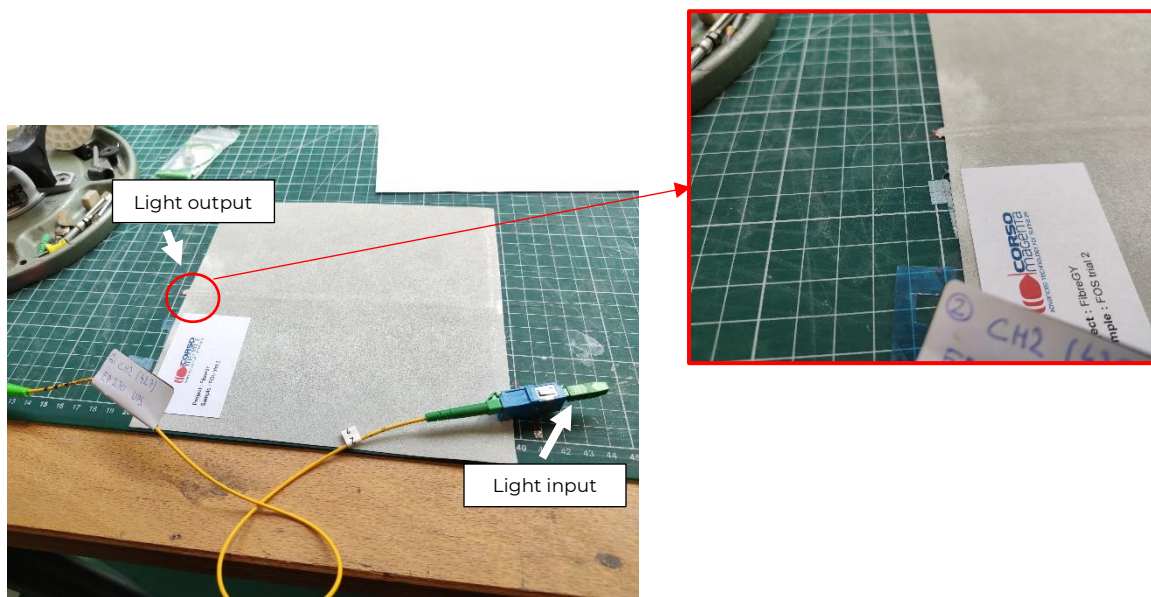
Figure 80 – Workability of the embedded FOS

2.3.2. Conclusion

Different types of sensors can be integrated at the backing of the dry coating. However, the choice of the sensors depends of its thickness and its sensitivity. Thickness under 500 µm cannot be embedding at the backing of the dry coating, as it is approximately the average thickness of the dry coating.

With an adapted sensor, such as the RFID tag or a thin protected optical fibre, this technology offers the advantage of eliminate two steps of the production: the first one is the paint step (which implies in general several coats and many hours of drying) and the second one is the installation of the sensors after the production.

However, the following aspects have to be validated for the final application:

- The infusion process shall not damage the sensor. Indeed, the pression when vacuuming or the curing temperature may have an impact on the sensor.

- The responses given by the sensor in service is representative to the behaviour of the composite material.
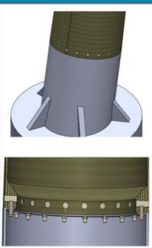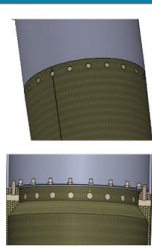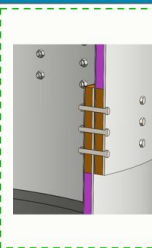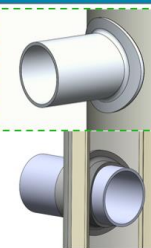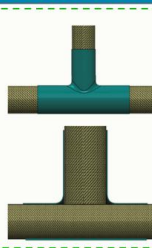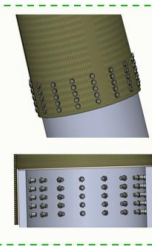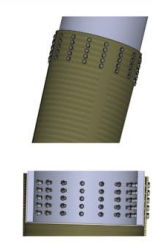
3. MIDDLE SCALE TEST ON CONNECTIONS

3.1. Evaluation of connection at subcomponent level

3.1.1. Subcomponent definition

The first step was to define which subcomponent (connection) will be tested under fatigue loadings. From the previous connections developed in WP2, the main ones are highlighted in Table 34.

Table 34 – Main connections developed in WP2

	Tower to Column	Tower to Nacelle	Tower to Tower	Tube to Column	Tube to Tube
Real Scale (1:1)					
Prototype (1:6)			N/A	N/A	N/A

From discussion with the task partners, it was decided that the ones marked with a green dashed rectangle are among the most interesting to test. This is due to their importance to the prototype to be built, or due to their novel nature, having little information from other similar structures (often inexistent) increasing the difficulty to validate them without physical testing. Hence, some possible geometries and types of loadings for the corresponding subcomponent, including its setup, were drafted or modelled (Figure 81).
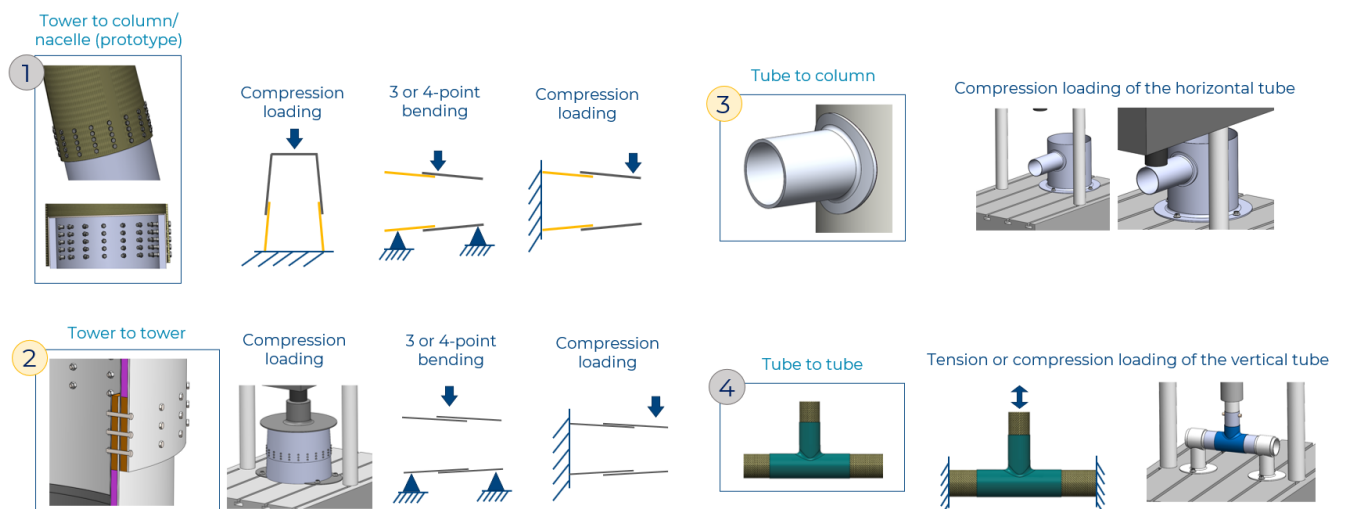
Figure 81 – Possible testing setups

Considering the points above and the concern regarding the peeling stresses on the bonded tube-to-column connection, the first idea was to choose it as the subcomponent to test. However, when idealizing

the testing setup, it was found that due to the axial misalignment of the column with the action/reaction forces applied to the tube, the actuator of the testing machine would likely bend thus permanently damaging it (Figure 82). An alternative setup was thought (Figure 83), but that would be a complex and expensive setup, plus very difficult to control as it is not possible to ensure that the same load is applied to both tubes, and the test would have to be stopped immediately after the failure of the first one to avoid bending the actuator's shaft. Furthermore, the geometry of the column would be very difficult to replicate at this scale due to their grid design (Figure 84).
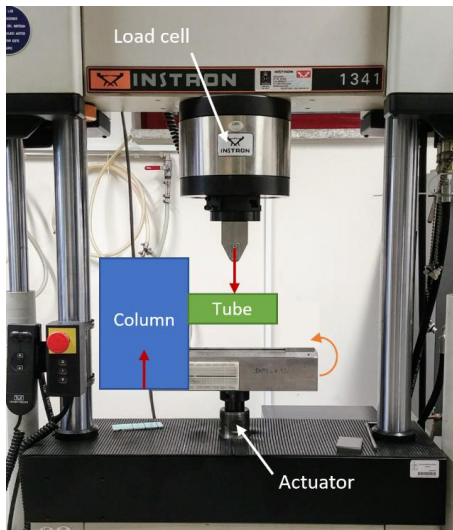
Figure 82 – Possible setup for testing the tube-to-column connection
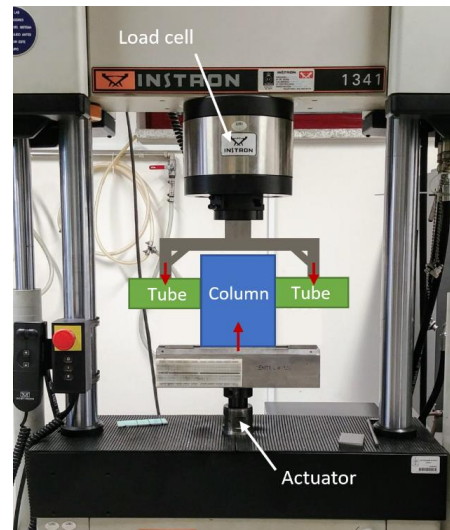
Figure 83 – Possible alternative setup for testing the tube-to-column connection
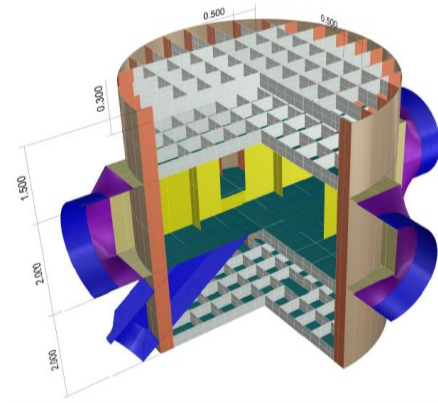
Figure 84 – Designed column using an internal grid structure

Since the testing of the tube-to-column was found to be unfeasible, it was decided to test tower-to-tower connection, which is also quite similar to the tower-to-column at the prototype scale. It will consist of two GFRP flanges tubes bolted together with 3 rows of 16 M3 bolts (48 bolts in total). Two metal sleeves will be placed on the inside and outside, having the double purpose of acting as a template for drilling the holes in the composite (sleeves will be drilled during their manufacturing) and as "washers" to avoid damaging the composite (i.e., causing delamination) when tightening the bolts with the final torque.

With IXBLUE's input regarding the manufacturability of these flanges tubes, it was decided to use the following OTS flanges [14]:

- ROTEC TFS-100-300(3);
- ROTEC TFS-125-300(3).

Figure 85 – ROTEC flange at IXBLUE's premisses

These flanges were then overlaminated by IXBLUE using multiaxial fibreglass fabric infused with the Infugreen 810 epoxy resin (the same used in the WP2 static and fatigue tests) to meet the desired thickness, assuring that the gap between flanges is of 0.5±0.5 mm.

The sleeves (Figure 87) were built in 304 stainless steel, calendered and with laser-cut ⌀3,5 mm holes. IXBLUE has performed the manual drilling of the GFRP tubes through the holes of the sleeves. The holes made in the GFRP tubes can be seen in Figure 86.

Figure 86 – Drilled GFRP tubes

The bolts used were M3X25 I4017 (D933) A2 stainless steel with hex head, and M3 (DIN 934) hexagon nuts. INEGI has performed the final bolting of the connection using a torque wrench (Figure 88) with controlled torque of 1.3 N/m as per specifications [15]. A detailed cut section of the bolted connection can be found in Figure 87, and an image of the interior in Figure 90.

A drawing of the subcomponent assembly can be found in Figure 91, and the complete technical drawings of the main components can be found in Annex 3.

Figure 87 – Stainless steel sleeves

Figure 88 – "Snap-on" calibrated torque wrench

Figure 89 – Detailed cut-section of the bolted connection

Figure 90 – Interior of the GFRP tubes after bolting
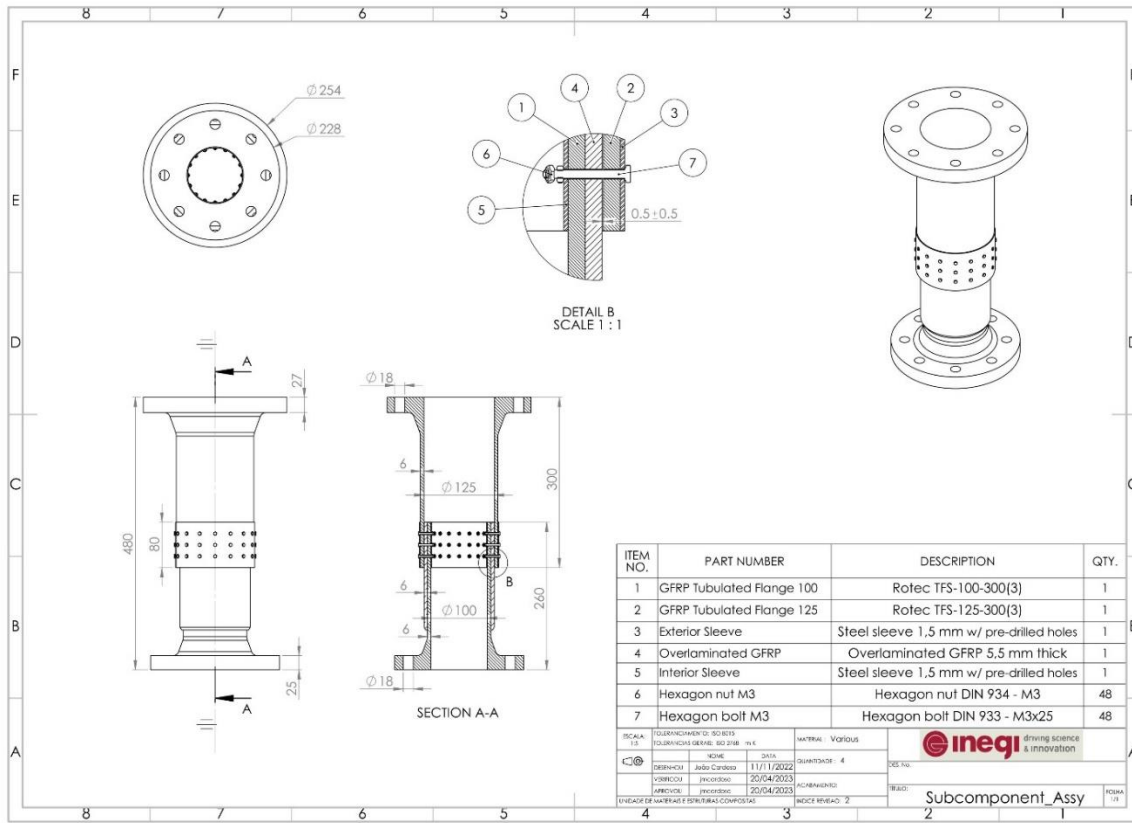
Figure 91 – Technical drawing of the subcomponent

A rendered mockup and a real picture of the finished (bolted) subcomponent can be found in Figure 92 and Figure 93, respectively.

Figure 92 – Rendered mockup of the subcomponent

Figure 93 – Picture of the produced subcomponent

Considering that this connection will be tested under axial loadings, it was necessary to develop a set of fixtures (Figure 94), specifically designed and manufactured by INEGI, that could transmit the loads to the component while being completely rigid. The solution came from designing two plates that can be bolted to the tube's flanges using M8 bolts, and the plates were then attached to forks through ⌀16 mm pins. As illustrated in Figure 95, this configuration for freedom of movement in two planes, thus compensating for axial misalignments that can occur and induce bending in the subcomponent to be tested.

Figure 94 – Set of fixtures
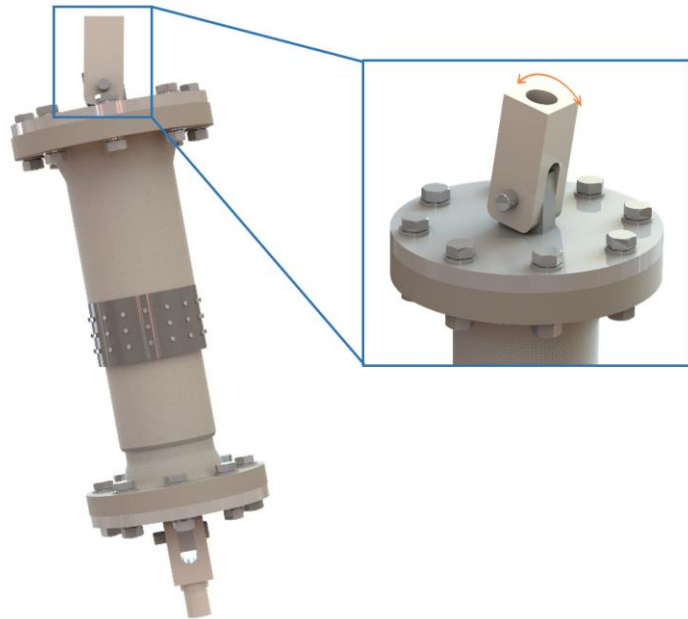
Figure 95 – Representation of the freedom of movement of the fixtures along a plane

The upper part of the setup (Figure 96) has a female clockwise thread to match the male thread of the Instron's load cell, while the bottom part of the setup (Figure 97) has a male counterclockwise thread for attachment with the Instron's main hydraulic shaft.
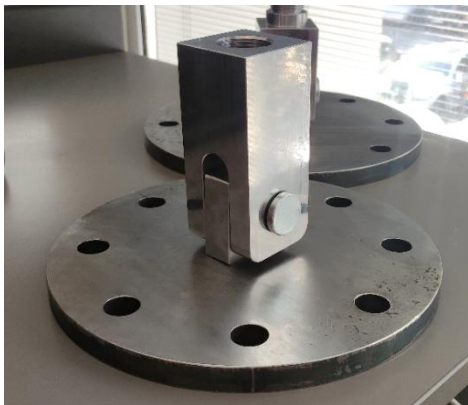
Figure 96 – Upper part of the setup

Figure 97 – Bottom part of the setup

The flanges tubes are then bolted to the steel plates using eight M16X60 hexagon head steel zinc plated Class 8.8 (ISO 4017/ DIN 933) bolts and M16 steel zinc plated hexagon Class 8 (DIN 934) nuts on each side. The clevis pins are 16X65 mm and made of free-cutting steel, zinc plated (ISO 2341 B).

The complete technical drawings of the setup can be found in Annex 3.
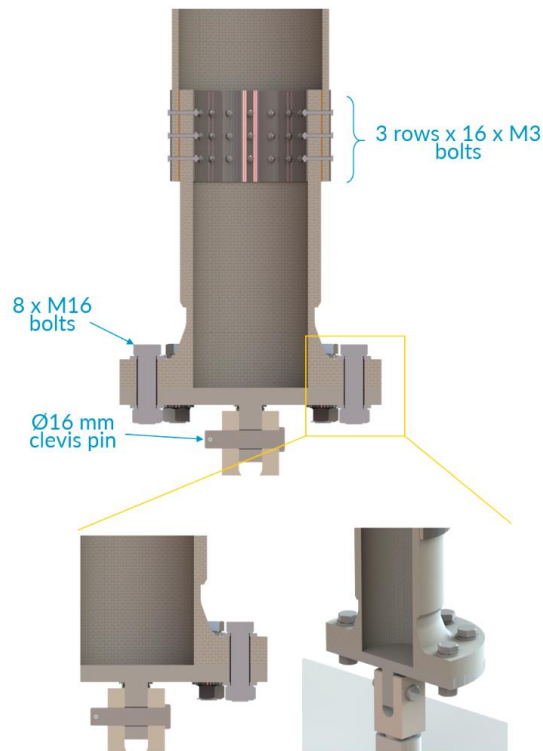
Figure 98 – Attachment of the flanges tubes to the setup plates

3.1.2. Test plan

This subsection will outline the approach to conducting fatigue tests on the selected subcomponent. This test plan has been designed to ensure the reliability, repeatability, and accuracy of the obtained results, while being aware of the limitation of only being able to test, at maximum, four subcomponents. The procedures, testing parameters, and necessary equipment were discussed among task partners, following a preliminary study carried out by INEGI regarding the topic of fatigue in composites, namely in bolted composite joints.

To do so, during the first discussion with the task partners, INEGI identified some of the most relevant guidelines mainly focused on fatigue assessment through a modelling and analysis perspective (Table 35). Most of these guidelines are from BV and DNV, and following them ensures compliance with industry standards and best practices, having a systematic approach to evaluating material and promoting reliability and consistency in results, which will ultimately lead to the development of safer and more durable (fatigue-resistant) structures in offshore applications.

Table 35 – Relevant guidelines for fatigue assessment
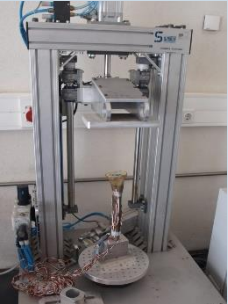
	Guidelines	Certification entity	Main highlights
2.1	**NI611 – Guidelines for Fatigue Assessment of Ships and Offshore Units**	BV	Loads to be considered for fatigue analysis (useful for WP4)
			Stress analysis of bolted connections (useful for WP4)
			Approaches for fatigue assessment
			Basic design S-N curves for steel details
			Factors affecting fatigue strength of steel details
			Fatigue damage calculation and acceptance criteria
			Data statistical treatment
2.2		DNVGL	Overview of hull fatigue analysis

	DNVGL-RP-C206 - Fatigue methodology of offshore ships		Overview of modelling techniques for fatigue analysis
			Load conditions (useful for WP4)
			Hot spot analysis (useful for WP4)
			Hull/turret interface fatigue design
			Fabrication and fatigue
2.3	**DNVGL-RP-C203 - Fatigue design of offshore steel structures**	DNVGL	Fatigue analysis
			Bolts
			Stress concentration factors
2.4	**NR546 - Hull in Composite Materials and Plywood, Material Approval, Design Principles, Construction and Survey**	BV	Fatigue analysis methodology
			Damage accumulation
			Mechanical tests on laminate test panels
2.5	**NI603 – Current and Tidal Turbines**	BV	Design Conditions and Load Cases (useful for WP4)
			Structural Design (useful for WP4)
			Fatigue Analysis
			Bolt Connections
2.6	**DNVGL-ST-0376 - Rotor blades for wind turbines**	DNVGL	Fibre failure and fatigue strength
			Adhesive joints (useful for CORSO)
			Root connections
			Intermediate level testing (sub-component testing)
			Full-scale blade testing
			Fatigue bending tests
			Fatigue data analysis
			Testing of inserts for bolted connections
2.7	**DNVGL-ST-0126 - Support structures for wind turbines**	DNVGL	Site conditions and loads (useful for WP4)
			Fatigue limits
			Design fatigue factors
			Cumulative Damage
			Connections (bolted connections)
2.8	**DNVGL-ST-0361 - Machinery for wind turbines**	DNVGL	Fatigue Strength Analysis
			S/N Curves for metallic materials
			Calculation of synthetic S/N Curves
			Partial Safety Factors
			Bolted Connections
			Dynamic analysis of wind turbine drive trains
			Prototype tests of gearboxes
2.9	**IEC 61400-23 - Wind turbines – Part 23: Full-scale structural testing of rotor blades**	IEC	Static and fatigue load testing
			Test requirements
			Reporting

In order to assist in the decision of the specific fatigue machine to use, a survey was also carried out of the available fatigue testing machines that are available to perform these tests (Table 36).

Table 36 – Most suitable equipment for fatigue testing available to INEGI

Equipment for Fatigue Testing				
Image	Reference	Local	Main Characteristics	Potential of use
	SIFAMA Structure	LET - FEUP	Strain or load controlled Axial forces or bending 10 kN Frequency: not defined	Dependable on the laboratory's availability Need for the development of a clamping device
	MTS 100 kN	LET - FEUP	Axial forces 100 kN Frequency: <15 Hz	Dependable on the laboratory's availability Dimensions limitations
	-	LET - FEUP	Strain controlled 3-Point Bending Max. Frequency: 23 Hz	Dependable on the laboratory's availability Dimensions limitations
	Instron ElectroPuls E10000	INEGI Alentejo	Axial forces Frequency up to 100 Hz ±10 kN (dynamic load) ±7 kN (static load)	Load limitations Dislocation to Évora to perform the tests

	Instron 1341	Universidade da Beira Interior (UBI)	Max. frequency: 20 Hz (recommendable to use only up to 10 Hz) 100 kN (dynamic load) 200 kN (static load)	Dependable on the laboratory's availability
	TESTRESOURCES - 830–E3–AR2M(830)-16-36	Mechanical Engineering Department at Universidade de Aveiro (UA)	Multiaxial dynamic fatigue (axial and torsion) ±8.4 kN Max. frequency: 15 Hz (linear actuator)	Dependable on the laboratory's availability Dislocation to UA to perform the tests
	-	Structures Laboratory – University of Minho (UMinho)	Max. frequency: 2 Hz Displacement of 2 mm	Dependable on the laboratory's availability Specimens up to 5 m (versatile portico)
	-	LEM - Instituto Superior Técnico de Lisboa	2 VHCF equipments Servohydraulics with a load capacity up to 250 kN Max. frequency: 20 to 50 Hz	Dependable on the laboratory's availability
	-	Element Seville	Maximum load: 4 MN Frequency: ≥10 Hz	Performs fatigue tests on composite materials at subcomponent level Can perform setup design and manufacturing; testing reports.
	-	ISQ (Instituto de Soldadura e Qualidade)	-	Performs fatigue tests on composite materials at subcomponent level

			Perform a wide range of fatigue tests, with different load capacities Ability to design and manufacture the clamping fixtures
	-	The Welding Institute - UK	-
	RUMUL Testronic 150 kN	INEGI – UMAI (Advanced Monitoring and Structural Integrity Unit)	Universal (static and dynamic tests) Dynamic load: 150 kN Frequency range: 40-260 Hz	Resonant fatigue testing machine

The choice of the Instron 1341 equipment was mainly due to its availability, cost, possibility to perform both static and dynamic tests, and relatively high capacity of the load cell. As previously seen, the setup was specifically designed for attachment to it. A rendered mockup and a picture of the subcomponent and its setup in the Instron equipment can be found in Figure 99 and Figure 100, respectively.
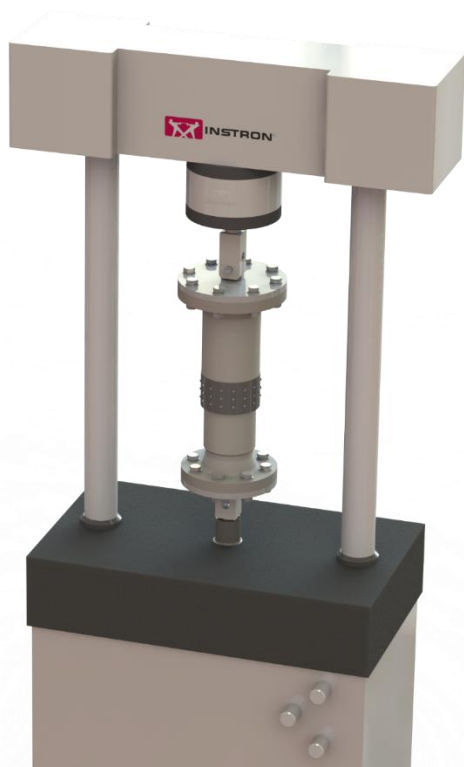
Figure 99 – Renderized mockup of the subcomponent on the fatigue machine

Figure 100 – Subcomponent before testing

Furthermore, the decision of using a servo-hydraulic testing machine rested on the fact that, although it would be desirable to test the subcomponent until a higher number of cycles – up to 10^7 or 10^8 – the resonant fatigue testing machine "RUMUL Testronic 150 kN" (Figure 101), located at INEGI's premisses, only operates in the range of 40-260 Hz (depending on the stiffness of the specimen – Figure 102) which, despite increased a lot the speed of the test, is not suitable for testing this composite bolted connections, has it is known that

at that the composite might not respond accurately to these high-frequency loads, namely due to significant heating of the plastic matrix, leading to potential discrepancies in test results. Furthermore, composite materials generally exhibit higher damping properties compared to metals, meaning that composites can absorb and dissipate more energy during loading, which can affect the resonant frequency of the test. Resonant fatigue testing machines might not account for these damping effects accurately, leading to potential misinterpretations of test results. For these reasons, it was decided to use a servo-hydraulic fatigue testing machine, better suited for this particular scenario as it can (with the trade-off of only being able to perform tests at smaller frequencies) simulate a wide range of loading conditions and frequencies more accurately.
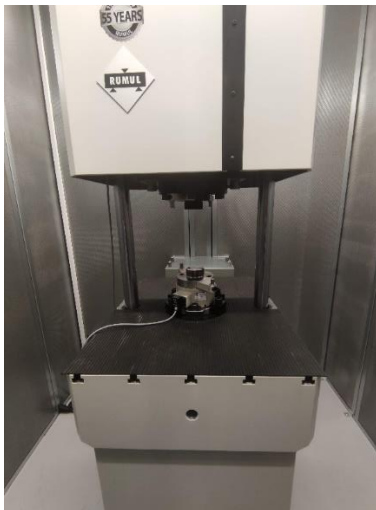
Figure 101 – RUMUL Testronic 150 kN at INEGI's premises
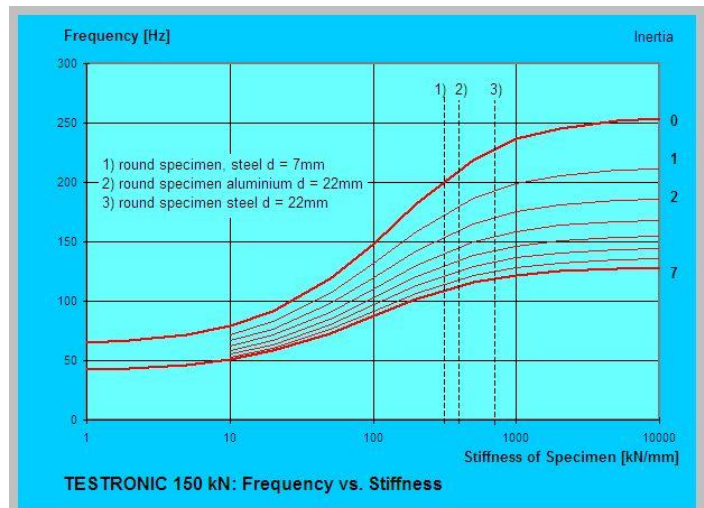
Figure 102 – RUMUL Testronic frequency range

It was decided that the fatigue tests will be monitored using a thermographic camera to understand the variation of temperature in the subcomponent in the different areas and possibly identify hotspots or early damage initiation and progression, correlating temperature with material response. The equipment chosen was the Testo 871 thermal imager (Figure 103), which provides images with a resolution of up to 480 x 360 pixels and has a temperature measuring range from -30°C to +650°C, detecting temperature differences from 0.08°C.

Figure 103 – Testo 871 thermal imager

The thermographic records were taken at the following timestamps:

- 0 min (before the start of the test);
- 5 min after start;
- 15 min after start;
- 30 min after start;
- 60 min after start;
- 120 min after start;
- 180 min after start;
- 240 min after start;

It was not possible to register data after this point because the rest of the test was run overnight and the thermographs had to be manually taken. Two thermographs were taken for each timestamp.

Regarding the loading and frequency conditions, it was decided to carry out one static test and two dynamic tests (and 1 subcomponent as spare), according to the following plan (Table 37):

Table 37 – Test plan

Specimen number	Type of test	Parameters	End criteria
#1	Static	Crosshead speed = 0.5 mm/min	Until failure or load cell limit

Specimen number	Type of test	Parameters	Frequency	End criteria
#2	Fatigue – displacement control	d_a = 0.2 mm d_{min} = 0.3 mm d_{max} = 0.7 mm $R \approx 0.4$ Sinusoidal	10 Hz	Until failure or 5×10^5 cycles

Specimen number	Type of test	Parameters	Frequency	End criteria
#3	Fatigue – displacement control	d_a = 0.3 mm d_{min} = 0.4 mm d_{max} = 1 mm R = 0.4 Sinusoidal	10 Hz	Until failure or 5×10^5 cycles

[Minimum displacement] d_{min}	[Displacement amplitude] $d_a = \dfrac{d_{max} - d_{min}}{2}$	[Mean displacement] $\begin{aligned}\Delta d &= d_{max} - d_{min} \\ &= 2d_a\end{aligned}$
[Maximum displacement] d_{max}	[Mean displacement] $d_m = \dfrac{d_{max} + d_{min}}{2}$	[Displacement ratio] $R_d = \dfrac{d_{min}}{d_{max}}$
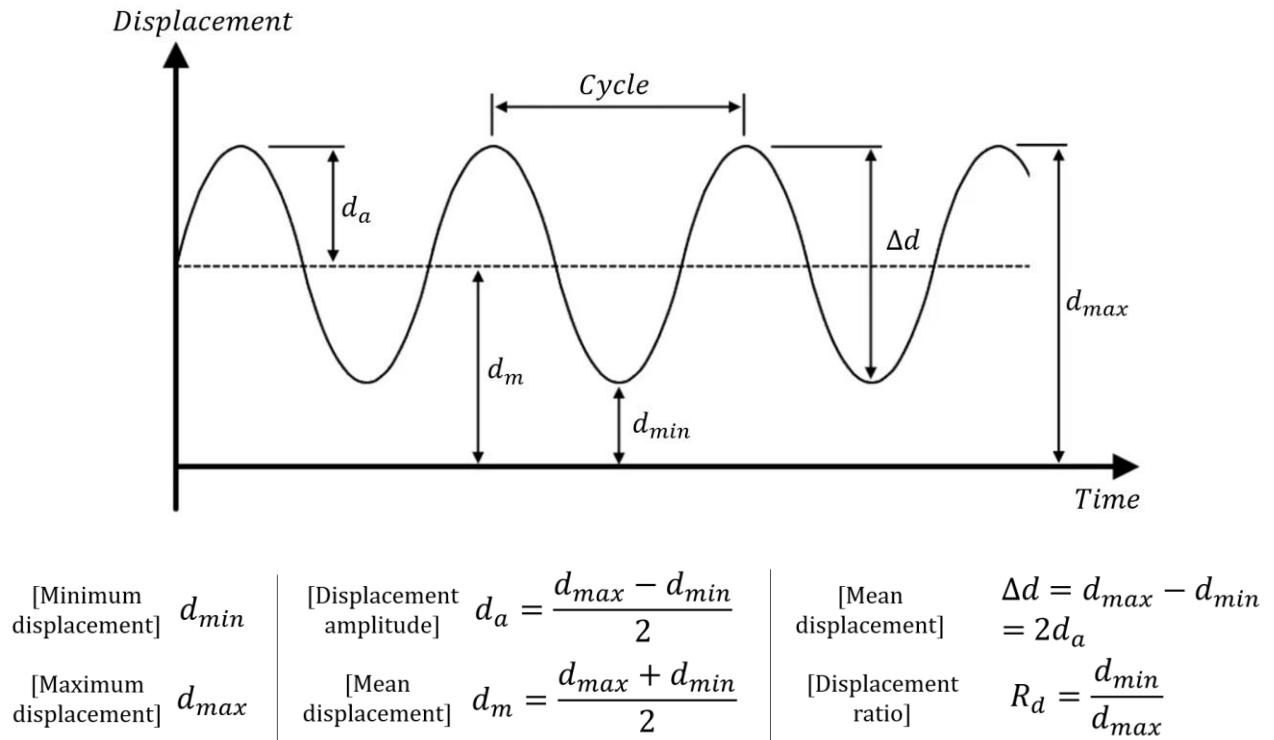
Figure 104 – Testing parameters

The main objective of the static was to obtain the ultimate tensile strength (UTS), in the case that the specimen fails below the load cell limit (this would also be the first point in the S-N curve), its stiffness, and observe the failure mechanisms that may be relevant for the subsequent fatigue tests. Furthermore, it is important to have an idea of the load-interval for the fatigue tests: despite being displacement-controlled, it is important that at maximum displacement (0.7 or 1 mm), the corresponding load is below ≈70% of the UTS, otherwise it is likely that the connection will fail after a low number of cycles, which is not intended since we are aiming to understand the behaviour of it under High Cycle Fatigue (HCF). High Cycle Fatigue (HCF), usually considered above 104 or more [16], is a major cause of failure in offshore wind turbine blades [17], [18].

The installation of the subcomponent into the fatigue testing machine was done by first bolting the tubed flanges to the plates of the setup, and then threading the setup to the load cell (top) and then to the hydraulic shaft (bottom). The bolts were slightly loose to avoid tensioning or compressing the subcomponent. After that, the bolts of the setup were tightened and the subcomponent was carefully set to the equilibrium of loads (the load cell was calibrated beforehand), corresponding to the zero displacement.

The first step of the fatigue tests, i.e., the movement to the average displacement (initial point of the cyclic sine waveform – 0.5 mm in specimen #2 and 0.7 mm in specimen #3), was carried at a programmed rate of 0.5 mm/min, the same used for the static test. The minimum displacement was always positive ($0 < R < 1$), and the connection was always in the tension-tension regime. ISO 13003 [19] was followed as guidance for defining the general procedure for fatigue testing.

3.1.3. Results

In this section, the results of the static and fatigue tests performed on the bolted composite connection will be presented. Conclusions from the mechanical behaviour and failure mechanisms of the connection will be drawn, ultimately providing valuable insights for their future design and optimization, contributing to the development of safer and more reliable composite structures, particularly for offshore applications.

3.1.3.1.Static test

Mechanical results

The results of the static test are illustrated in Figure 105. The stiffness at the elastic region was also calculated, between 0.2 and 1.2 mm of displacement (Figure 106), being around 22.1 kN/mm (slope of the linear trendline), assuming that at these low displacements the connection obeys Hooke's law. Unfortunately, the limit of the load cell (100 kN) has not allowed for continuing the test up to the failure of the connection (and subsequently determining fatigue loading parameters from it). However, as it will be seen further, some interesting conclusions can be drawn.
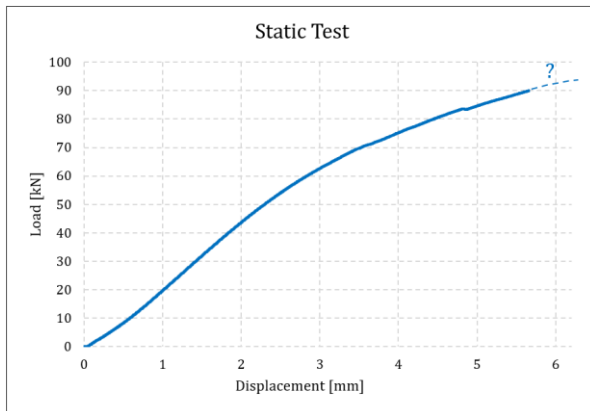
Figure 105 – Results of the static test
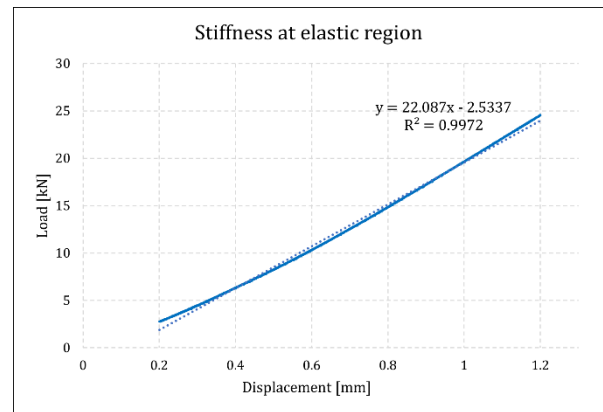
Figure 106 – Stiffness during the static test

Visual inspection

Visual inspection after testing reveals that no bolts or nuts were broken during the static test. The inside and exterior surfaces of the connection are illustrated in Figure 107 and Figure 108, respectively.
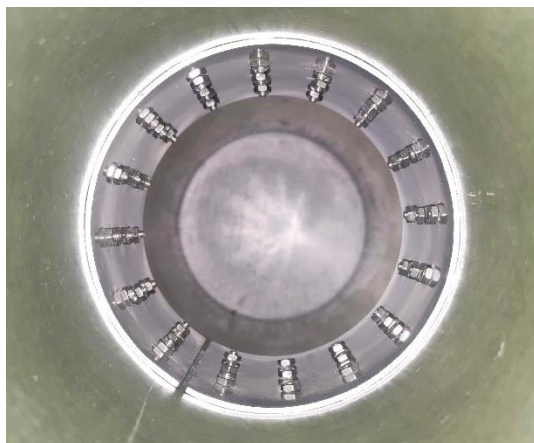
Figure 107 – Post-testing inspection from the inside (specimen #1)

Figure 108 – Post-testing inspection from the outside (specimen #1)

However, after inspection upon removal, it was observed that most of the bonds exhibited some bending meaning that their yield strength was surpassed, entering the plastic region.

Figure 109 – Bending of the M3 bolts (Specimen #1)

Another observation, after the removal of the sleeves, was that some compressed resin particles were found around most of the 3 mm holes. These were also observed on the fatigue-tested specimens, but were more prominent on the static-tested one. Presumably, this occurred due to the elongation of the holes (from increased stress concentration around them), breaking the resin matrix which, having nowhere to escape (between the tube and the sleeve) has compacted to a ring shape around the hole. Besides this, no delamination or any type of fibre failure of the cured FRP tube was found.
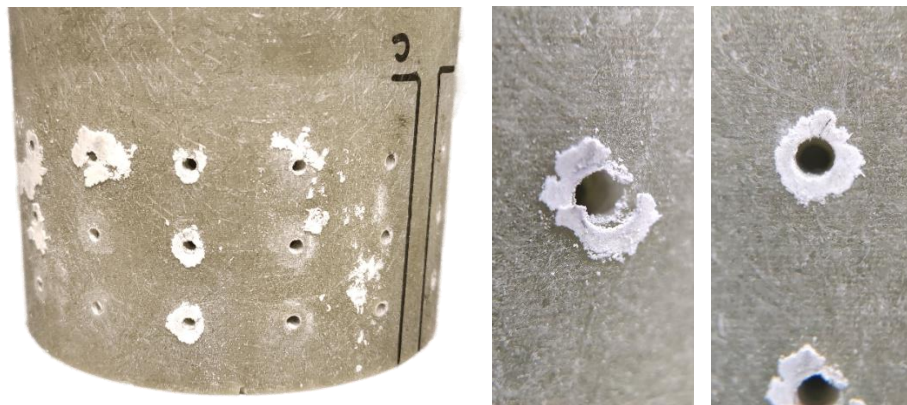
Figure 110 - Compressed resin particles

3.1.3.2. Fatigue test

Mechanical results

The results of the fatigue tests performed in both #2 and #3 specimens can be found in Figure 111 and Figure 112, respectively, plotting the maximum and minimum load during the entire test duration.
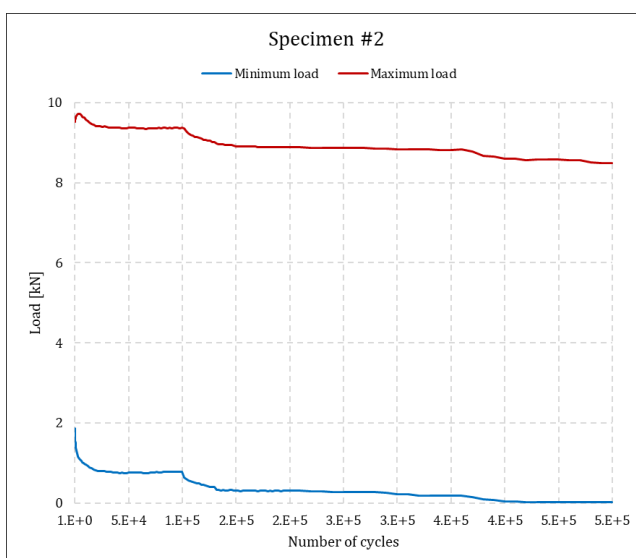
Figure 111 – Minimum and maximum load for each cycle of specimen #2
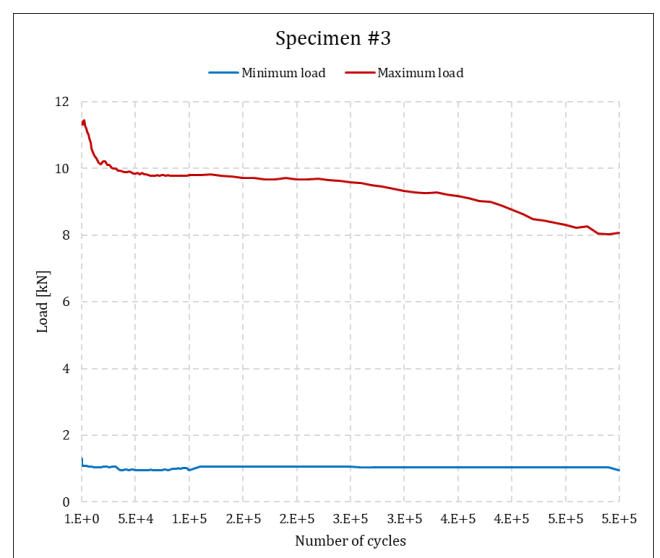
Figure 112 – Minimum and maximum load for each cycle of specimen #3

Since the connection didn't catastrophically fail during the duration of the test, they were carried out up to the predetermined number of 500 000 cycles (13,9 hours after starting the test). As expected, the minimum load carried out by specimen #3 were higher than specimen #2 on almost the entire test (Figure 113), presumably due to its higher minimum displacement (0.4 mm vs 0.3 mm). However, while the minimum load on specimen #3 stays approximately constant after 100 000 cycles, on specimen #2 it continues to decrease until reaching approximately zero (the neutral point where the connection is not loaded, neither in tension nor comprehension). While it was not possible to register any specific event at this time mark, it is possible that one or more bolts were broken, resulting in an inferior load-bearing capability of the connection. On the other hand, the maximum load (Figure 114) exhibits an interesting behaviour: expectably, it decreases during the entire duration of the test and is typically higher for specimen #3 (higher maximum displacement), but an inversion is seen around 400 000 cycles – which can be due to higher damage of the connection, with more broken or weakened bolts, and therefore less capability than the specimen #2 to support loadings after this point. It can also be depicted, backed by the literature on this subject [20], that when the bolts become loose during the test and the clamping force reduces, the load transfer during fatigue loading from friction forces decreases, potentially to zero. This will reduce the area to which the load is transferred, and transfer it to the bolts, which will, inevitably, fail.
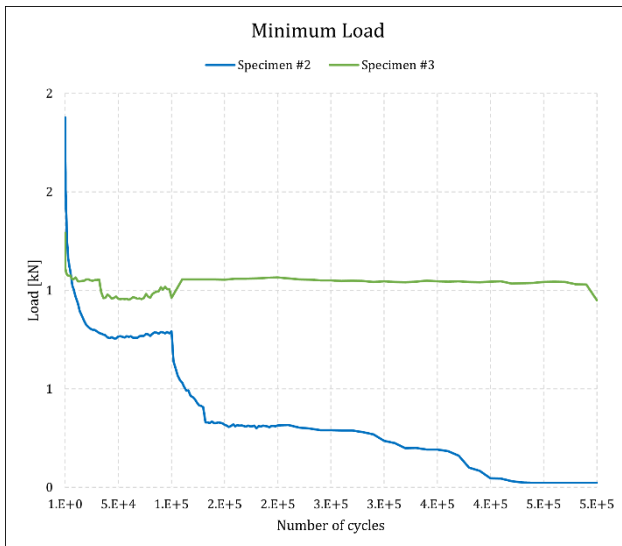
Figure 113 – Minimum load
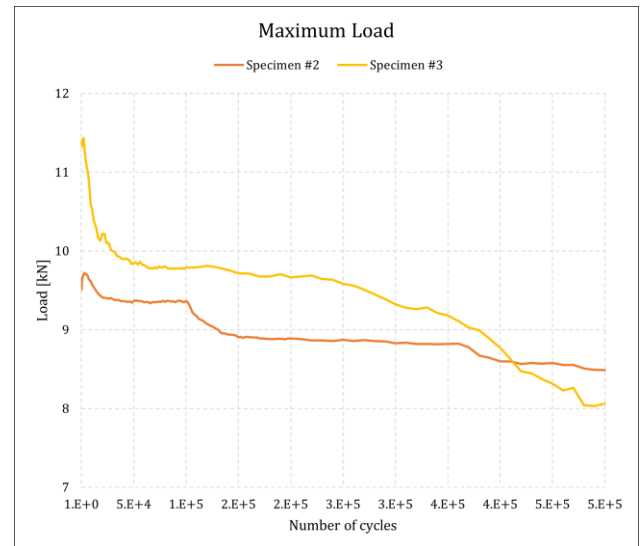
Figure 114 – Maximum load

Additionally, to the previous analysis, a more specific analysis of the final 10 cycles of the testing can be seen, drawing further observations. In Figure 115 and Figure 116 it is plotted the displacement variation during these last 10 cycles which, as expected (being displacement-controlled testing) maintain the predefined parameters of 0.3 mm – 0.7 mm and 0.4 mm – 1 mm for specimens #2 and #3, respectively. A small difference for cycle 500 001, only because it is not part of the test *per se* and is not responsible for taking the specimen to the start position (d_m).
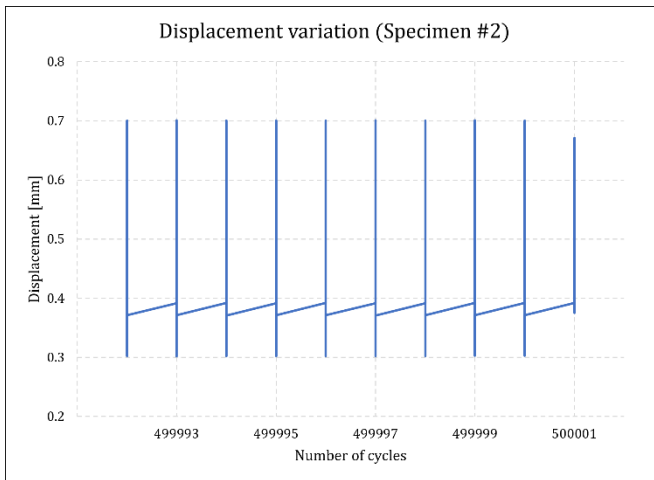
Figure 115 – Displacement variation (specimen #2)
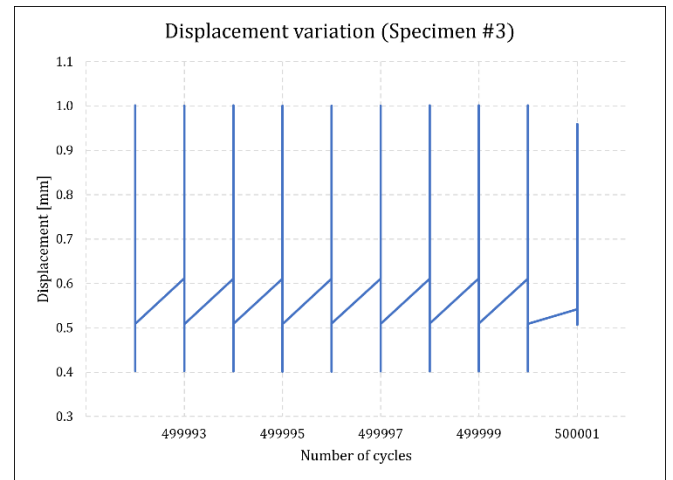
Figure 116 – Displacement variation (specimen #3)

To what concerns the load variation (Figure 117 and Figure 118), it is also approximately constant during the last 10 cycles, being the minimum load higher for specimen #3, and the maximum load higher for specimen #2, as already previously depicted in Figure 113 and Figure 114.
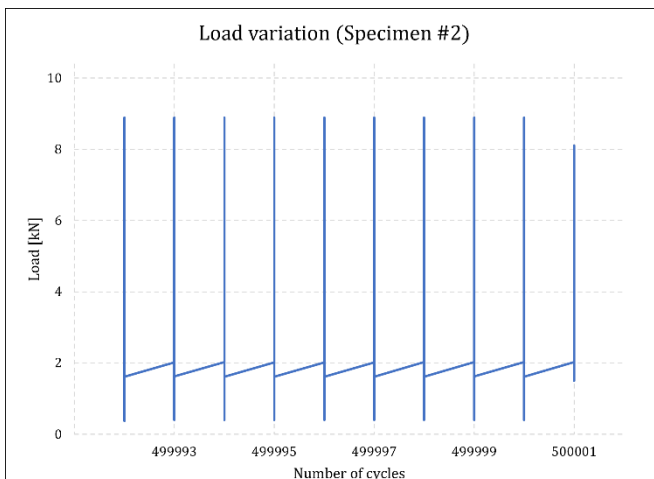
Figure 117 – Load variation (specimen #2)
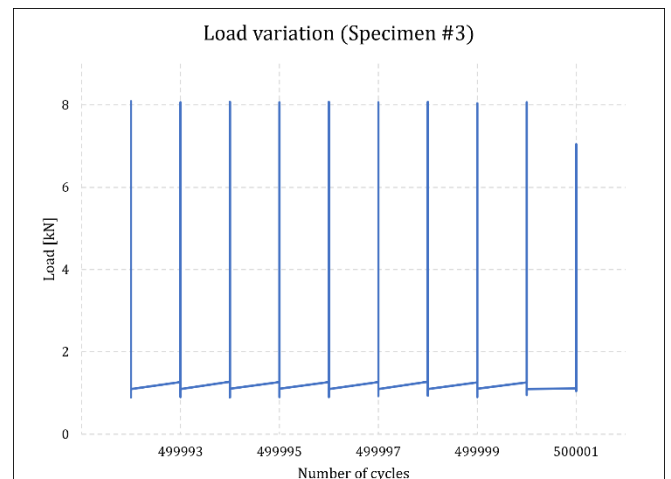
Figure 118 – Load variation (specimen #3)

Furthermore, the stiffness (average load/displacement) was calculated for both specimens by sampling and using a linear trendline from the load-displacement curve, for an approximately linear region of the cycle number 499 997. The results are illustrated in Figure 119 and Figure 120 for specimens #2 and #3, respectively, and indicate that at this point, very near the end of the test, there is a reduction of the stiffness of the specimen, when compared to the initial stiffness of 22.1 kN/mm. This reduction, although small, is more significant for specimen #3, presumably due to the higher displacement amplitude, causing more damage to the connection, including ovalized holes, hence reducing its stiffness.
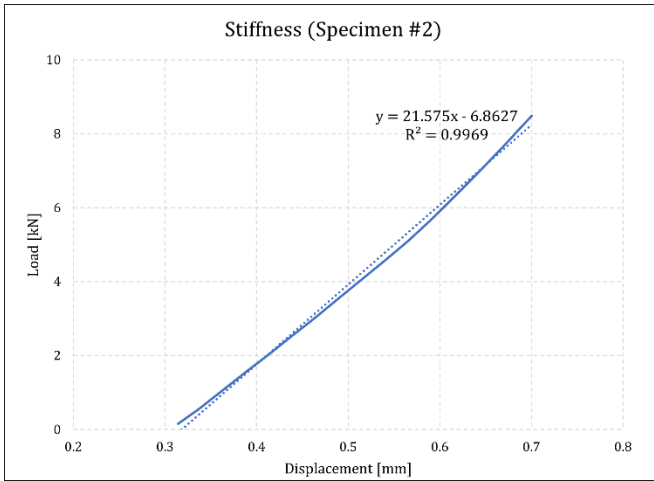
Figure 119 – Stiffness (specimen #2)
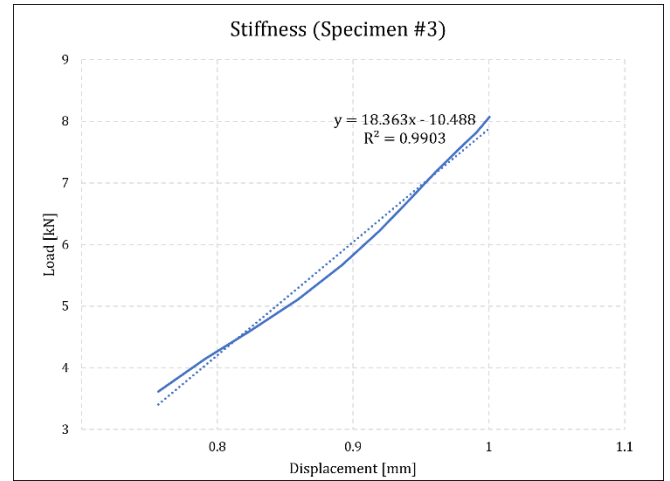
Figure 120 – Stiffness (specimen #3)

Visual inspection

Visual inspection reveals that some bolts were broken during the cyclic testing. Specimen #2 had three broken bolts, two near the bolt head, and one near the nut. Similarly, but with a higher number of damaged bolts, Specimen #3 had seven broken bolts (five near the bolt head and two near the nut), being that two of them were broken when unscrewing them from the sleeve (possibly already broken, but stayed in place). Removal of the bolts showed that all bolts were quite loose, without needing almost any torque load to unscrew them. None of the bolts exhibited plastic bending and, among the ones that broke, all of them did it near one of the ends (example in Figure 121 for specimen #3).

Figure 121 – Broken bolts of specimen #3

Figure 122 illustrates, as an example, bolts that broke near the bolt head.

Figure 122 – Broken bolt near the head cap

While Figure 123 illustrates bolts that broke near the bolt end (nut).

Figure 123 – Broken bolt near the bolt end

While none of the nuts had broken, in some bolts (particularly those that didn't fail by the nut end), it was possible to see that the bolt threads were damaged in the area where the nut was, making it difficult to manually remove the nut.

Figure 124 – Damaged thread

The inside and outside surfaces of specimens #2 and #3 are illustrated in Figure 125 to Figure 128.

Specimen #2	Specimen #3

Figure 125 – Post-testing inspection from the inside (specimen #2)
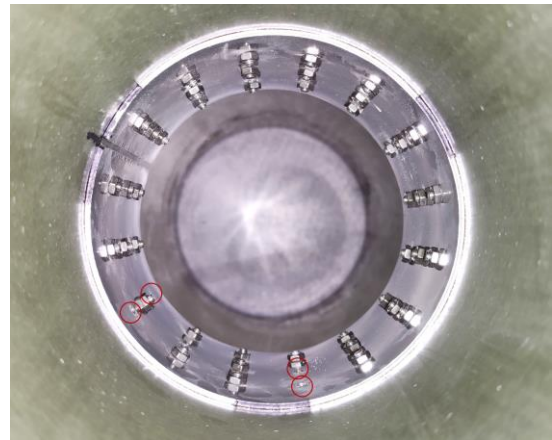
Figure 126 – Post-testing inspection from the inside (specimen #3)

Figure 127 – Post-testing inspection from the outside (specimen #2)

Figure 128 – Post-testing inspection from the outside (specimen #3)

Furthermore, the sleeves were not bent or cracked, only exhibiting some circle marks (wear and tear) around the hole (due to tightening and friction between the bolt head cap and the sleeve) and some minor metal shavings and chamfering of the hole (only visible after close inspection), as illustrated in Figure 129. No delamination of the FRP tubes was found, being the damage limited to the area around the holes, where it appears to have been some roughing of the resin matrix.
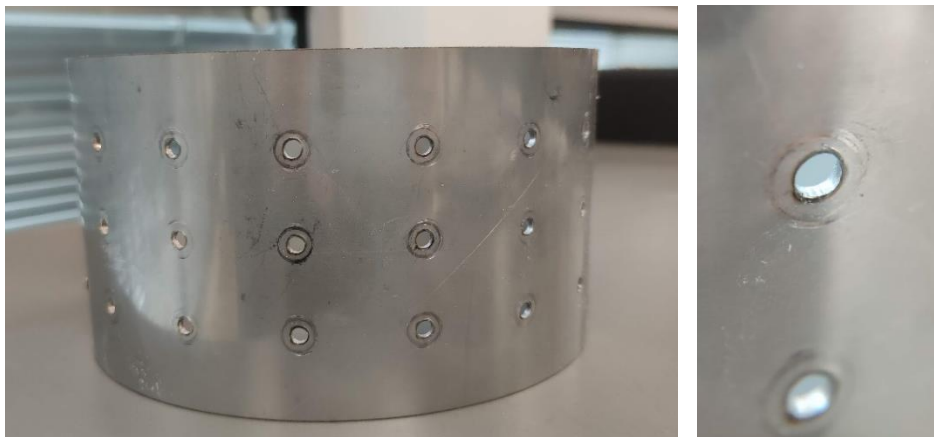
Figure 129 – Post-testing inspection of the sleeves (exterior sleeve; specimen #3)

3.1.3.1. Thermography

The results of the thermographs taken during the two fatigue tests are plotted in Figure 130 and Figure 131 for specimens #2 and #3, respectively.
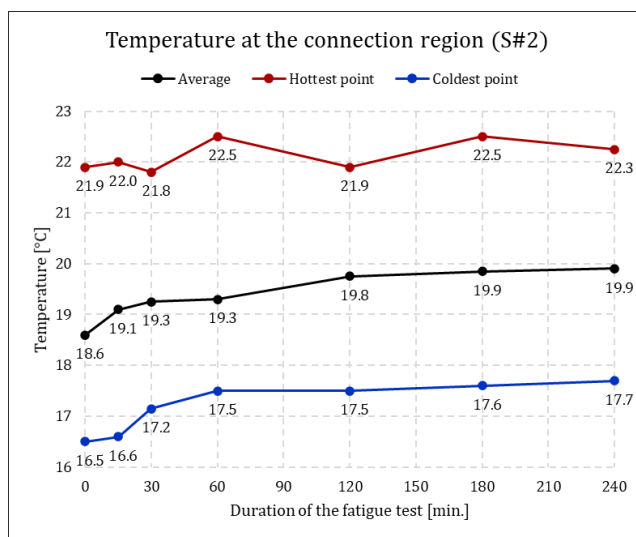
Figure 130 – Thermography results of specimen #2
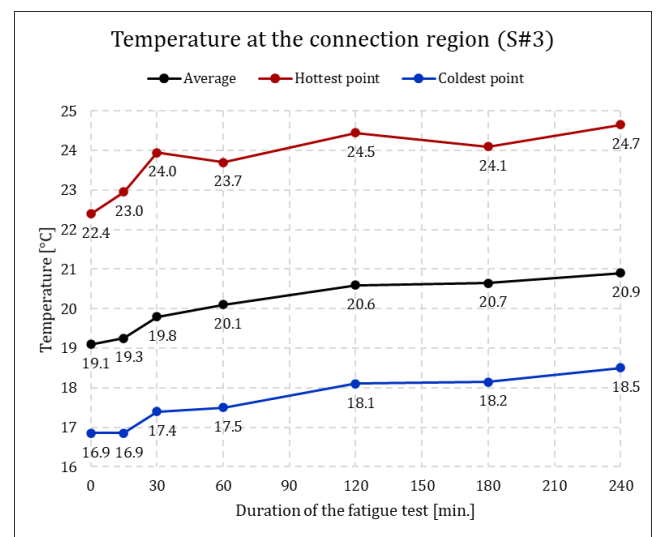
Figure 131 – Thermography results of specimen #3

As illustrated in Figure 132, these results were obtained from the "testo IRSoft" thermography analysis software [21] and limiting the results area to a rectangle where the connection is. The output was the average temperature within this area, the hottest point and the coldest point. From the analysis of the plotted results (Figure 130 and Figure 131), it can be concluded that there is a clear increase in the average temperature, as well as the hottest and coldest points, over the 240-minute period. Upon comparing the two sets of results, it is evident that specimen #3, tested over a displacement amplitude of 0.3 mm, had a more pronounced increase in average temperature, hottest point, and coldest point over the period under evaluation. In contrast, specimen #2, tested over a smaller displacement amplitude of 0.2 mm, exhibits a more gradual and relatively smaller change in temperature values. This is somewhat expected, due to the higher load carried by specimen #3, but it can also partially be due to the highest (about 0.5 °C) ambient temperature during the testing of specimen #3 (although the temperature variation after 240 minutes, when compared to the specimen #2, was considerably higher than 0.5 °C).
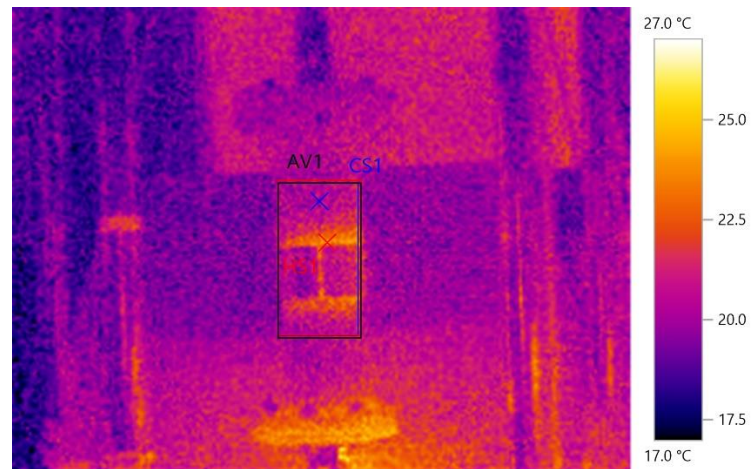
Figure 132 – Example of analysis performed at one timestamp

Several studies have shown that the fatigue life of composite components is reduced [22]-[24]. For example, in one study [23] it was concluded that the fatigue life of vinyl ester/ E-glass fibre composite specimens (R = 0.1, f = 10 Hz) in aqueous environments at 65°C is about the same as that at 30°C, but the fatigue life at 4°C is significantly longer than that at 30°C. Figure 133 shows the experimental results and linear regressed S-N curves. Another study [24]] has concluded from the D-N graphs that, with increasing temperature, the cumulative fatigue damage is increased and vice versa. Figure 134 illustrates the variation of fatigue damage with temperature.

Although it is difficult to say if the observed temperature variations, being quite small (less than 2°C from before the test to the 240 minutes mark), do affect the fatigue behaviour, it is known that parameters such as Young's modulus of the composite, E_c, composite ultimate tensile strength, σ_{ult}, and ultimately the fatigue life of composite, N_f, are temperature dependent and therefore future fatigue and predictive models should also be temperature dependent.
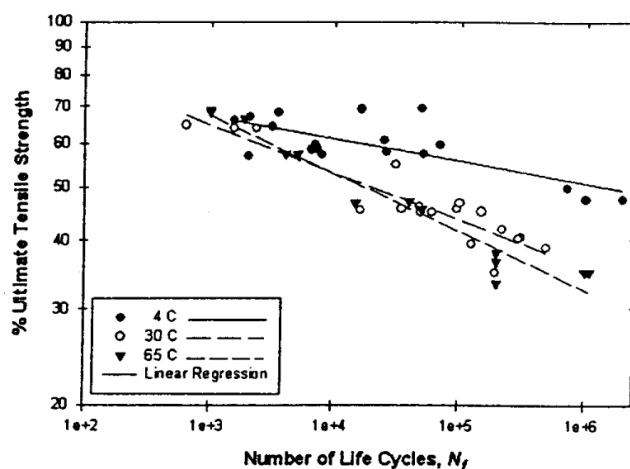
Figure 133 – S-N curves of vinyl ester/ E-glass fibre composite specimens for three different temperatures (4°C, 30°C and 65°C), R = 0.1, f = 10 Hz
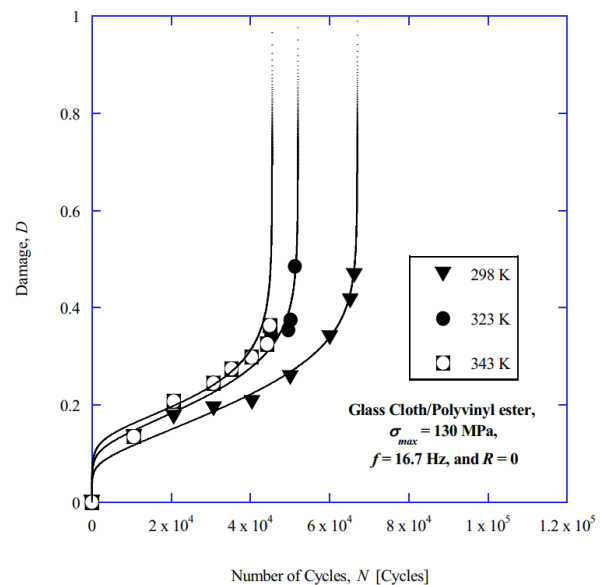
Figure 134 – Fatigue damage of glass cloth/polyvinyl ester versus number of cycles under σ_{max}= 130 MPa, f = 16.7 Hz, and R = 0 at 298 K (25 °C), 323 K (52°C) and 343 K (70°C)

It can be noted from the current observations of the thermographs that the friction-generated heat dissipates through both contact surfaces, increasing the temperature mostly above and below the steel sleeves (well visible in Figure 142). Such heat will create thermal stresses and can impact on pitting, micropitting, scuffing, and wear on the surface – reducing the fatigue life of the structure. Caution should also be taken if the reversible adhesive is used between the steel sleeves and the composite, since this area concentrates the most heat and should ultimately result in unwanted debonding of the adhesive if the temperature is raised to its debonding temperature.

In the following figures, some thermographs of both specimens at different timestamps (0, 30 and 240 minutes after the beginning of the test) are presented as an example.

Specimen #2:

Figure 135 – Photography before the test
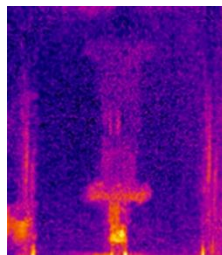
Figure 136 – Thermography before the test
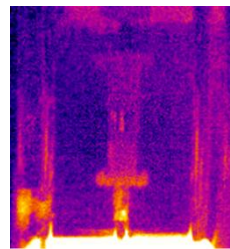
Figure 137 – Thermography after 30 minutes
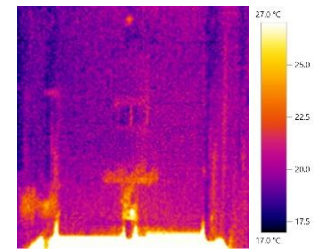
Figure 138 – Thermography after 240 minutes

Specimen #3:

Figure 139 – Photography before the test
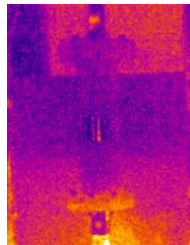
Figure 140 – Thermography before the test
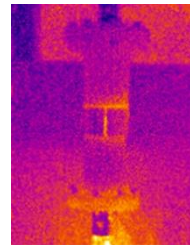
Figure 141 – Thermography after 30 minutes
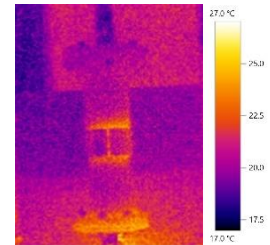
Figure 142 – Thermography after 240 minutes

3.2. Evaluation of the reversible adhesive as an option for connections

When a structure has to be destroyed or need a maintenance operation, the main disadvantage of using an adhesive is the impossibility of disassembly the different part without damaging the structure. The use of a reversible adhesive, developed by Corso Magenta, may be useful. As a standard adhesive, this adhesive permits to bound two pieces but after the service, it can be disbound. This can be possible by the action of heat.

A first characterisation of the performance of the adhesive was done in the deliverable D2.4 "Connections in offshore structure". The fatigue performance of the adhesive was also described int the D2.2 "Fatigue performance of composites". This chapter will be an overview of the utilization of this adhesive: the performance in service and its dismantling capacities to have its behaviour at the end of life. An application on a large coupon, more representative of a use case, will also be performed.

3.2.1. Performance in service

Two tests were selected to evaluate the performance of this new adhesive: the single lap joint test to access the adhesion of the adhesive on composite and the fatigue resistance to obtain the performance of the adhesive itself.

3.2.1.1. Samples and materials description

All the samples (composites laminates and bounding) were prepared by INEGI.

For the preparation of the coupons tested by single lap joint, refer to D2.4 "Connections in offshore structure" as the produced that will be described after is very similar.

In the following subchapters, the procedure for preparing the bonding specimens will be presented: fatigue coupons preparation and coupons used in Chapter3.2.3. As will be seen, two different sizes of specimens were manufactured and bonded with CORSO's reversible adhesive. However, all the substrates (coupons) were cut from similar vacuum-infused CFRP plates. The process for manufacturing these plates, which took place at INEGI's premises, will now be described.

3.2.1.1.1.CFRP Plates Manufacturing

The laminate for these plates is constituted by CFRP multidirectional fabrics (ZOLTEK PX35 50K +/-45° and 0/90°, both with 600gr/m2 [6]) and the epoxy resin SR InfuGreen 810 (with the SD 4771 hardener [7]). Both materials are illustrated in Figure 143 and Figure 144, respectively. Because the fabrics were provided by iXblue which at that time only had available the +/-45° fabric, the 0/90° layers were cut from the same material (ID PX35MD060A-127) by cutting it at a 45° angle – resulting in layers with 0° fibres in one side and 90° fibres on the opposite stitched side.
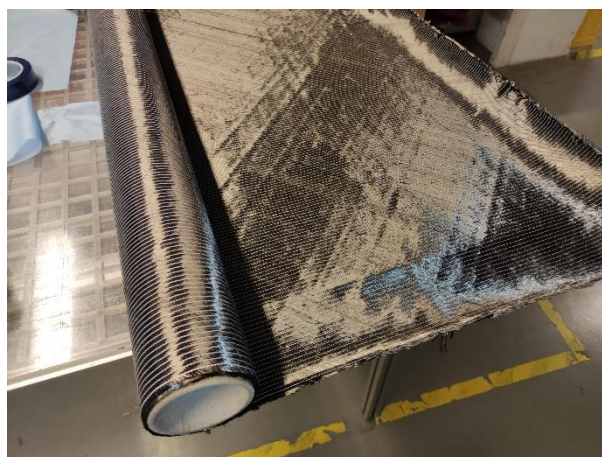
Figure 143 – Zoltek PX35 50K +/-45° carbon fabric

Figure 144 – SR InfuGreen 810 and SD 4771

It was decided to use a quasi-isotropic, symmetric and balanced stacking sequence of the carbon fibres, as this would allow for constant strength and stiffness of the material regardless of the direction in which it is loaded, a typical layout and very close to the one that will be used on the demonstrators. The complete sequence is the one indicated in Figure 145.

Since these tests follow the tests already conducted in tasks 2.3 (static) and 2.4 (fatigue), the fibres, resin system, and laminate stacking, were the same as used in those tasks to ensure comparable results.

Figure 145 – Stacking sequence

Concerning the setup, a prismatic steel mould tool, displayed in Figure 146, was once again used. Figure 147 depicts the complete setup, including the resin container, the resin inlet and outlet hoses, the resin trap and the vacuum pump.
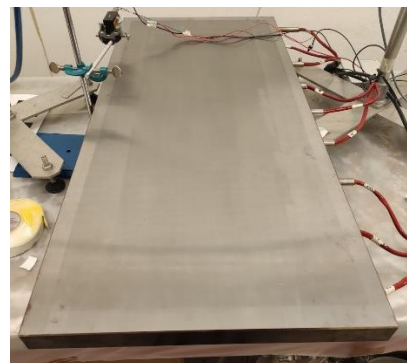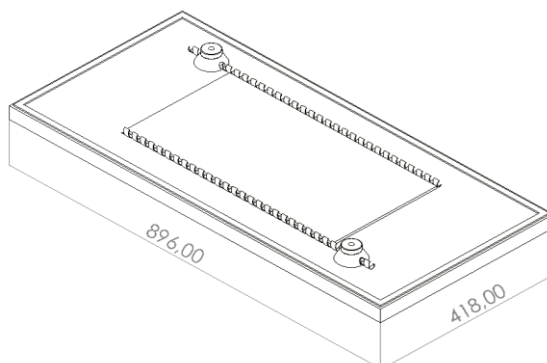
Figure 146 – Illustration of the mould tool
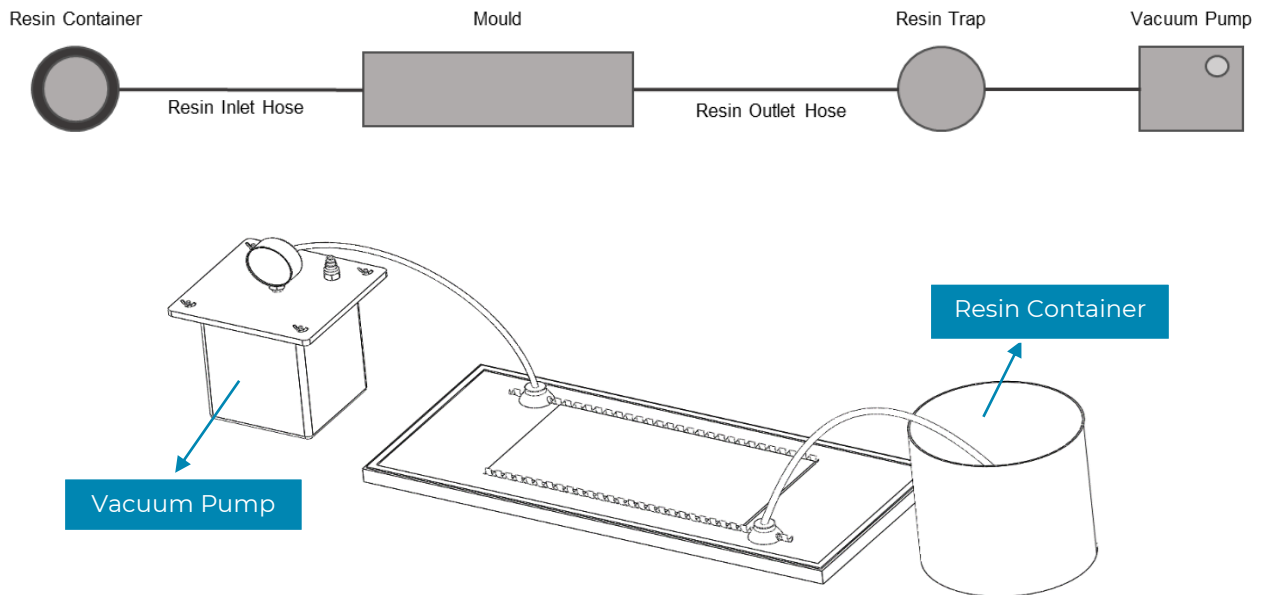
Figure 147 – Representation of the used vacuum infusion setup

After gathering the necessary components to perform the vacuum infusion process, the steps presented in Table 38 were followed. First, the mould has been degreased with acetone, then it was cleaned with a mould cleaner and a cotton cloth. Subsequently, it was applied a mould sealer (*Loctite® Frekote®* B-15), 3 coats of release agent (*Loctite® Frekote®* 770-NC) with an interval of 10 minutes between coats, and a final wax coating.

Procedure	
1	Preparation of the mould
2	Placement of the bottom peel ply
3	Cutting and stacking of the carbon fibre layers
4	Placement of the spiral wraps and T-fittings
5	Placement of the peel ply and flow distribution mesh
6	Preparation and sealing of the vacuum bag
7	Connection of the resin inlet and resin outlet hoses
8	Clamping off the resin line and switch on the vacuum pump
9	Apply vacuum and test for leaks/losses of vacuum pressure
10	Open the resin line
11	Resin flow until it impregnates the full length and width of the carbon fibre layers
12	Clamping off the resin line
13	Cure of the CFRP composite
14	Demoulding of the cured laminate sheet

Table 38 – Procedure steps of the vacuum infusion process

The following step was placing a bottom layer of peel ply before the carbon fibre layers, which were then cut and stacked according to the desired sequence (Figure 145). The spiral wrap (Figure 148) and T-fittings (Figure 148) were placed next to the stacked fibres, as they are responsible for allowing and facilitating the resin flow. An upper peel ply was also placed after the last layers of fabric, and a distribution mesh (above the peel ply) covering about 70% of the part's length. Afterwards, sealant tape was bonded to the vacuum bag, which was then placed above the *Flashbreaker®* blue adhesive tape (Figure 148) that was on the mould's surface. The tape was carefully pressed against the mould to assure complete air tightness. The system was connected to a vacuum pump, which was switched on to compact the components and fix present leaks. The illustration of the final vacuum bag setup can be found in Figure 149.

Figure 148 – (a) Spiral Wrap; (b) T-fitting; (c) Airtech Flashbreaker 1 Tape
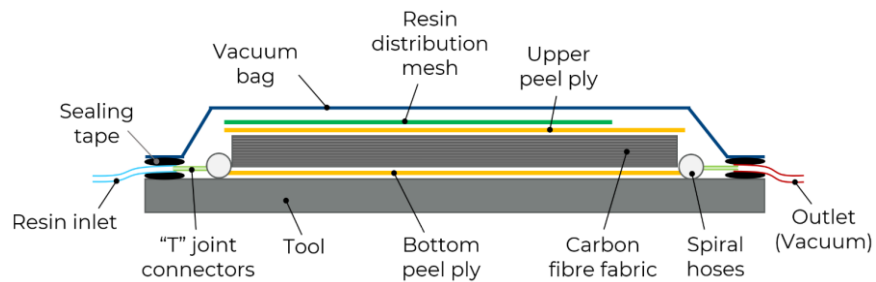
Figure 149 – Vacuum bag setup (components not at scale)

The next step concerned the preparation of the resin. As the laminate is composed of four layers (600gr/m^2), it was recommended to use approximately 700 g of resin, with a mix ratio (epoxy to hardener) of 100/29, calculated using the formulas in Table 39. Once the mixture was prepared, the resin inlet hose was immersed in the resin container and the vacuum pump (Figure 150) was switched on (vacuum pressure of -0,5 bar), leading to the beginning of the impregnation of the fibres by the resin. The vacuum infusion process was performed at ambient temperature (mould was also at T_{amb}) and is illustrated in Figure 151.

Formulas	
Number of layers	[Fibre Fraction Volume x Fibre Density x Desired Thickness] / Areal Weight
Resin Weight	[Resin Ratio / (Resin Ratio + Hardener Ratio)] x Desired Weight
Hardener Weight	[Hardener Ratio / (Resin Ratio + Hardener Ratio)] x Desired Weight

Table 39 - Formulas

Figure 150 – Magnus Venus Plastech vacuum pump

About 10 minutes after, the resin has impregnated the full length and width of the fabric, the resin inlet was ceased and the sample was left to cure at T_{amb}. According to the datasheet of the SR InfuGreen 810 and SD 4771, the composite laminate was cured after 24 hours at T_{amb}, nonetheless, the plates were only demoulded after 48 hours.
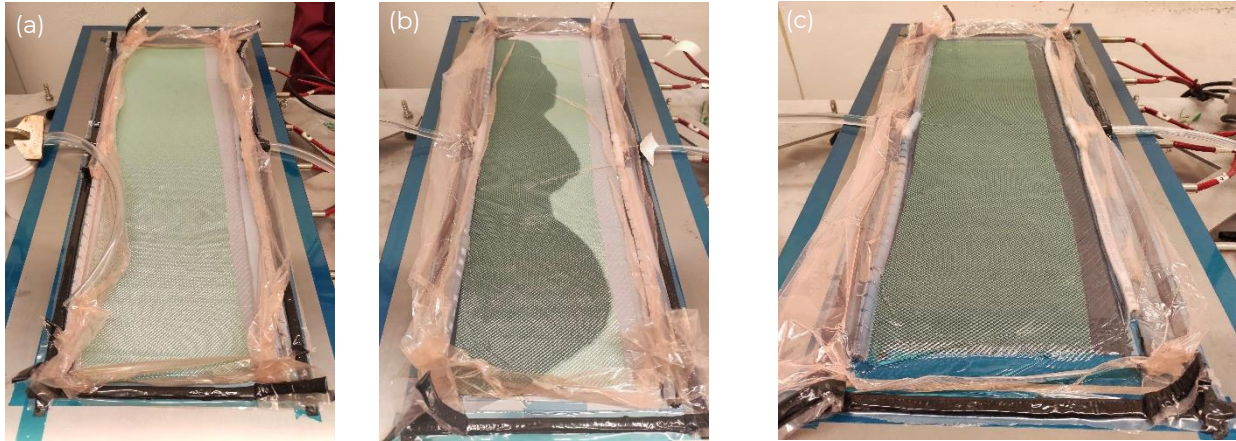
Figure 151 – Infusion process: (a) Before infusion; (b) During infusion; (c) After infusion

3.2.1.1.2.   CFRP Coupons

After demoulding, the different coupons were cut off from the plate using an abrasive diamond disc (Figure 152).

Figure 152 – Abrasive diamond disc

Two types of size configurations of coupons were cut from the CFRP plate:

-    Small-scale: 36 x 160 mm coupons, with a bonding area between coupons of 36 x 36 mm (1296 mm^2) – Figure 153;

-    Large-scale: 72 x 150 mm coupons, with a bonding area between coupons of 72x 72 mm (5184 mm2) – Figure 154.
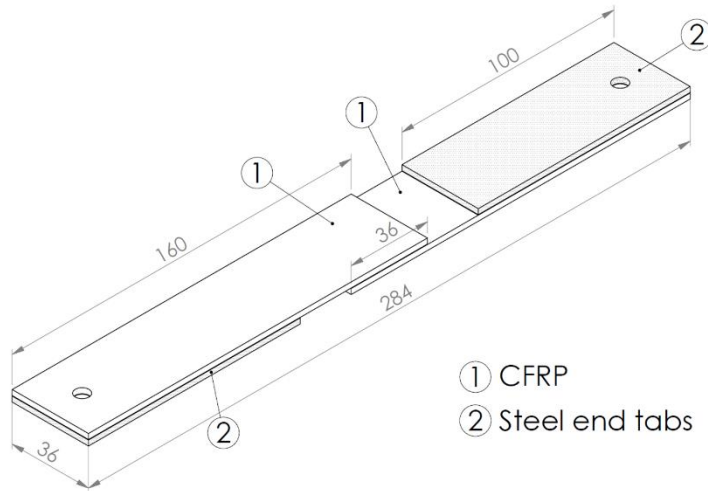
Figure 153 – Small-scale specimens' geometry and main dimensions (isometric view)
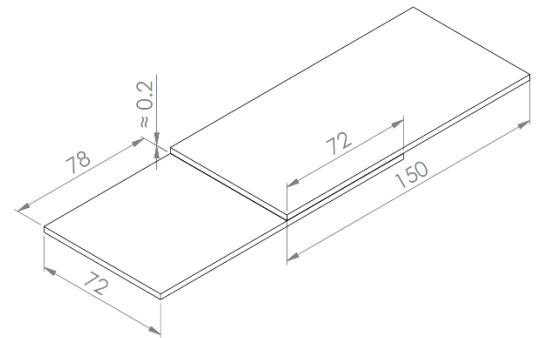
Figure 154 – Large-scale specimens' geometry and main dimensions (isometric view)

The small-scale specimens will be tested under dynamic tensile loads, and it was agreed to use the same geometry of the specimens used in task 2.4 (and based on the ASTM D5961 [8]). Steel end tabs (100 mm in length and about the same thickness as the CFRP coupons) were designed to reduce the eccentricity of the load path which causes out-of-plane bending moments and consequently high peel stresses and non-uniform shear stresses in the adhesive layer. Furthermore, the length of each coupon was increased from the 135 mm used in task 2.3 (static tests) to 160 mm in order to fit the specimens into ULIM's fatigue machine test frame, as per ULIM's request. Nevertheless, the critical test section dimensions remain the same as in ASTM D5961 [8] and as with the previous static (task 2.3) and fatigue (task 2.4) tests. Seven bonded specimens were produced using this configuration.

More detailed dimensioning of the small-scale specimens can be seen in Figure 155.
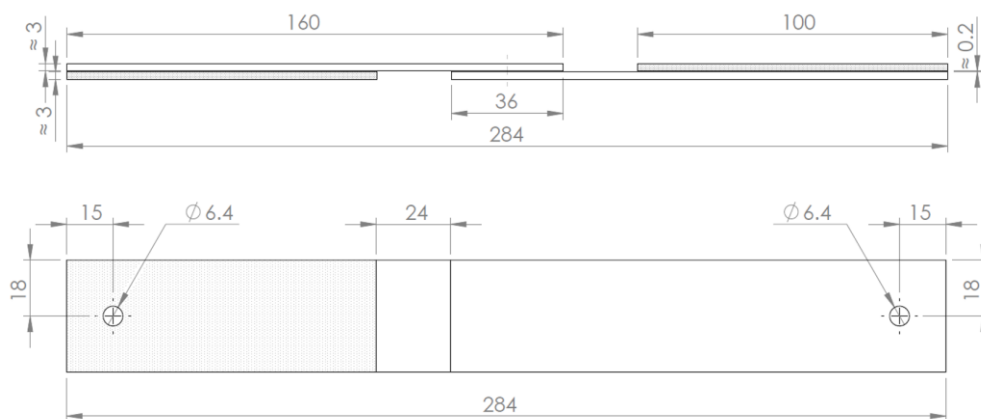
Figure 155 – Additional small-scale specimens' dimensions

For the large-scale specimens, which bonding area is 4 times larger than the small-scale specimens, tests to be performed are aimed to evaluate the heat energy and time needed to separate the bonded joint. No steel end tabs were necessary, and two bonded specimens were produced using this configuration.

3.2.1.1.3.   Bonding and Final Preparation

On the side that was in contact with the mould (controlled surface), the peel ply was maintained in all coupons and was only removed before bonding to protect the surface from water ingression or any contaminants during cutting and subsequent procedures, as it will also be the method used for bonding

surface treatment. Although other surface preparations methods, such as abrasion, have been shown to lead to higher bonding strengths [9], this was decided to be the simplest method to provide a clean and roughened surface with high repeatability and satisfactory results, which is why it continues to be the most frequently specified surface preparations for bonding fibre-polymer composites [10].

All the CFRP coupons (adherends), both small and large-scale, were bonded at INEGI's premises using the reversible adhesive from Corso Magenta and their instructions. This adhesive is a 3-component epoxy and, apart from Figure 156.. From the task 2.3 results [11], it is known that its lap shear strength at 25°C is around 3 MPa. However, it was also mentioned by INEGI that most specimens failed at lower values, possibly due to the difficult preparation of the bonded joint.
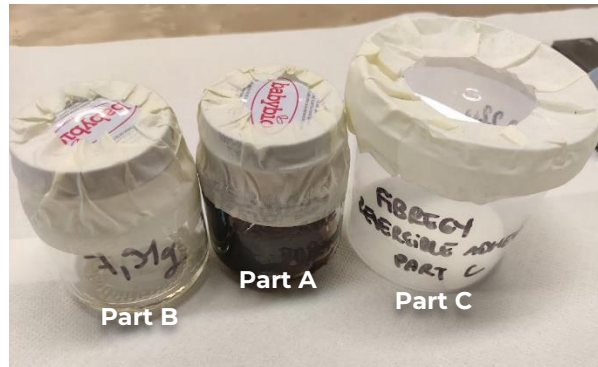
To aid in the mixing of components, the paste epoxy (component A) was subjected to heat treatment in a laboratory oven (Venticell 404 standard [12]) at 50°C for 20 minutes. This process effectively reduced the viscosity of the epoxy, rendering it more amenable to handling.

Furthermore, because previous observations [11] have noted that the epoxy returned to its original viscosity (similar to caramel at ambient temperature, Figure 157) just after one minute at room temperature (time between the removal from the oven and the transport to the scale), making it impossible to mix with the hardener (component B), it was decided to perform the mixing process of A+B using a laboratory hot plate (set to 50°C) to keep the temperature of the paste epoxy above 45°C (it was found that below this temperature it was very difficult to perform the mixture). All components were weighted according to the mixing ratio.

Figure 157 – Epoxy (Component A) becoming solidified after a few minutes at T_{amb}.

After obtaining a close-to-homogeneous paste (A+B), component C was added and manually mixed for 10 minutes.

Immediately after removing the peel ply, the reversible adhesive was laid out into the surface using wooden spatulas to cover the entire bonding surface evenly. The container with the mixed paste was maintained in the hot plate until the adhesive was applied to all specimens, however, this process was still very challenging due to the difficulties of applying the adhesive after cooling, being nearly impossible to do repeatable adhesive applications.

As can be seen in Figure 158, another small modification from the previous procedure used in tasks 2.3 and 2.4 was made to the small-scale specimens, placing a strip of *Flashbreaker®* blue adhesive tape delimiting the bonding area, and taking it off after the adhesive application, consequently removing any excess adhesive in this process.
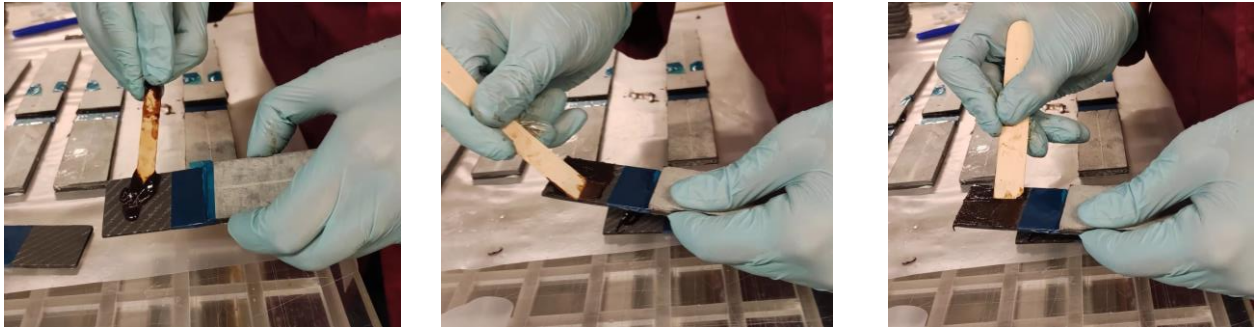
Figure 158 – Reversible adhesive application

After applying the adhesive on both surfaces, the adherends were pressed together and placed into a bonding jig setup. This setup was made using 3 mm steel plates and shim tapes, assuring that the gap between the bottom and upper adherends is constant and the same as the desired adhesive thickness (Figure 159), around 0,2 mm, as suggested in the literature [13]. The alignment of the adherends was assured visually and by using blue adhesive tape (Airtech *Flashbreaker®*) to fix them, as illustrated in Figure 160.

A = Tool
B = Adhesive bondline
C = Shim tape
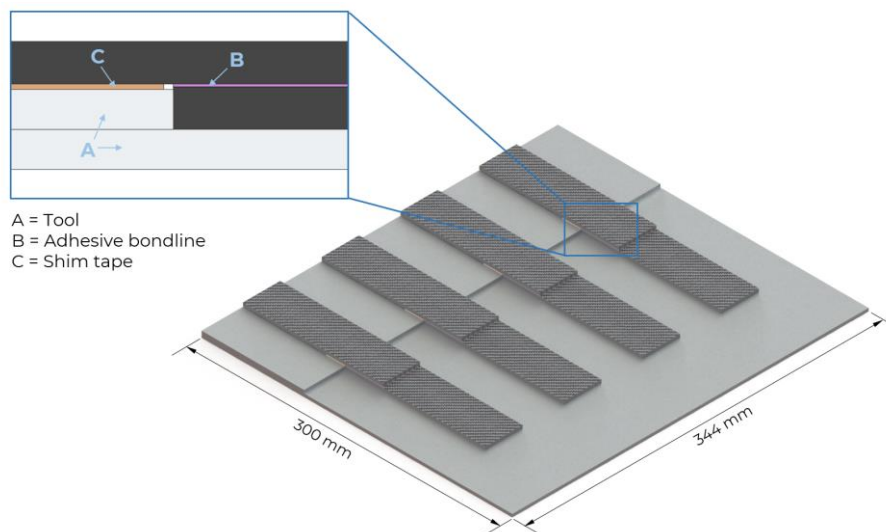
Figure 159 – Bonding jig setup
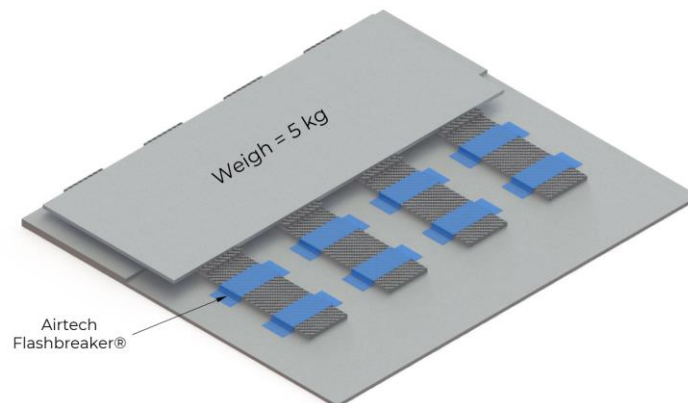
Figure 160 – Bonding jig setup during curing

The specimens were finally left to cure at 40°C for 24 hours inside a laboratory oven Venticell 404 standard [12]. All specimens were allowed to cool down to ambient temperature before testing.

Regarding the small-scale specimens, and in order to perform the ageing, it was also necessary to have a ø6.4 mm hole on both ends (Figure 155). This hole was made as a final step by laser-cutting ø6.4 mm holes on the steel tabs, and drilling another ø6.4 mm hole on the composite coupons (through the laser-cut holes) after bonding the pre-drilled steel tabs to them. No delamination nor chipping was visible using this method.

3.2.1.2. Results

The adhesion strength of the adhesive is carried out by the single lap joint test (ASTM 5961). Two flat laminates are glued together then a tensile machine measure the shear strength of the adhesive. Details are described in D2.4 "Connections in offshore structure".

Fatigue testing is a mechanical test where cyclic loading is applied on samples. It allows to identify degradation of the mechanical properties in a structure when exposed to fatigue and predict damages that can occur in real life. It can be used at coupon level as well as for real structure. One result generated from those tests is the S-N curve or fatigue limit. To build this curve, cyclic stresses are applied on the samples with a constant amplitude until its failure. In the FibreGY project, the fatigue study is performed by Ulim on the composite itself but also on connections, see "D2.2 Fatigue performance of composites".

The graphs given by both tests are reminded after.
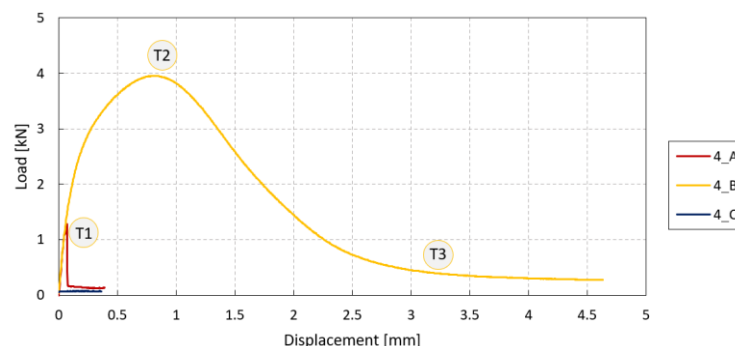
Figure 161 – Adhesion strength result by single lap joint, extract from D2.4
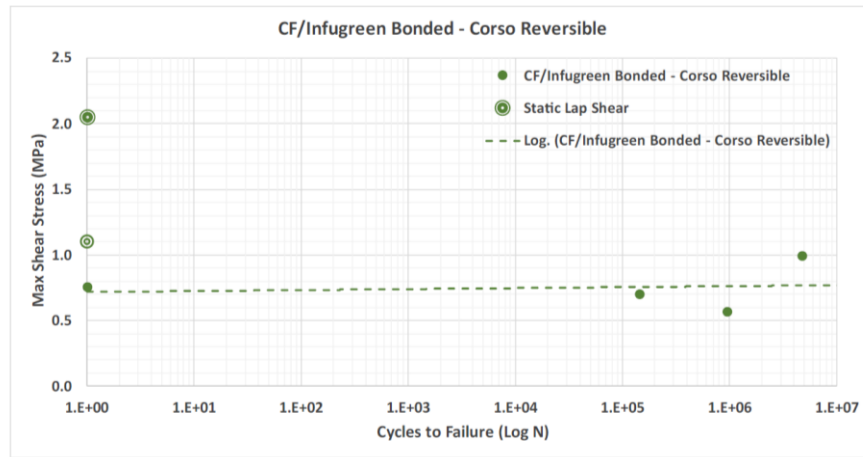
Figure 162 – S-N curve / fatigue result, from D2.2

For both test type, the responses give a cohesive failure: this means the result is representative to the real adhesive performance.

Two trends are emerging:

- The results are not repeatable: there is a lack in the coupons preparation. This is probably coming from the difficulty to mix and apply the adhesive; this issue is described in the previous subchapter.

- The mechanical responses are low compared to a traditional marine glue Araldite 2015-1 which has a maximum load of about 15 kN in single lap joint test and has a max shear stress of 9 MPa for 1 cycle in fatigue. Moreover, materials having this range of performance in static lap shear are not usually tested in fatigue as the results become not accurate.

To conclude, the reversible adhesive does not have the minimum required properties to be used for connections. What is more, trials on aged coupons (aged by static shear) are intended to be tested in fatigue in D2.2. Knowing the unaged specimen's performance, no better results are expected.

3.2.2. Behaviour at the end of life

Even though, the previous chapter showed the poor performance in service of the adhesive, the principle of the reversible adhesive is to allow a debonding of 2 glued parts. This technology, based on the sensitivity of the reversible adhesive to heat, has to be evaluated.

The ideal scenario is to disbound at the lowest temperature with the lowest latency. The couple temperature/duration instruction is 120°C for 1 hour.

3 scenarios are selected:

- 120°C, 1 h: the actual indications for the disbanding.

- 120°C, 30 min: testing less time is interesting as it is unknow the minimal time needed to disbound.

- 150°C, 30 min: in the case of a failure with the previous couple, increase the temperature may solve the issue.

3.2.2.1. Test description

The set-up employed to test the previous scenarios is to use the pull-off materials, see chapter 2.2.2.2.2.. Instead of testing the adhesion of the coating on the substrate, the dolly is directly glued to a substrate (non-coated) with the adhesive to be tested, here the reversible adhesive. The substrate was a laminate composed of carbon fibres and epoxy resin. The method of its preparation is the same as described in the chapter 3.2.1.1.

3.2.2.2. Result

After curing and leaving the samples so their temperature is the ambient one, the pulling of the dollies was performed. The next graph shows the force needed to disconnect the dolly from the substrate and the next pictures illustrated the weakest interface obtained.
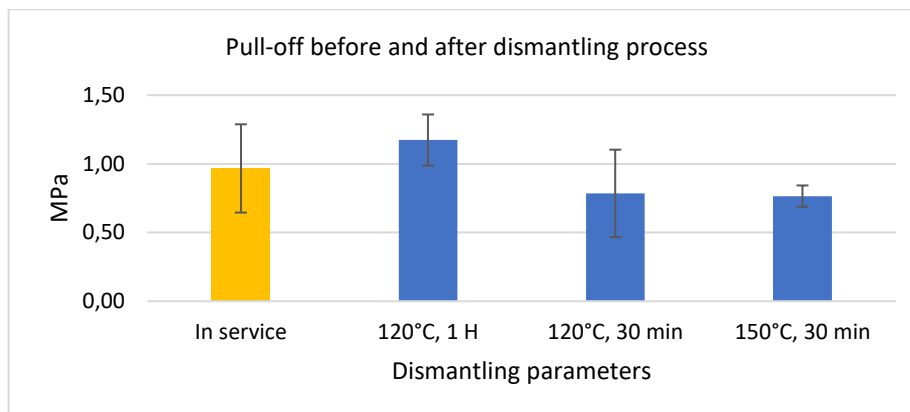
Figure 163 – Pul off results after dismantling
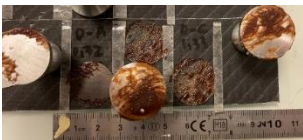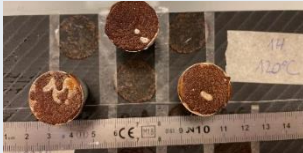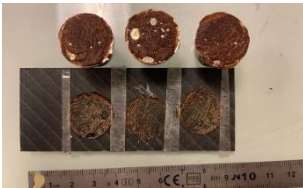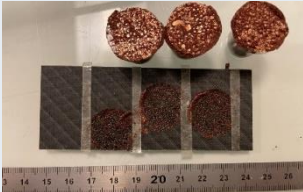
Dismantling parameters	Pictures	Weakest interface
In service (without dismantling process)	Figure 164 – Failure interface – No dismantling	Cohesive
120°C, 1H	Figure 165 – Failure interface – After 1H at 120°C	Cohesive
120°C, 30 min	Figure 166 – Failure interface – After 30 min at 120°C	Cohesive
150°C, 30 min	Figure 167 – Failure interface – After 30 min at 150°C	Cohesive

Table 40 – Interfaces obtained after different dismantling parameters

Based on the value on the graph and taking into account deviations, no significant decrease in the force is observed between the configuration in service and on the three conditions tested. However, on the pictures, the texture of the adhesive has significantly changed on the sample at 150°C, 30min compared to the

120°C/30min samples: the adhesive seems foamed. This can be read as the most appropriate couple of time and temperature to allow the debonding of the adhesive.
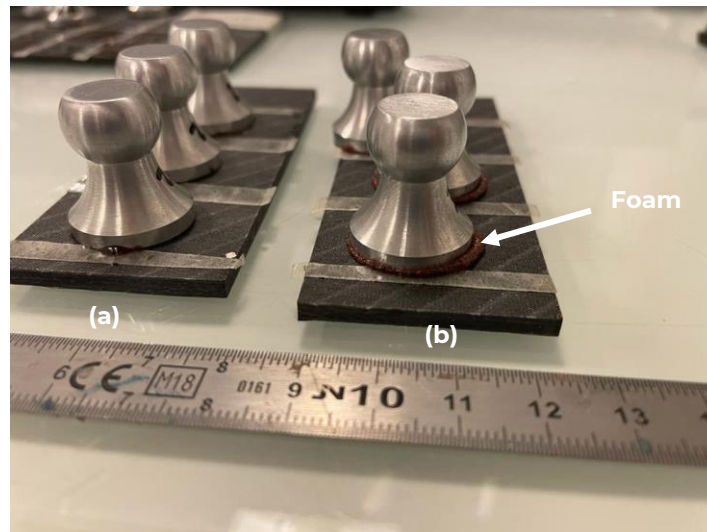
Figure 168 – Adhesive structure after dismantling process – (a)120°C, 30 min (b)150°C, 30 min

3.2.3. Application at a more representative scale

The previous chapter permits to validate a couple of time and temperature to disbound two pieces bound together with the reversible adhesive. To remind the goal of the use of it, the ideal scenario is to disconnect the assembly just with human force. To evaluate if this schema is possible, the dismantling capacities is evaluated at a more representative scale. It was chosen to work on a bonded area four time bigger than the one used for the previous testing in service. The preparation of the specimens is described in 3.2.1.1.

As seen before, the couple 150°C / 30 min gives a significant change in the adhesive structure by giving a sort of foam. It was decided to apply this to the larger component.

The result is that, the 2 parts are separated from each other after applying the dismantling parameters. No force was needed. The next Figure gives the interface obtained. It can be seen that the adhesive as the same texture of foam as observed earlier. Moreover, a thin layer of the adhesive seems to still adhere to one of the adherents.

Before dismantling	After dismantling
Figure 169 – Bonded large component without dismantling	Figure 170 – Dismantled larger component
Figure 171 – Bonded larger component without dismantling – bonded area	Figure 172 – Dismantled larger component – bonded area

Table 41 – Pictures of larger components

If the dismantling was not evident to demonstrate by the previous characterisation by pull-off, here it appears that it works.

To conclude, even though a couple has been found to permit the dismantling of two pieces bounded with the reversible adhesive, its difficulty during the preparation and application and also its performance in service that are too low makes it a bad candidate for offshore marine connections.

4. CONCLUSION

<u>Middle scale on dry coatings</u>

First of all, the coating has an impact on the structure. Indeed, the mechanical response of a coated laminate is different to a non-coated laminate. It cannot be said if it ameliorates or not the properties.

When looking at the coating itself, the dry coating performs as well as the liquid paint. From the real sea exposition on the Hempathane 55210 applied on Infugreen by infusion or liquid paint, the behaviour on colour, gloss, visual aspect is the same. From the immersion in the sea, both dry and liquid paint didn't act as a fouling barrier.

From the point of view of adhesion, dry coatings adhere better to the composite substrate even after exposition to real sea environment.

From the protection point of view, dry coatings protect the composite against water as well as the liquid paint. Against UV aggression and corrosion atmosphere, dry coatings can act as a protection but it is very dependant of the choice of the coating (transformed) and the nature of the composite. Comparing the Hempathane 55210 form: liquid and dry, the liquid performs better. At this stage, we assume that it is thanks to the primer underneath more than the coating form.

So even if the coatings have a good visual aspect after aging, that not means that the composite material has not be damaged.

Finally, integrate sensors at the backing of the dry coatings is feasible. The key parameters to keep in mind for further investigations are the thickness of the sensors, their robustness to the process of manufacturing the dry coating, their resistance to the vacuum infusion process and last but not least, their usability to collect data.

<u>Middle scale tests on connections</u>

Regarding the work performed on connections, particularly at subcomponent level, the test campaign results are extremely relevant for further development in designing and validating connections with FRP substrates, especially bolted composite joints. Tension-tension high-cycle fatigue tests were conducted on two subcomponent specimens at room temperature up to 500,000 cycles. Progressive failure was observed for both specimens, caused by broken bolts and elongated/oversized holes due to wear and tear from the combined friction and stress around the holes. Additional interesting observations included stripped threads on some bolts, compacted resin particles near the FRP holes, and metallic shavings around the holes on the stainless-steel sleeves. Thermographic analysis concluded that the exterior surface temperature of the connection did not exceed 25°C; however, a 2°C increase was observed from the test's beginning to 240 minutes later. Areas with higher temperature concentration were also identified.

Although limited to a small number of specimens, as foreseen in the building block approach, these conclusions are important for further validating predictive models. For this reason, they have also been provided to the partners responsible for developing numerical models, offering practical implications for future work and revealing critical factors influencing the performance and durability of connections as the one studied. Pending further, more in-depth future analyses, the reported work has improved understanding of the damage mechanisms in bolted composite joints and leads to more reliable connection design when using such composite laminates under the studied load and environmental conditions. In fact, one key conclusion was that with an increased number of cycles, clamping pressure is reduced (bolts become loose), and load transfer from friction forces decreases, shifting to the bolts instead. This occurs while holes become elongated from wear of the composite matrix, ultimately leading to bolt failure. No visible fibre failure was found in the tested specimens.

Regarding the use of the reversible adhesive, its initial adhesion and performance are poor. Then, its use is questionable, even though the principle of dismantling works.

5. REFERENCES

[1]   M. Bruyneel, P. Jetteur, J. P. Delsemme, S. Siavoshani, and A. Cheruet, "Modeling and simulating progressive failure in composite structures for automotive applications," SAE Tech. Pap., vol. 1, no. July, 2014, doi: 10.4271/2014-01-0962.

[2]   CORSO et al., "FIBREGY D2.3 (WP2): Environmental protection of composites," 2022.

[3]   https://www.sharklet.com/

[4]   https://sensing.konicaminolta.asia/what-is-cie-1976-lab-color-space/

[5]   Corger D. La colorimétrie, décembre 2018

[6]   Zoltek Corporation, "Technical Datasheet ZOLTEK TM PX35 Multi-Directional Fabrics Technical Datasheet ZOLTEK TM PX35 Multi-Directional Fabrics," vol. 300, pp. 1–2, [Online]. Available: http://zoltek.com/wp-content/uploads/2016/01/PX35-MD-Fabrics.pdf.

[7]   Sicomin, "SR InfuGreen 810 Technical Datasheet." pp. 1–9, 2017.

[8]   A. International, "ASTM D5961: Standard Test Method for Bearing Response of Polymer Matrix Composite Laminates," 2017. doi: 10.1520/D5961_D5961M-13.

[9]   J. V Cardoso, P. V Gamboa, and A. P. Silva, "Effect of surface pre-treatment on the behaviour of adhesively-bonded CFRP T-joints," Eng. Fail. Anal., vol. 104, pp. 1188–1202, 2019, doi: https://doi.org/10.1016/j.engfailanal.2019.05.043.

[10]   L. J. Hart-Smith, "Adhesively Bonded Joints in Aircraft Structures BT - Handbook of Adhesion Technology," L. F. M. da Silva, A. Öchsner, and R. D. Adams, Eds. Berlin, Heidelberg: Springer Berlin Heidelberg, 2011, pp. 1101–1147.

[11]   INEGI et al., "FIBREGY D2.4 (WP2): Connections in offshore structures," 2022.

[12]   Venticell, "Venticell - Laboratory Ovens with Forced Air Convention," no. Rj 45.

[13]   D. Gleich, M. Van tooren, and A. Beukers, "Analysis and evaluation of bondline thickness effects on failure load in adhesively bonded structures," J. Adhes. Sci. Technol. - J ADHES SCI TECHNOL, vol. 15, pp. 1091–1101, Jan. 2001, doi: 10.1163/156856101317035503.

[14]   Rotec, "Tubulated Flanges." [Online]. Available: https://www.rotecgrp.com/products/flanges/tubulated-flanges.

[15]   Merco Service, "Torque Specifications." [Online]. Available: http://www.melco-service.com/docs/AMAYA_OS_v10/AMAYA/Torque_Specifications.htm.

[16]   efunda, "High-Cycle Fatigue." [Online]. Available: https://www.efunda.com/formulae/solid_mechanics/fatigue/fatigue_highcycle.cfm.

[17]   K. Ravikumar, R. Subbiah, N. Ranganathan, J. Bensingh, A. Kader, and S. K. Nayak, "A review on fatigue damages in the wind turbines: Challenges in determining and reducing fatigue failures in wind turbine blades," Wind Eng., vol. 44, no. 4, pp. 434–451, May 2019, doi: 10.1177/0309524X19849851.

[18]   J. C. Marín, A. Barroso, F. París, and J. Cañas, "Study of fatigue damage in wind turbine blades," Eng. Fail. Anal., vol. 16, no. 2, pp. 656–668, 2009, doi: 10.1016/j.engfailanal.2008.02.005.

[19]   International Organization for Standardization, "ISO 13003: Fibre-reinforced plastics — Determination of fatigue properties under cyclic loading conditions." p. 17, 2003.

[20]   J. Schön, "7 - Fatigue of bolted composite joints," in Woodhead Publishing Series in Composites Science and Engineering, P. Camanho and L. B. T.-C. J. and C. Tong, Eds. Woodhead Publishing, 2011, pp. 245–256.

[211   testo, "testo IRSoft v5.0 - PC software." [Online]. Available: https://www.testo.com/en-UK/software-testo-irsoft/p/0501-8809.

[22]   M. Kawai and T. Taniguchi, "Off-axis fatigue behavior of plain weave carbon/epoxy fabric laminates at room and high temperatures and its mechanical modeling," Compos. Part A Appl. Sci. Manuf., vol. 37, no. 2, pp. 243–256, 2006, doi: https://doi.org/10.1016/j.compositesa.2005.07.003.

[23]   H. Tang, T. Nguyen, T. Chuang, J. Chin, F. Wu, and J. Lesko, "Temperature Effects on Fatigue of Polymer Composites," Jul. 2001.

[24]   H. Mivehchi and A. Varvani-Farahani, "The effect of temperature on fatigue strength and cumulative fatigue damage of FRP composites," Procedia Eng., vol. 2, no. 1, pp. 2011–2020, 2010, doi: https://doi.org/10.1016/j.proeng.2010.03.216.

6. ANNEX

Annex 1 – Samples prepared for D2.3 "Environmental protection of composites" test campaign

Coating	Composite Resin	Pictures
Dry coating A: Hempathane 55210	Infugreen	Figure 173 – Infugreen infused with dry coating Hempathane 55210
Dry coating B: Alexit 471	Elium	Figure 174 – Elium infused with dry coating Alexit 471
Dry coating C: Alexit 411-77	Infugreen	Figure 175 – Infugreen infused with dry coating Alexit 411-77

	Elium	
		Figure 176 – Elium infused with dry coating Alexit 411-77
Liquid paint: Hempathane 55210	Infugreen	
		Figure 177 – Infugreen painted with liquid Hempathane 55210
	Elim	
		Figure 178 – Elium painted with liquid Hempathane 55210

Table 42 - Samples prepared for D2.3 "Environmental protection of composites" test campaign

Annex 2 – Bending tests overview

This annex contains a description of the work performed in Task 6.1 during months 1-30 of the FibreGY project encompassing an extensive experimental test campaign involving flexural testing of coated composite specimens under various ageing conditions and the associated results. The main objectives addressed in this document can be summarised as follows:

- To present an overview of the experimental test campaign conducted to study the effect of ageing on the mechanical response of coated Glass-Fibre (GF) reinforced laminates under static flexural loading.

- To describe the methodology employed for extensive experimental testing campaign conducted to evaluate the flexural behaviour of the coated composites.

- To analyse and present the data obtained from the flexural experiments to understand the effect of ageing on flexural response of specimens.

In Task 2.3 of this project, the rationale behind selection of different coatings was described. Further the ageing conditions were explained in the report D2.3. The mechanical response of a few Ultra-violet (UV) aged specimens was discussed in D2.3. In the current report the mechanical response of all the Un-aged, Salt Sprayed and UV-aged specimens is described. An overview of the test matrix for the flexural testing of coated specimens (including the ones reported in D2.3) have been shown below in Table 43. For completeness of this report, the results obtained in Task 2.1 for the unaged controlled (without coating) samples are also provided along with coated Un-aged results.

Table 43 - Overview of the specimen types tested under different ageing conditions

Sr. No.	Material ([0°]$_n$ and [90°]$_n$)	Aging Environment
1.	Laminate- Glass Fibre- InfuGreen Coating- HEMP/55210 Dry	Un-aged Salt Spray UV- aged
2.	Laminate: Glass Fibre-Elium Coating: ALEXIT/471 Dry	
3.	Laminate: Glass Fibre-InfuGreen Coating- ALEXIT/411-77	
4.	Laminate: Glass Fibre-Elium Coating: ALEXIT/411-77	
5.	Laminate- Glass Fibre-InfuGreen Coating- HEMP/55210 Liquid Paint	
6.	Laminate: Glass Fibre-Elium Coating: HEMP/55210 Liquid Paint	

FIBREGY

This project has received funding from the European Union's Horizon 2020 research and innovation programme under grant agreement No 952966.

1. TEST CAMPAIGN

   a. Test Matrix

The mechanical tests were performed under 3-pt flexural loading for at least 3 specimens under each combination of laminate/coating and the ageing type. A detailed tabular listing of total specimens tested under each category is provided in Table 44.

Table 44 - Overall test campaign matrix showing the number of specimens tested for mechanical performance for each laminate and coating type under different ageing conditions

Sr. No.	Material	Unaged		Salt Spray Aged		UV Aged	
		0°	90°	0°	90°	0°	90°
1.	Laminate- Glass Fibre- InfuGreen Coating- HEMP/55210 Dry	3	3	4	3	4	5
2.	Laminate: Glass Fibre-Elium Coating: ALEXIT/471 Dry	3	3	3	3	4	5
3.	Laminate: Glass Fibre-InfuGreen Coating- ALEXIT/411-77	3	4	3	3	3	3
4.	Laminate: Glass Fibre-Elium Coating: ALEXIT/411-77	3	4	3	3	4	3
5.	Laminate- Glass Fibre-InfuGreen Coating- HEMP/55210 Liquid Paint	4	4	3	3	4	5
6.	Laminate: Glass Fibre-Elium Coating: HEMP/55210 Liquid Paint	3	3	3	3	4	5
	Total Samples Tested (126)	19	21	19	18	23	26

   b. Flexural Test Procedure

The samples were tested in a three-point-bending loading mode in accordance with ISO14125. The samples were tested on a Tinius Olsen electro-mechanical straining frame with load cell of 5 kN rating for Flexural 0° and 1 kN for Flexural 90° specimens. A displacement transducer was used to record the deflection of the central region of the specimens. The tests were conducted under displacement control with a displacement rate of 1 mm/min. The roller diameters at the load nose and support points were 10 mm and 4 mm respectively. The next figure depicts a sample being tested under 3-point loading. Data reduction was performed for the calculations of the required properties. The following results were extracted from the Flexure 0° and 90° test data, viz. Flexural Strength (σ_f) at failure initiation, Flexural Strength (σ_{max}) at maximum load, Flexural Modulus (E$_f$), Flexural strain (ε_f) at failure initiation, Flexural strain (ε_f) at maximum load. The strain to failure (ε_f) is the strain at which a first sign of load drop is observed in the mechanical response curves. The calculations were performed using the following formulae,

$$Flexural\ Strength\ (\sigma) = \frac{3 \times F \times L}{2 \times b \times h^2}$$

$$Flexural\ Strain\ (\varepsilon) = \frac{6 \times s \times h}{L^2}$$

$$Flexural\ Modulus\ (E) = \frac{(\sigma'' - \sigma')}{(\varepsilon'' - \varepsilon')}$$

Where, F is the applied load, L is the span, b is the sample width, h is the sample thickness, s is the deflection, σ'' is the stress at which strain (ε'') is 0.0025 and σ' is the stress at which strain (ε') is 0.0005. The strength/load at failure and the strain at failure are reported at the point of initiation of the failure in the specimen.
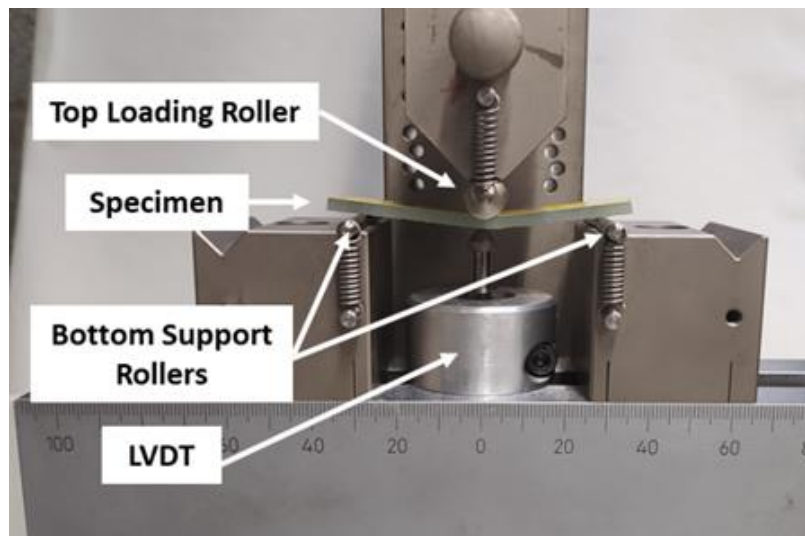
Figure 179 - Flexure test sample under 3-pt bend loading configuration

2. RESULTS

A tabulated summary of the average mechanical properties obtained is presented in the next tables for all 0° and 90° specimens respectively. Following sections present the average results for Un-aged, Salt Sprayed and UV-aged specimens separately. The appendix Appendix-A, Appendix-B, and Appendix-C presents the detailed tabulated results for each specimen tested under Un-aged, Salt Sprayed and UV-aged condition.

Table 45 - Tabular summary of average results obtained for all 0° specimens

Sr. No.	Material (0°)	Un-aged		Salt Spray Aged		UV-aged	
		Strength (MPa)	Modulus (GPa)	Strength (MPa)	Modulus (GPa)	Strength (MPa)	Modulus (GPa)
1.	Laminate- Glass Fibre-InfuGreen Coating- HEMP/55210 Dry	1065.8 (24.5)	32.4 (0.5)	813.3 (39.4)	28.5 (1.3)	872.2 (90.5)	25.9 (1.6)
2.	Laminate: Glass Fibre-Elium Coating: ALEXIT/471 Dry	1222.4 (29.3)	34.4 (1.0)	1062.8 (16.7)	32.0 (1.4)	1080.5 (41.7)	29.5 (2.0)
3.	Laminate: Glass Fibre-InfuGreen Coating- ALEXIT/411-77	973.2 (85.0)	29.4 (1.2)	940.1 (72.4)	29.5 (1.0)	934.3 (63.2)	30.2 (0.6)
4.	Laminate: Glass Fibre-Elium Coating: ALEXIT/411-77	1105.9 (37.9)	30.9 (0.9)	914.1 (30.6)	29.2 (1.1)	978.9 (99.7)	26.6 (5.1)
5.	Laminate- Glass Fibre-InfuGreen Coating- HEMP/55210 Liquid Paint	852.9 (139.0)	30.7 (1.2)	838.7 (27.4)	29.8 (1.7)	929.5 (47.8)	28.8 (1.6)
6.	Laminate: Glass Fibre-Elium Coating: HEMP/55210 Liquid Paint	1087.3 (35.2)	34.6 (0.7)	1054.5 (76.5)	35.6 (0.5)	1142.3 (36.8)	32.2 (1.5)
7.	Laminate: Glass Fibre-Elium Coating: No Coating	939.5 (51.3)	30.3 (1.8)	-	-	-	-
8.	Laminate: Glass Fibre-InfuGreen Coating: No Coating	1075 (61.8)	39.3 (1.8)	-	-	-	-

Note-Standard deviation in parenthesis.

Table 46 - Tabular summary of average results obtained for all 90° specimens

Sr. No.	Material (90°)	Un-aged		Salt Spray Aged		UV-aged	
		Strength (MPa)	Modulus (GPa)	Strength (MPa)	Modulus (GPa)	Strength (MPa)	Modulus (GPa)
1.	Laminate- Glass Fibre-InfuGreen Coating- HEMP/55210 Dry	60.8 (2.7)	11.2 (0.3)	34.7 (0.5)	9.7 (0.1)	56.3 (4.3)	9.2 (0.5)
2.	Laminate: Glass Fibre-Elium Coating: ALEXIT/471 Dry	53.9 (7.3)	11.3 (0.6)	24.6 (1.5)	8.8 (0.9)	38.0 (1.4)	9.6 (0.5)
3.	Laminate: Glass Fibre-InfuGreen Coating- ALEXIT/411-77	56.5 (2.4)	10.7 (0.3)	33.9 (5.9)	9.9 (0.6)	55.7 (1.9)	10.3 (0.4)

Sr. No.	Material						
4.	Laminate: Glass Fibre-Elium Coating: ALEXIT/411-77	49.0 (3.25)	10.8 (0.1)	38.3 (1.1)	10.0 (0.1)	49.5 (9.8)	10.4 (0.1)
5.	Laminate- Glass Fibre-InfuGreen Coating- HEMP/55210 Liquid Paint	60.8 (5.4)	9.9 (0.4)	36.7 (1.3)	9.5 (0.4)	62.0 (3.5)	10.1 (0.2)
6.	Laminate: Glass Fibre-Elium Coating: HEMP/55210 Liquid Paint	39.0 (7.3)	10.0 (0.3)	41.9 (5.9)	10.1 (1.2)	40.1 (4.5)	9.6 (0.3)
7.	Laminate: Glass Fibre-Elium Coating: No Coating	70.6 (4.4)	11.1 (0.8)	-	-	-	-
8.	Laminate: Glass Fibre-InfuGreen Coating: No Coating	58.4 (2.2)	9.1 (0.4)	-	-	-	-

a. Un-aged Specimen

This section presents the results obtained for Un-aged specimens. Next tables present the tabulated summary of average values obtained for 0° and 90° Un-aged specimens. Next figures depict the Flexural response curves obtained for tested specimens and show the post-test images of the 0° and 90° specimens respectively. A more detailed information about each tested specimen is presented in Appendix A.

a.1. 0° Un-aged Specimen

The key observations are summarised below:
- Linear stress-strain response curves observed.

- Rapid drop in load towards the end of the test.

- The point of first drop in load in the curve is being reported as the failure load and corresponding strain is reported as the failure strain. For many of the 0° samples the maximum load and the failure load are very close or equal. However, it is recommended to compare both for different types of specimens.

Table 47 - Tabular summary of results of Un-aged 0° tests

Sr. No.	Material	No. of samples	Load at Failure (kN))	Failure Strength σ_f (MPa)	Flexural Modulus, E_f (GPa)	Strain-at-failure ε_f (%)	Max Load(kN)	Max Strength σ_{max} (MPa)	Strain at Max Load ε_{max} (%)
1.	Laminate- Glass Fibre-InfuGreen Coating- HEMP/55210 Dry	3	1.988 (0.048)	1065.8 (24.5)	32.4 (0.5)	3.43 (0.13)	2.009 (0.044)	1076.8 (21.8)	3.49 (0.11)
2.	Laminate: Glass Fibre-Elium Coating: ALEXIT/471 Dry	3	2.144 (0.033)	1222.4 (29.3)	34.4 (1.0)	3.89 (0.15)	2.150 (0.030)	1226.2 (28.9)	3.89 (0.15)
3.	Laminate: Glass Fibre-InfuGreen Coating-	3	2.003 (0.154)	973.2 (85.0)	29.4 (1.2)	3.32 (0.31)	2.028 (0.143)	984.7 (74.0)	3.39 (0.24)

	ALEXIT/411-77							
4.	Laminate: Glass Fibre-Elium Coating: ALEXIT/411-77	3	2.130 (0.079)	1105.9 (37.9)	30.9 (0.9)	3.69 (0.11)	2.136 (0.077)	1109.2 (38.2)	3.72 (0.07)
5.	Laminate-Glass Fibre-InfuGreen Coating-HEMP/55210 Liquid Paint	4	1.764 (0.195)	852.9 (139.0)	30.7 (1.2)	2.81 (0.22)	1.814 (0.146)	875.9 (116.3)	2.76 (0.24)
6.	Laminate: Glass Fibre-Elium Coating: HEMP/55210 Liquid Paint	3	1.918 (0.116)	1087.3 (35.2)	34.6 (0.7)	3.25 (0.21)	1.934 (0.099)	1096.4 (26.4)	3.37 (0.15)
7.	Laminate: Glass Fibre-Elium Coating: No Coating	6	1.436 (0.092)	939.5 (51.3)	30.3 (1.8)	3.31 (0.18)	-	-	-
8.	Laminate: Glass Fibre-InfuGreen Coating: No Coating	7	1.759 (0.108)	1075 (61.8)	39.3 (1.8)	2.75 (0.17)	-	-	-

Note-Standard deviation in parenthesis.
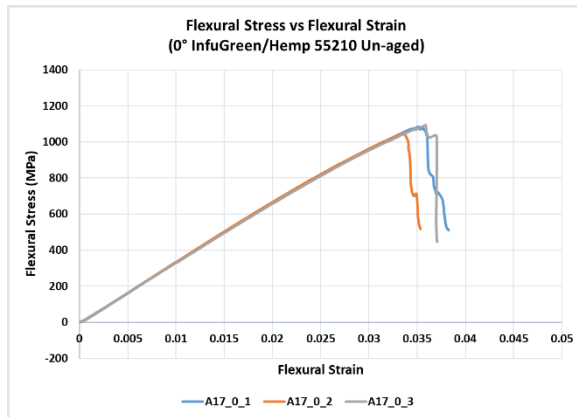
(i)
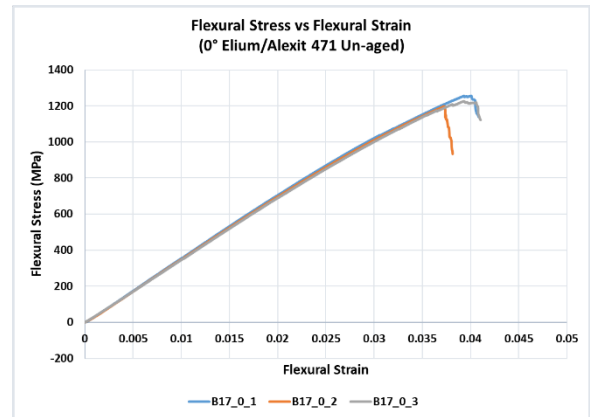
(ii)
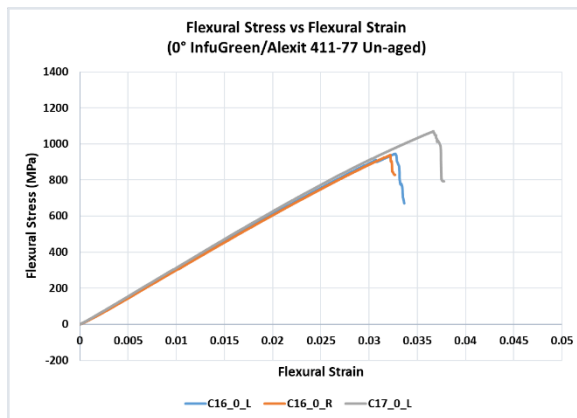
(iii)
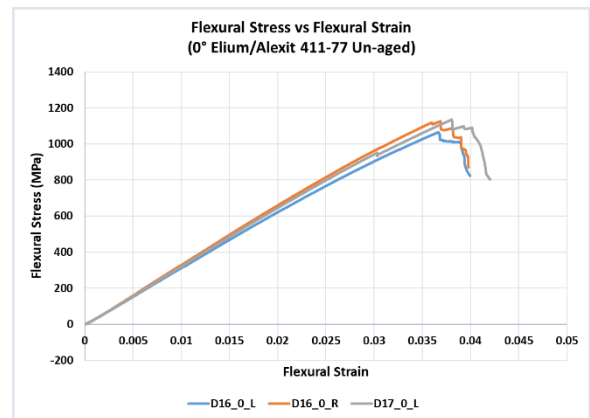
(iv)

(v)

(vi)
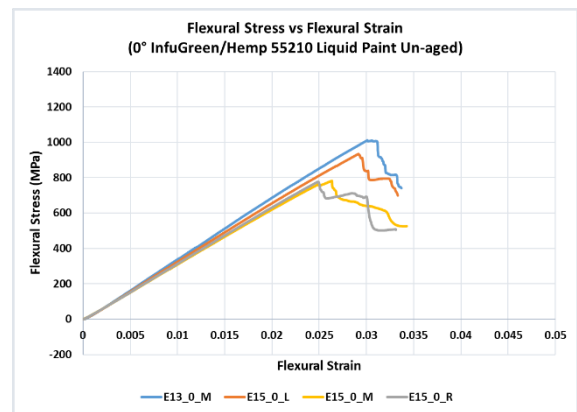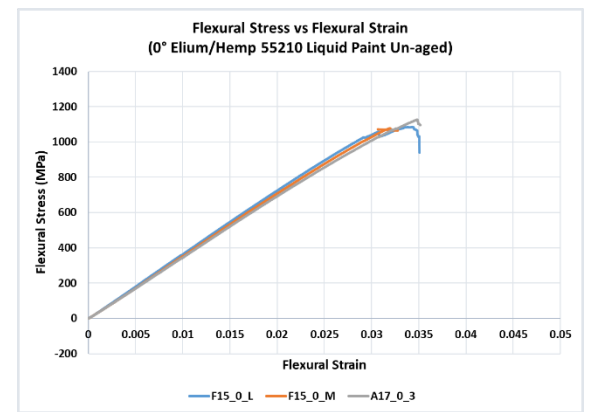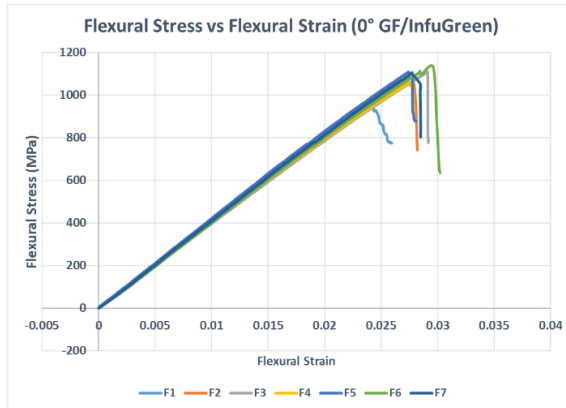
(vii)
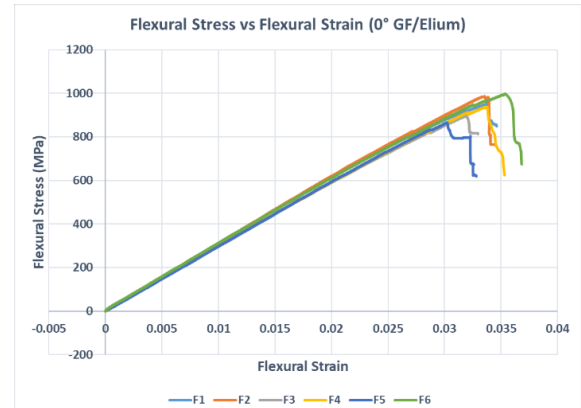
(viii)

Figure 180 - Flexural stress v flexural strain plots for Un-aged 0° (i) InfuGreen/Hemp 55210 (ii) Elium/Alexit 471 (iii) InfuGreen/Alexit 411-77 (iv) Elium/Alexit 411-77 (v) InfuGreen/Hemp 55210 Liquid Paint (vi) Elium/Hemp 55210 Liquid Paint (vii) GF/InfuGreen (No Coating) (viii) GF/Elium Control (No Coating)

(i)

(ii)

**0° Compressive Side
GF InfuGreen/Alexit 411-77 Un-aged**

**0° Tensile Side
GF InfuGreen/Alexit 411-77 Un-aged**

(iii)

**0° Compressive Side
GF Elium/Alexit 411-77 Un-aged**

**0° Tensile Side
GF Elium/Alexit 411-77 Un-aged**

(iv)

**0° Compressive Side
GF InfuGreen/Hemp 55210
Liquid Paint Un-aged**

**0° Tensile Side
GF InfuGreen/Hemp 55210
Liquid Paint Un-aged**
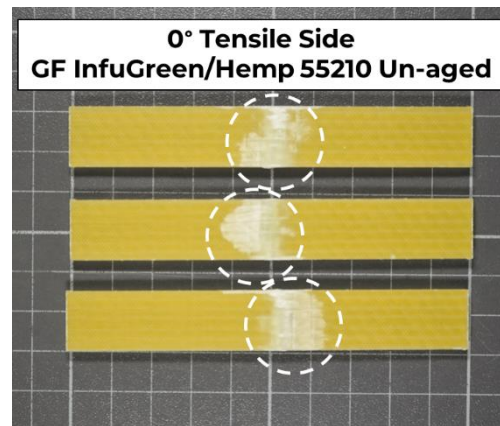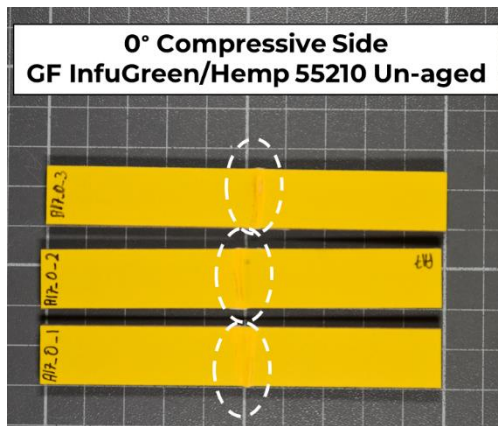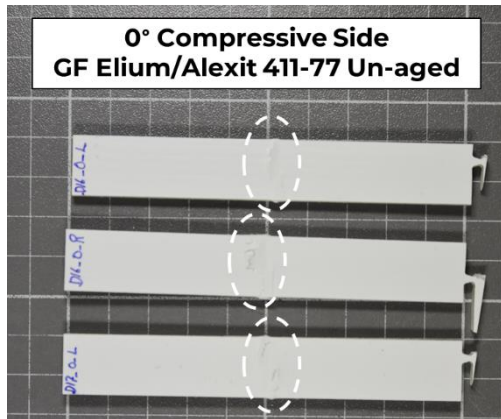
(v)

(vi)

Figure 181 - Post-test specimen images for Un-aged 0° (i) InfuGreen/Hemp 55210 (ii) Elium/Alexit 471 (iii) InfuGreen/Alexit 411-77 (iv) Elium/Alexit 411-77 (v) InfuGreen/Hemp 55210 Liquid Paint (vi) Elium/Hemp 55210 Liquid Paint

a.2. 90° Un-aged Specimen

The key observations are summarised below:

- Bilinear stress-strain response observed in majority of 90° specimens.
- For all the 90° specimens, typically small drops in load observed at various stages initiating at lower strains. For many of the specimens, these drops are very small and not visibly evident in the stress-strain plots. **Thus, this point may not be a true representation of failure. Hence a comparison of maximum load is also recommended between various tested specimen types.** Further, as the test progresses multiple small drops are observed and with a rapid drop towards the end of the test at higher strains.
- Failure load is reported as the load where the 1st drop in load is observed. This typically lies closer to the end of 1st linear portion of the curve. The failure strain and load are reported corresponding to this point in the curve.
- Further the max load is reported as the maximum load observed throughout the curve and the corresponding strain is reported as strain at maximum load.

Table 48 - Tabular summary of results of Un-aged 90° tests

Sr. No.	Material	No. of samples	Load at Failure (kN))	Failure Strength (MPa)	Flexural Modulus, E_f (GPa)	Strain-at-failure (%)	Max Load(kN)	Max Strength (MPa)	Strain at Max Load (%)
1.	Laminate-Glass Fibre-InfuGreen Coating-HEMP/55210 Dry	3	0.117 (0.005)	60.8 (2.7)	11.2 (0.3)	0.58 (0.05)	0.133 (0.003)	69.1 (1.7)	1.38 (0.17)
2.	Laminate: Glass Fibre-Elium Coating: ALEXIT/471 Dry	3	0.100 (0.012)	53.9 (7.3)	11.4 (0.6)	0.60 (0.10)	0.135 (0.004)	72.3 (1.6)	1.67 (0.17)
3.	Laminate: Glass Fibre-InfuGreen Coating-ALEXIT/411-77	3	0.115 (0.005)	56.5 (2.4)	10.7 (0.3)	0.56 (0.02)	0.133 (0.008)	65.7 (3.7)	1.33 (0.13)
4.	Laminate: Glass Fibre-Elium Coating: ALEXIT/411-77	4	0.096 (0.008)	49.0 (3.5)	10.8 (0.1)	0.52 (0.06)	17.66 (0.07)	0.131 (0.008)	1.65 (0.21)
5.	Laminate-Glass Fibre-InfuGreen Coating-HEMP/55210 Liquid Paint	4	0.116 (0.014)	60.8 (5.4)	9.9 (0.4)	0.72 (0.14)	0.122 (0.010)	64.1 (3.1)	0.96 (0.18)
6.	Laminate: Glass Fibre-Elium Coating:	3	0.070 (0.014)	39.0 (7.3)	10.0 (0.3)	0.54 (0.21)	0.097 (0.011)	54.0 (5.0)	1.34 (0.31)

	HEMP/55210 Liquid Paint							
7.	Laminate: Glass Fibre-Elium Coating: No Coating	5	0.117 (0.007)	70.6 (4.4)	11.1 (0.8)	0.72 (0.07)	-	-	-
8.	Laminate: Glass Fibre-InfuGreen Coating: No Coating	6	0.116 (0.004)	58.4 (2.2)	9.1 (0.4)	0.61 (0.05)	-	-	-

Note-Standard deviation in parenthesis.

(i)

(ii)

(iii)

(iv)

This project has received funding from the European Union's Horizon 2020 research and innovation programme under grant agreement No 952966.

(v)

(vi)
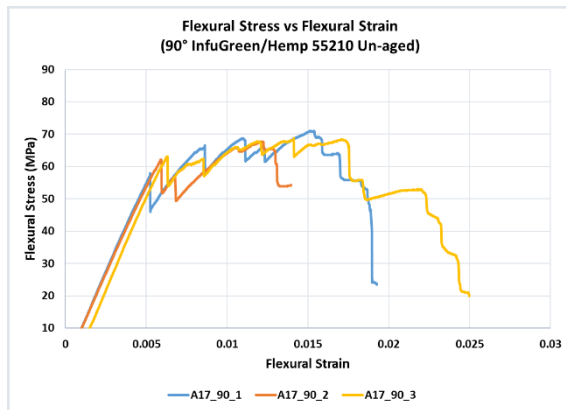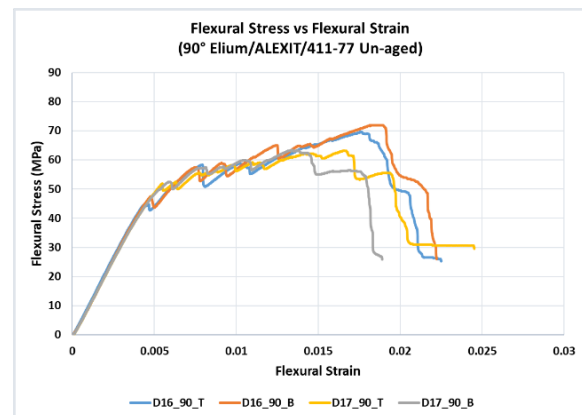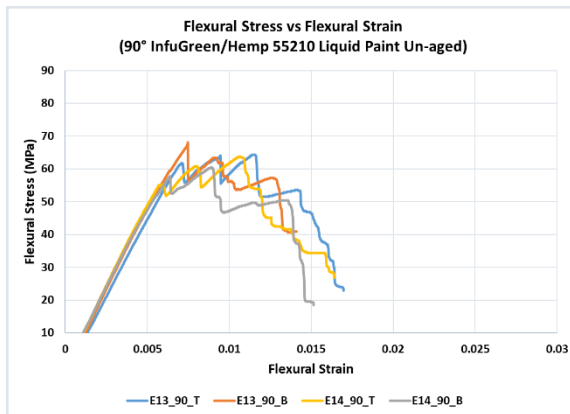
(vii)
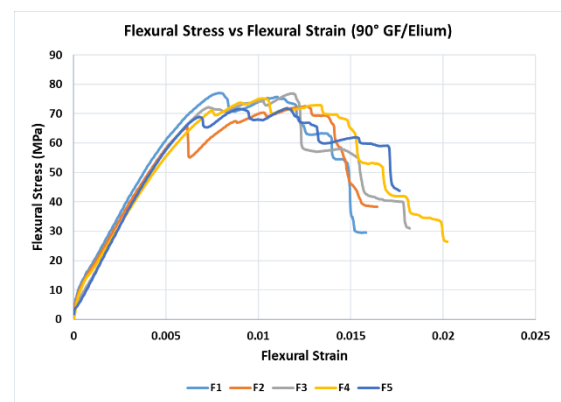
(viii)

Figure 182 - Flexural stress v flexural strain plots for Un-aged 90° (i) InfuGreen/Hemp 55210 (ii) Elium/Alexit 471 (iii) InfuGreen/Alexit 411-77 (iv) Elium/Alexit 411-77 (v) InfuGreen/Hemp 55210 Liquid Paint (vi) Elium/Hemp 55210 Liquid Paint (vii) GF/InfuGreen (No Coating) (viii) GF/Elium Control (No Coating)

(i)

90° Compressive Side
GF Elium/Alexit 471 Un-aged

90° Tensile Side
GF Elium/Alexit 471 Un-aged

(ii)

90° Compressive Side
GF InfuGreen/Alexit 411-77 Un-aged

90° Tensile Side
GF InfuGreen/Alexit 411-77 Un-aged

(iii)

90° Compressive Side
GF Elium/Alexit 411-77 Un-aged

90° Tensile Side
GF Elium/Alexit 411-77 Un-aged
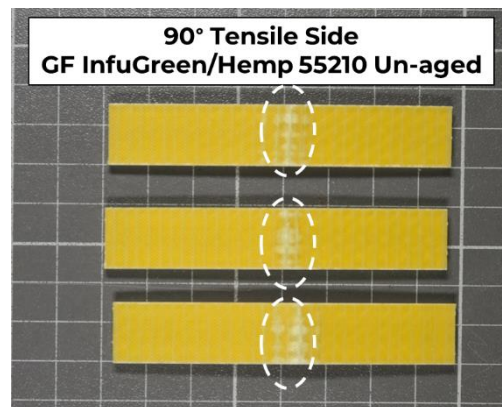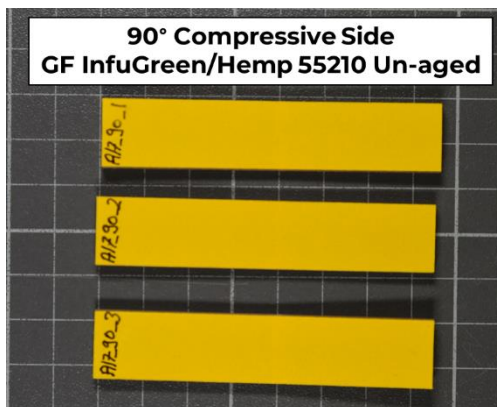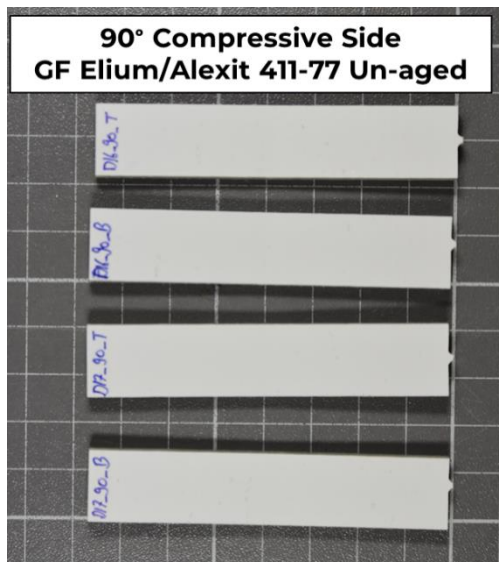
(iv)
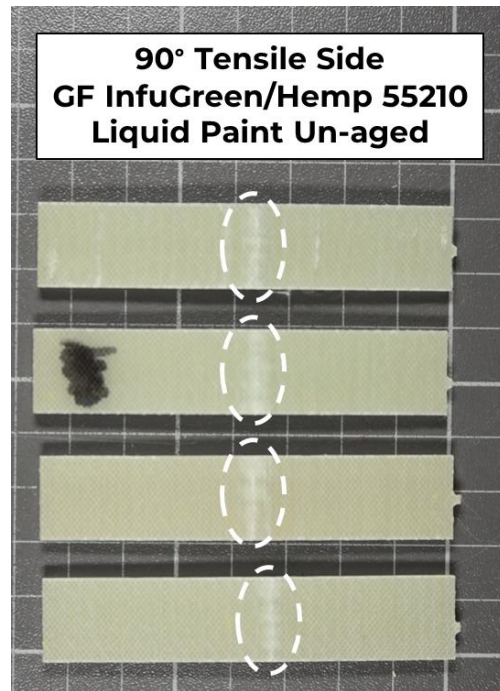
(v)
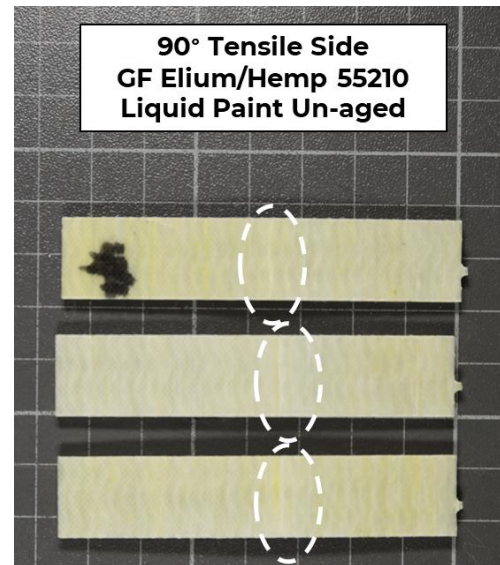
(vi)

Figure 183 - Post-test specimen images for Un-aged 90° (i) InfuGreen/Hemp 55210 (ii) Elium/Alexit 471 (iii) InfuGreen/Alexit 411-77 (iv) Elium/Alexit 411-77 (v) InfuGreen/Hemp 55210 Liquid Paint (vi) Elium/Hemp 55210 Liquid Paint

b. Salt-Spray Specimen

This section presents the results obtained for Un-aged specimens. Next tables present the tabulated summary of average values obtained for 0° and 90° Un-aged specimens. Next figures depict the Flexural response curves obtained for tested specimens and show the post-test images of the 0° and 90° specimens respectively. A more detailed information about each tested specimen is presented in Appendix B.

b.1. 0° Salt-Spray Specimen

The key observations are summarised below:
- Linear stress-strain response curves observed.
- Rapid drop in load towards the end of the test.
- The point of first drop in load in the curve is being reported as the failure load and corresponding strain is reported as the failure strain. For many of the 0° samples the maximum load and the failure load are very close or equal. However, it is recommended to compare the both for different types of specimens

Table 49 - Tabular summary of results of Salt-spray 0° tests

Sr. No.	Material	No. of samples	Load at Failure (kN))	Failure Strength (MPa)	Flexural Modulus, E_f (GPa)	Strain-at-failure (%)	Max Load(kN)	Max Strength (MPa)	Strain at Max Load (%)
1.	Laminate-Glass Fibre-InfuGreen Coating-HEMP/55210 Dry	4	1.636 (0.067)	813.3 (39.4)	28.5 (1.3)	2.77 (0.10)	1.637 (0.068)	813.9 (40.2)	2.77 (0.10)
2.	Laminate: Glass Fibre-Elium Coating: ALEXIT/471 Dry	3	1.807 (.034)	1062.8 (16.7)	32.0 (1.4)	3.43 (0.05)	1.824 (0.027)	1072.8 (20.3)	3.57 (0.25)
3.	Laminate: Glass Fibre-InfuGreen Coating-ALEXIT/411-77	3	1.827 (0.108)	940.1 (72.4)	29.5 (1.0)	3.21 (0.23)	1.836 (0.105)	944.3 (71.4)	3.23 (0.23)
4.	Laminate: Glass Fibre-Elium Coating: ALEXIT/411-77	3	1.686 (0.083)	914.1 (30.6)	29.2 (1.1)	3.11 (0.14)	1.788 (0.159)	969.2 (81.9)	3.41 (0.39)
5.	Laminate-Glass Fibre-InfuGreen Coating-HEMP/55210 Liquid Paint	3	1.729 (0.094)	838.7 (27.4)	29.8 (1.7)	2.68 (0.17)	1.755 (0.079)	851.5 (22.6)	2.78 (0.16)
6.	Laminate: Glass Fibre-	3	1.762 (0.112)	1054.5 (76.5)	35.6 (0.5)	3.14 (0.36)	1.846 (0.064)	1104.57 (51.20)	3.41 (0.23)

Elium Coating: HEMP/55210 Liquid Paint									

Note- Standard deviation in parenthesis.
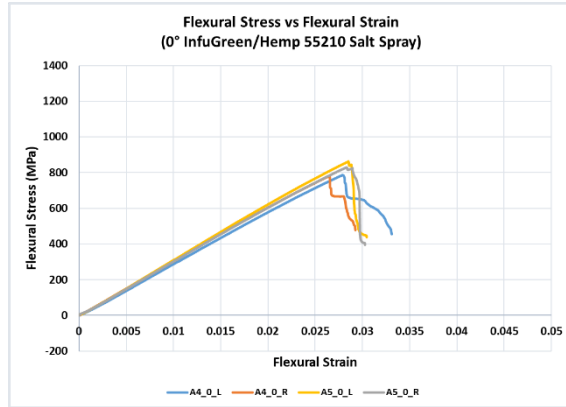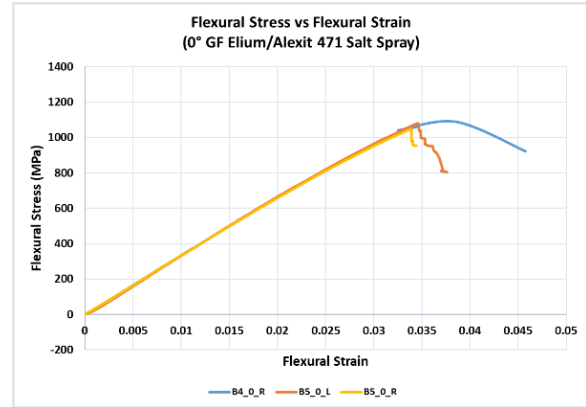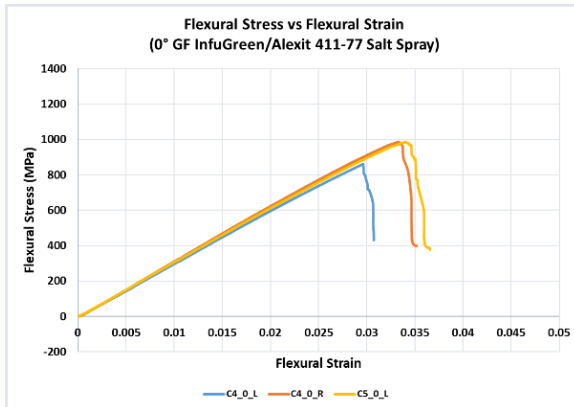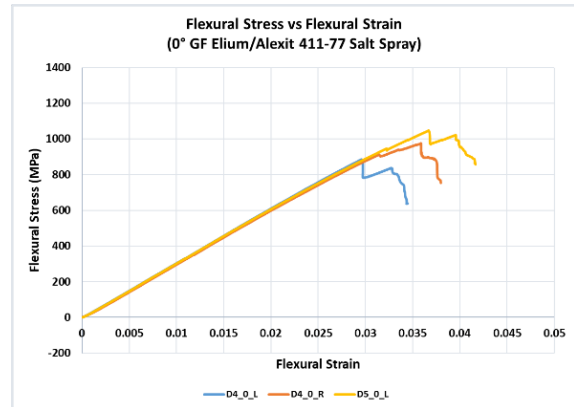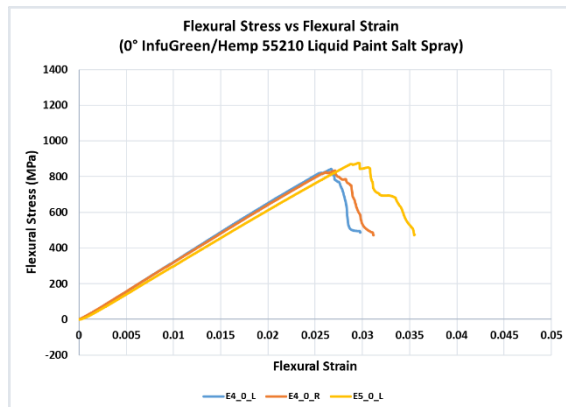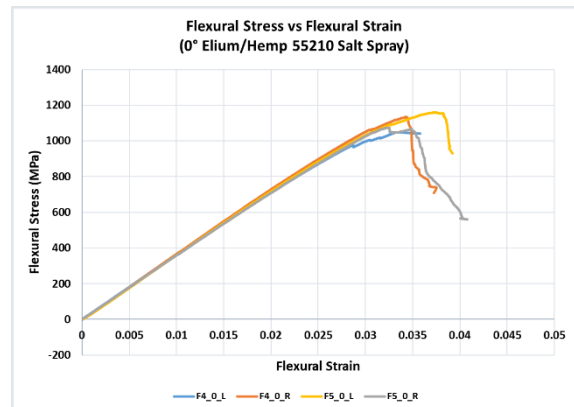
Figure 184 - Flexural stress v flexural strain plots for 0° (i) InfuGreen/Hemp 55210 Salt Spray (ii) Elium/Alexit 471 Salt Spray (iii) InfuGreen/Alexit 411-77 Salt Spray (iv) Elium/Alexit 411-77 Salt Spray (v) InfuGreen/Hemp 55210 Liquid Paint Salt Spray (vi) Elium/Hemp 55210 Liquid Paint Salt Spray

(i)

(ii)
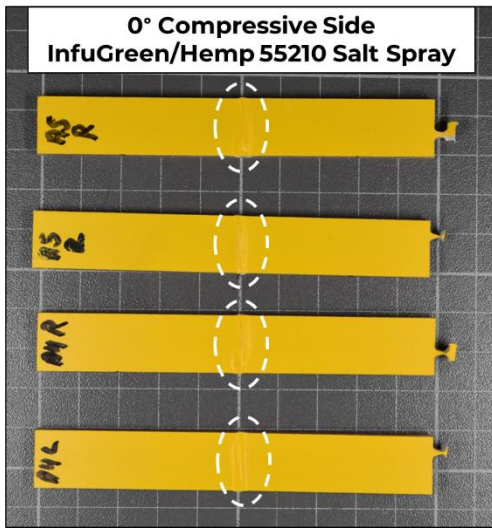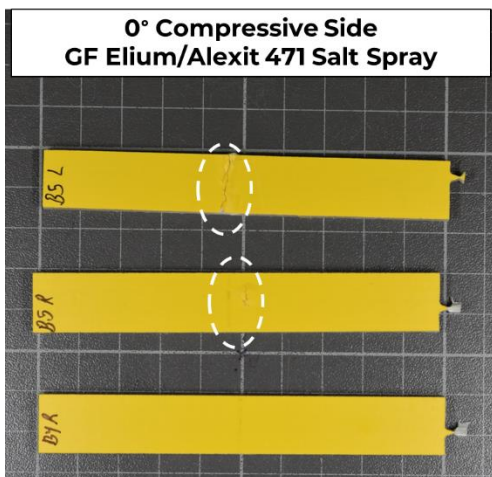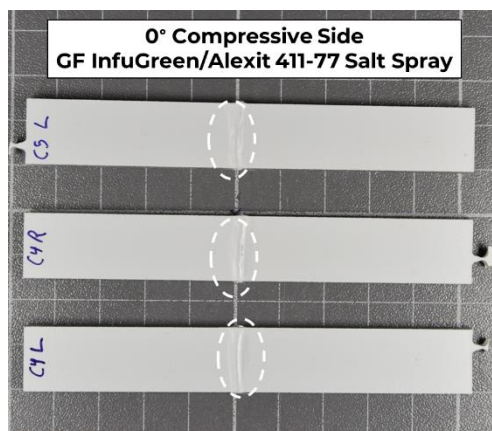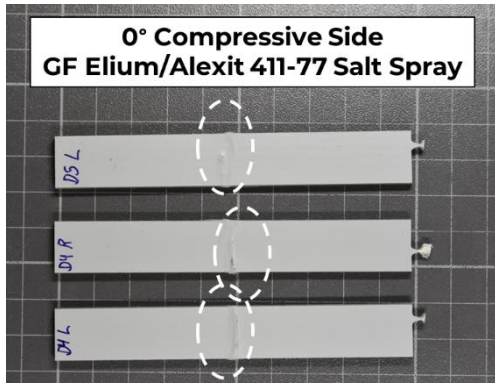
(iii)

Figure 185 - Post-test specimen images for 0° (i) InfuGreen/Hemp 55210 Salt Spray (ii) Elium/Alexit 471 Salt Spray (iii) InfuGreen/Alexit 411-77 Salt Spray (iv) Elium/Alexit 411-77 Salt Spray (v) InfuGreen/Hemp 55210 Liquid Paint Salt Spray (vi) Elium/Hemp 55210 Liquid Paint Salt Spray

b.2. 90° Salt-Spray Specimen

The key observations are summarised below:

- Bilinear stress-strain response observed in majority of 90° specimens.
- For all the 90° specimens, typically small drops in load observed at various stages initiating at lower strains. For many of the specimens, these drops are very small and not visibly evident in the stress-strain plots. Thus, this point may not be a true representation of failure. Hence a comparison of maximum load is also recommended between various tested specimen types. Further, as the test progresses multiple small drops are observed and with a rapid drop towards the end of the test at higher strains.
- Failure load is reported as the load where the 1st drop in load is observed. This typically lies closer to the end of 1st linear portion of the curve. The failure strain and load are reported corresponding to this point in the curve.
- Further the max load is reported as the maximum load observed throughout the curve and the corresponding strain is reported as strain at maximum load.

Table 50 - Tabular summary of results of Salt-spray 90° tests

Sr. No.	Material	No. of samples	Load at Failure (kN))	Failure Strength (MPa)	Flexural Modulus, E_f (GPa)	Strain-at-failure (%)	Max Load(kN)	Max Strength (MPa)	Strain at Max Load (%)
1.	Laminate-Glass Fibre-InfuGreen Coating-HEMP/55210 Dry	3	0.070 (0.001)	34.7 (0.5)	9.7 (0.1)	0.38 (0.00)	0.135 (0.01)	67.0 (3.5)	1.94 (0.19)
2.	Laminate: Glass Fibre-Elium Coating: ALEXIT/471 Dry	3	0.043 (0.003)	24.6 (1.5)	8.8 (0.9)	0.32 (0.06)	0.110 (0.007)	62.8 (4.3)	2.36 (0.13)
3.	Laminate: Glass Fibre-InfuGreen Coating-ALEXIT/411-77	3	0.066 (0.010)	33.9 (5.9)	9.9 (0.6)	0.36 (0.07)	0.125 (0.005)	63.8 (3.6)	1.74 (0.25)
4.	Laminate: Glass Fibre-Elium Coating: ALEXIT/411-77	3	0.072 (0.001)	38.3 (1.1)	10.0 (0.1)	0.44 (0.03)	0.123 (0.004)	65.5 (1.3)	2.05 (0.25)
5.	Laminate-Glass Fibre-InfuGreen Coating-HEMP/55210 Liquid Paint	3	0.075 (0.009)	36.7 (1.3)	9.5 (0.4)	0.41 (0.02)	0.125 (0.010)	61.3 (5.7)	1.38 (0.26)

| 6. | Laminate: Glass Fibre- Elium Coating: HEMP/55210 Liquid Paint | 3 | 0.070 (0.011) | 41.9 (5.9) | 10.1 (1.2) | 0.52 (0.05) | 0.102 (0.013) | 61.4 (7.5) | 1.60 (0.08) |

Note-Standard deviation in parenthesis.

(i)

(ii)
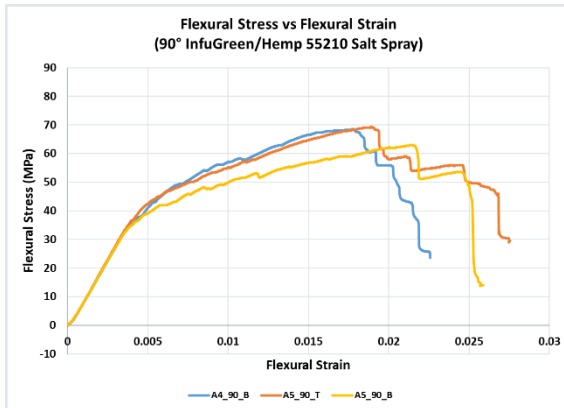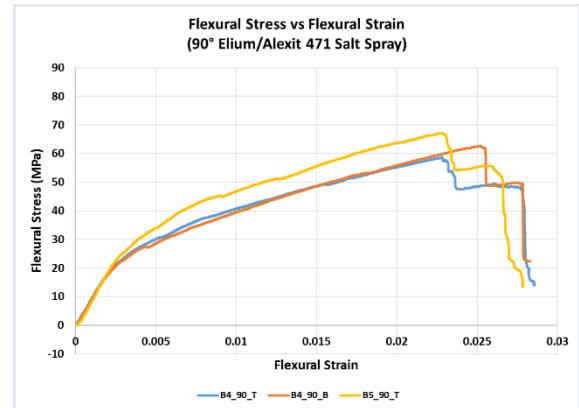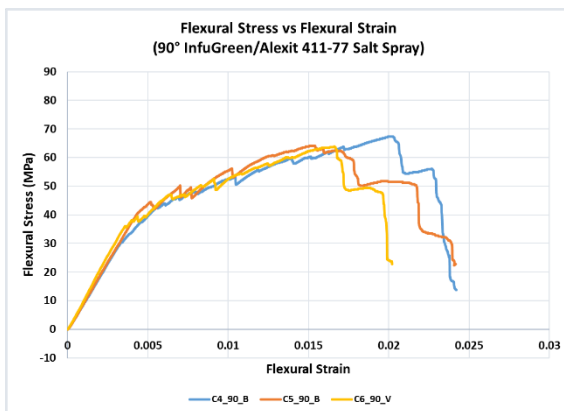
(iii)
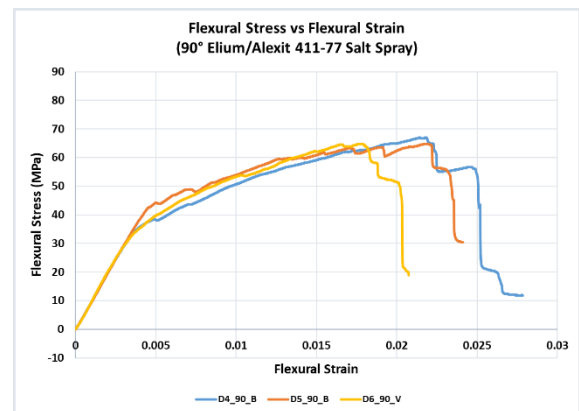
(iv)
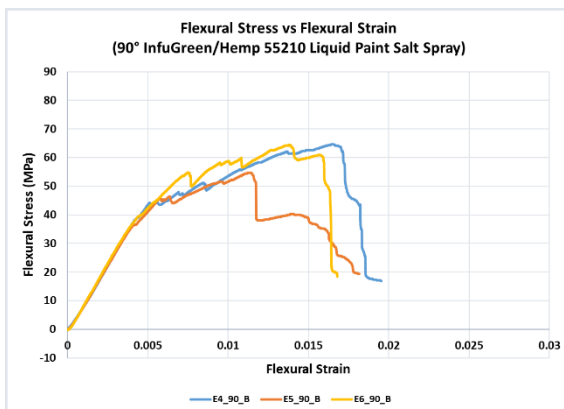
(v)
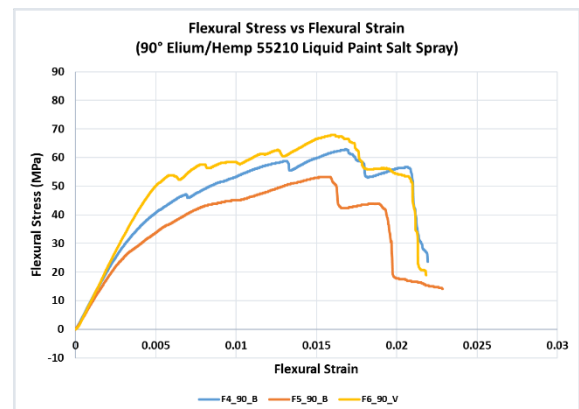
(vi)

Figure 186 - Flexural stress v flexural strain plots for 90° (i) InfuGreen/Hemp 55210 Salt Spray (ii) Elium/Alexit 471 Salt Spray (iii) InfuGreen/Alexit 411-77 Salt Spray (iv) Elium/Alexit 411-77 Salt Spray (v) InfuGreen/Hemp 55210 Liquid Paint Salt Spray (vi) Elium/Hemp 55210 Liquid Paint Salt Spray

(i)

(ii)
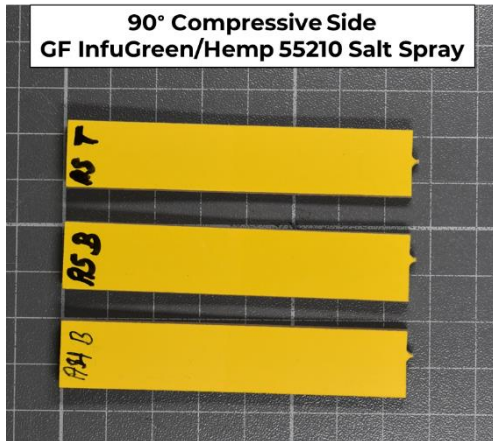
(iii)
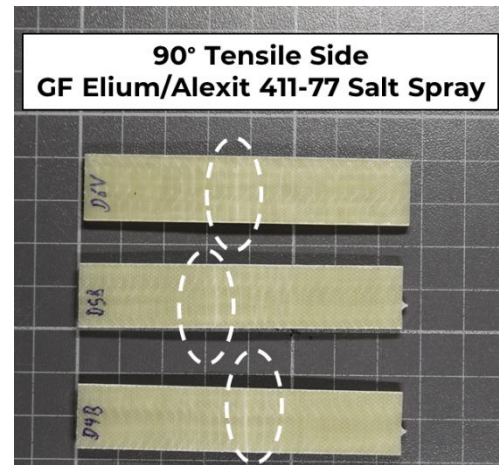
(iv)
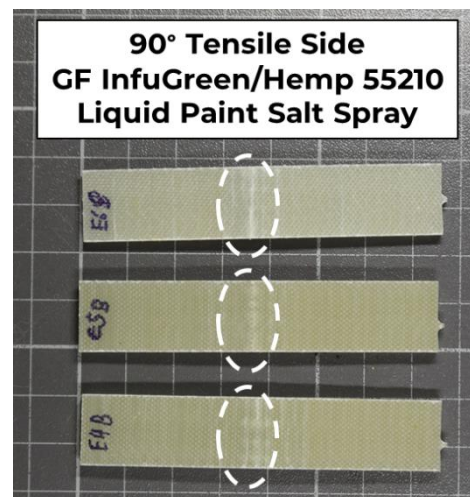
(v)

(vi)

Figure 187 - Post-test specimen images for 90° (i) InfuGreen/Hemp 55210 Salt Spray (ii) Elium/Alexit 471 Salt Spray (iii) InfuGreen/Alexit 411-77 Salt Spray (iv) Elium/Alexit 411-77 Salt Spray (v) InfuGreen/Hemp 55210 Liquid Paint Salt Spray (vi) Elium/Hemp 55210 Liquid Paint Salt Spray

c. UV-aged Specimen

This section presents the results obtained for Un-aged specimens. Next tables present the tabulated summary of average values obtained for 0° and 90° UV-aged specimens. Next figures depict the flexural response curves obtained for tested specimens. And show the post-test images of the 0° and 90° specimens respectively. A more detailed information about each tested specimen is presented in Appendix C.

c.1. 0° UV-aged Specimen

The key observations are summarised below:
- Linear stress-strain response curves observed.
- Rapid drop in load towards the end of the test.
- The point of first drop in load in the curve is being reported as the failure load and corresponding strain is reported as the failure strain. For most of the 0° samples the maximum load and the failure load are very close or equal.
- In general, the liquid coating appears to exhibit higher strength and modulus compared to the dry coating
- Regarding GF/Elium, the liquid/hemp coating appears to exhibit higher strength (+5%) and flexural modulus (+8%) than dry/alexit coating.
- Regarding GF/Infugreen, the liquid/hemp sample exhibits higher flexural strength (+6%) and modulus (+10%) compared to the dry/hemp sample
- Comparing to the control samples, the coated Elium samples have higher strength and comparable moduli. The InfuGreen control samples exhibit much higher strength (+16%) and modulus (+30%) than coated samples. There could be a possibility of UV ageing affecting this observation. This aspect needs further investigation. A comparison by considering the fibre volume fraction and SEM analysis could further provide more insight into this in future investigations.

Table 51 - Tabular summary of results of UV-aged 0° tests

| Sr. No.	Material	No. of samples	Load at Failure (kN))	Failure Strength (MPa)	Flexural Modulus, E_f (GPa)	Strain-at-failure (%)
1.	Laminate- Glass Fibre- InfuGreen Coating: HEMP/55210 Dry	4	1.777 (0.146)	872.2 (90.5)	25.9 (1.6)	3.27 (0.20)
2.	Laminate: Glass Fibre-Elium Coating: ALEXIT/471 Dry	4	1.892 (0.114)	1080.5 (41.7)	29.5 (2.0)	3.61 (0.24)
3.	Laminate: Glass Fibre-InfuGreen Coating: ALEXIT/411-77	3	1.835 (0.08)	934.3 (63.2)	30.2 (0.6)	3.15 (0.24)
4.	Laminate: Glass Fibre-Elium Coating: ALEXIT/411-77	4	1.861 (0.180)	978.9 (99.7)	26.6 (5.1)	3.42 (0.36)
5.	Laminate- Glass Fibre-InfuGreen Coating: HEMP/55210 Liquid Paint	4	1.678 (0.087)	929.5 (47.8)	28.8 (1.6)	2.97 (0.11)
6.	Laminate: Glass Fibre-Elium Coating: HEMP/55210 Liquid Paint	4	1.875 (0.077)	1142.3 (36.8)	32.2 (1.5)	3.51 (0.27)

Note-Standard deviation in parenthesis.
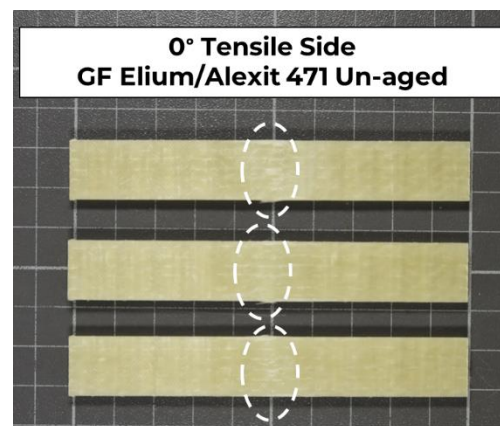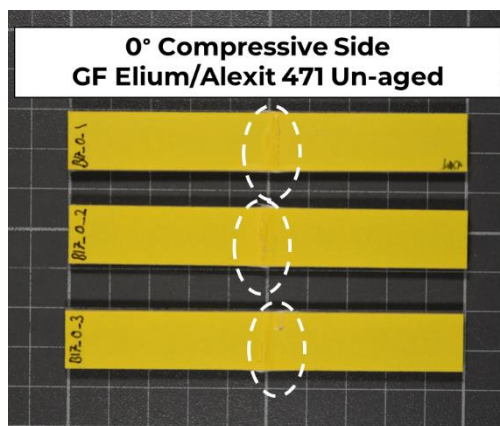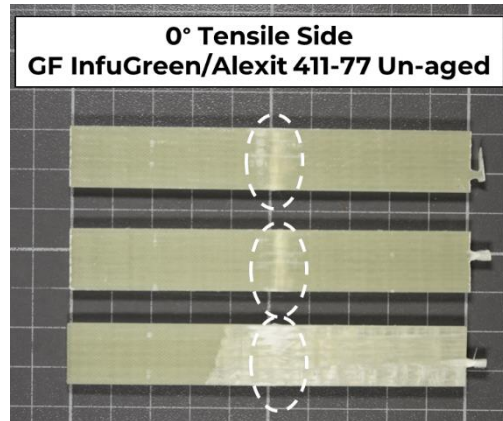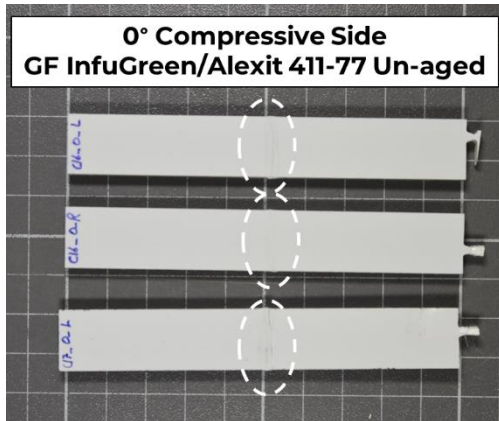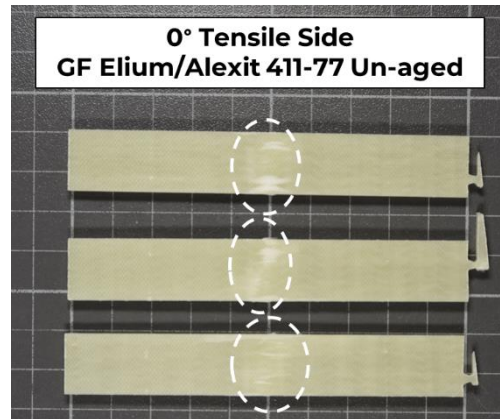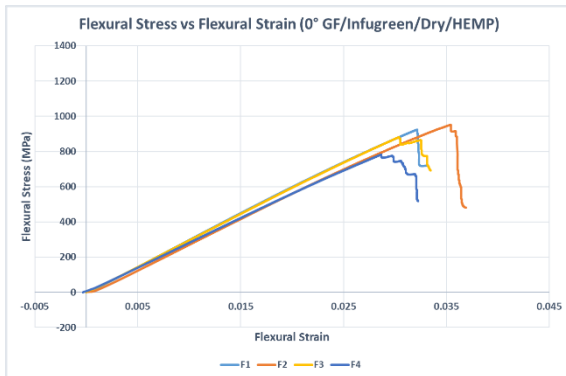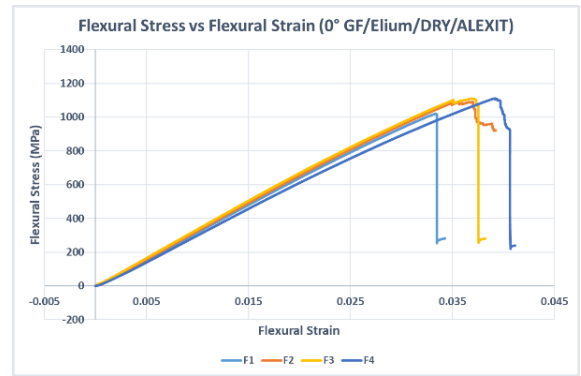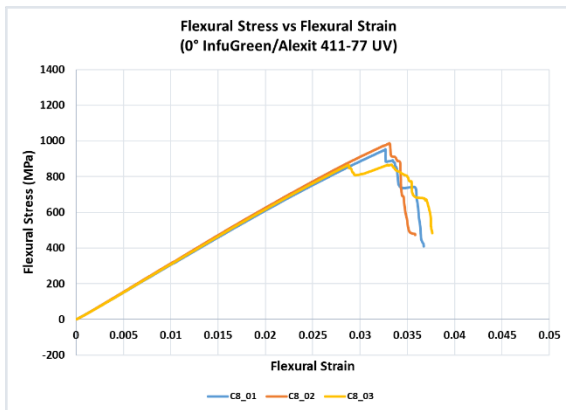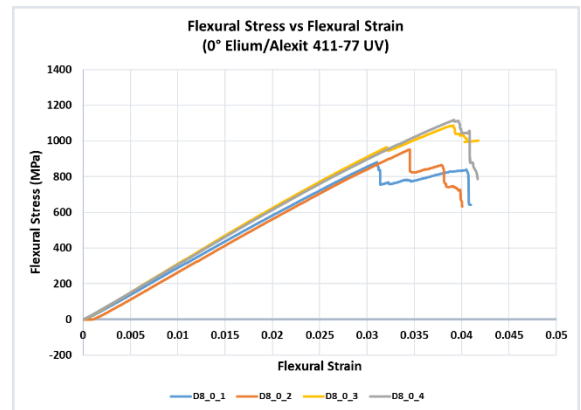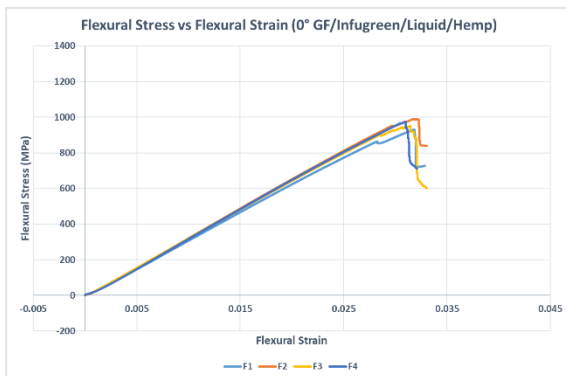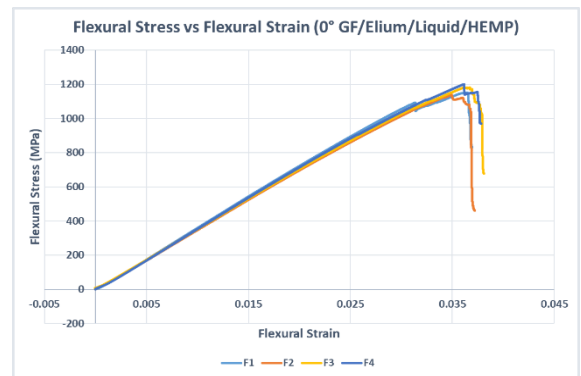
Figure 188 - Flexural stress v flexural strain plots for 0° (i) GF/Infugreen/Dry/HEMP (ii) GF/Elium/Dry/ALEXIT (iii) InfuGreen/Alexit 411-77 UV (iv) Elium/Alexit 411-77 UV (v) GF/Infugreen/Liquid/HEMP (vi) GF/Elium/Liquid/HEMP

(i)

(ii)
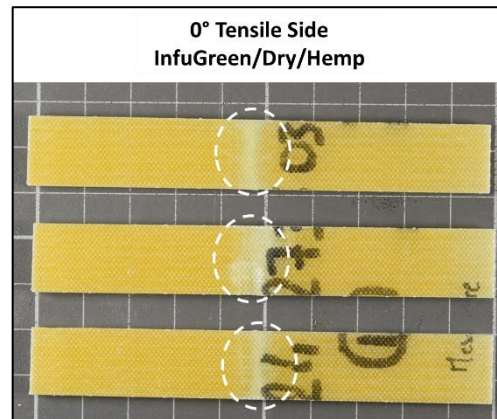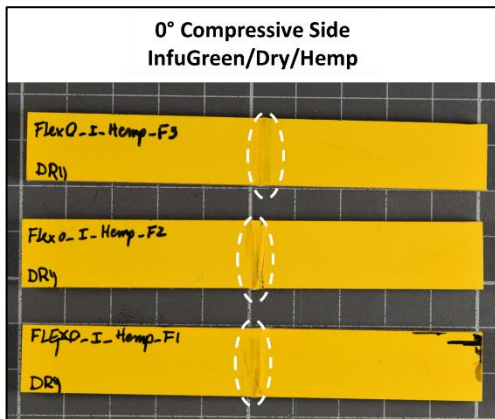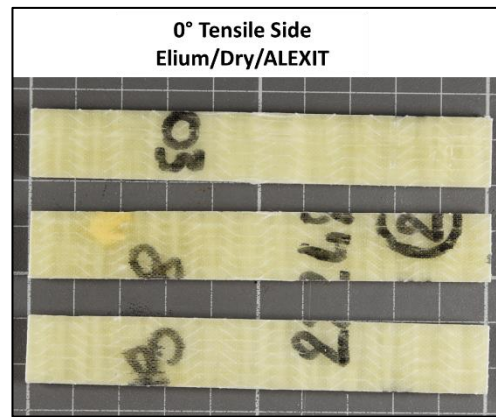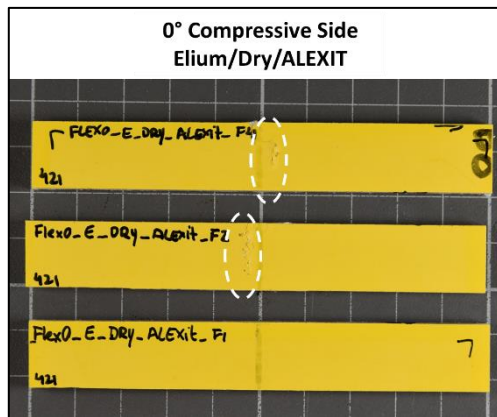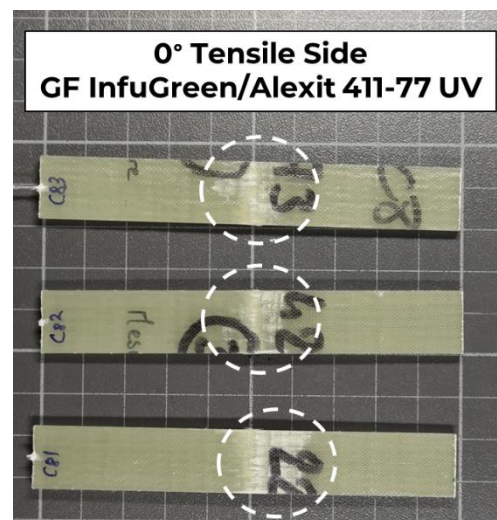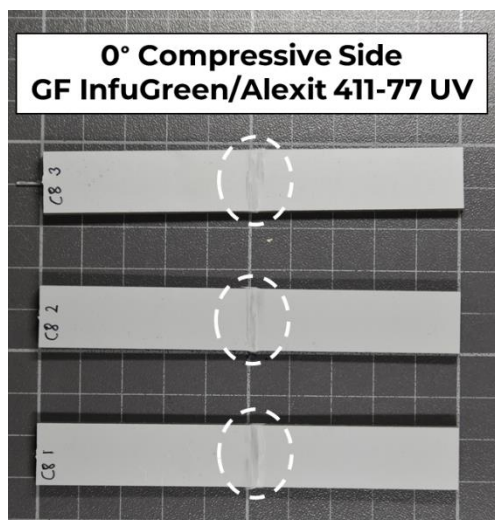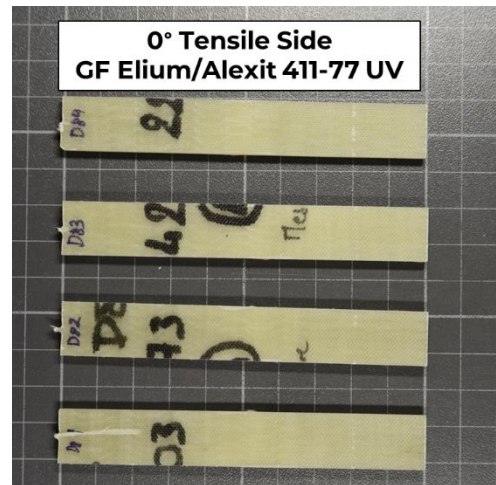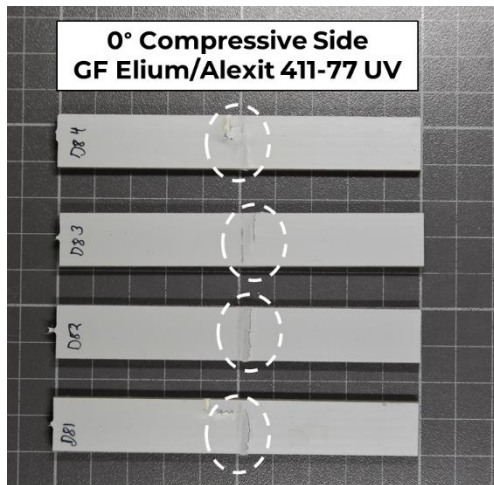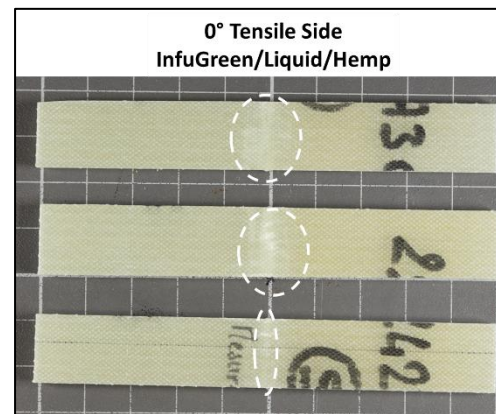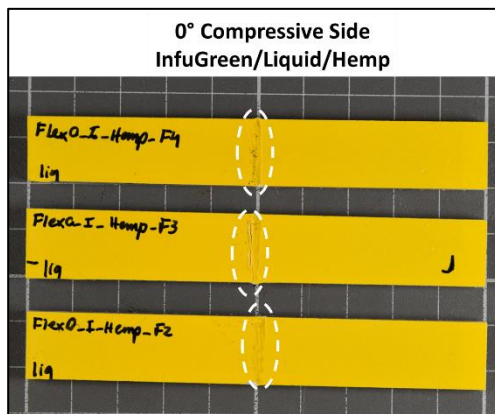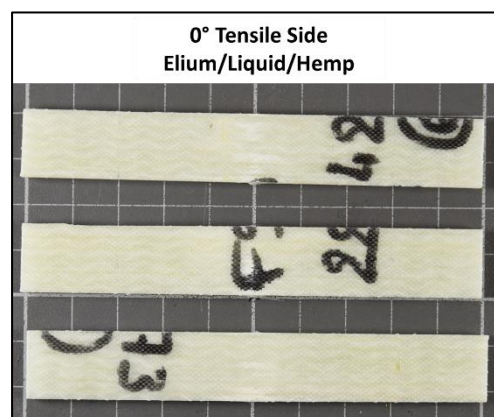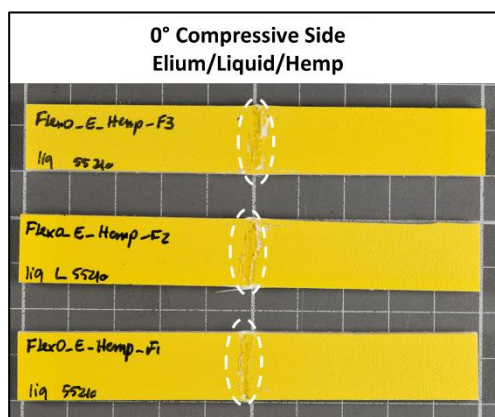
(iii)

Figure 189 - Post-test specimen images for 0° (i) GF/Infugreen/Dry/HEMP (ii) GF/Elium/Dry/ALEXIT (iii) InfuGreen/Alexit 411-77 UV (iv) Elium/Alexit 411-77 UV (v) GF/Infugreen/Liquid/HEMP (vi) GF/Elium/Liquid/HEMP

![FIBREGY logo]

This project has received funding from the European Union's Horizon 2020 research and innovation programme under grant agreement No 952966.

c.2. 90° UV-aged Specimen

The key observations are summarised below:

- Bilinear stress-strain response observed in 90° GF/Elium Dry and GF/Elium/Liquid specimens.
- For all the 90° specimens, typically small drops in load observed at various stages initiating at lower strains. As the test progresses multiple small drops are observed and with a rapid drop towards the end of the test at higher strains.
- Failure load is reported as the load where the 1st drop in load is observed. In GF/Elium Dry and GF/Elium/Liquid specimens, this typically lies closer to the end of 1st linear portion of the curve. The failure strain and load are reported corresponding to this point in the curve.
- Further the max load is reported as the maximum load observed throughout the curve and the corresponding strain is reported as strain at maximum load.
- In general, the liquid coating appears to exhibit marginally higher strength and at least comparable modulus compared to the dry coating.
- Regarding GF/Elium, the liquid/hemp sample exhibits marginally higher flexural strength (+5%) and the same modulus as the dry/hemp sample
- Regarding GF/Infugreen, the liquid/hemp sample exhibits marginally higher flexural strength (+9%) and higher modulus (+8%) compared to the dry/hemp sample.
- Comparing to the control samples, the coated Elium samples appear to exhibit the lower strength. The reason is that the reported failure strength in coated Elum samples is at the point closer to that section of the curve where the bilinear behaviour is observed. This point is lower than maximum load. However, the maximum load of Elium 90° coated samples is of the similar range of that of the failure load (at point of initiation of failure) observed in Control Elium 90° samples.

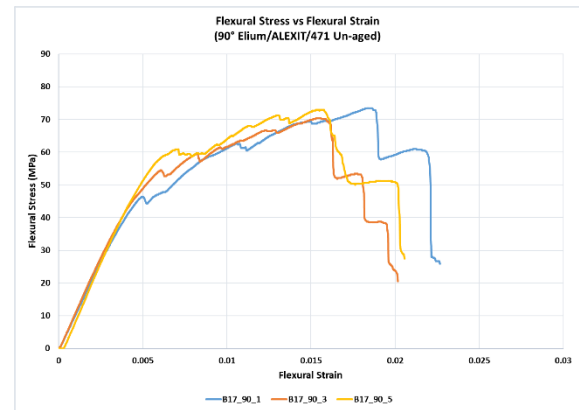Table 52 - Tabular summary of results of UV-aged 90° tests

Sr. No.	Material	No. of samples	Load at Failure (kN))	Failure Strength (MPa)	Flexural Modulus, E_f (GPa)	Strain-at-failure (%)	Max Load(kN)	Max Strength (MPa)	Strain at Max Load (%)
1.	Laminate-Glass Fibre-InfuGreen Coating-HEMP/55210 Dry	5	0.116 (0.007)	56.3 (4.3)	9.2 (0.5)	0.63 (0.08)	0.134 (0.007)	65.0 (3.9)	1.49 (0.38)
2.	Laminate: Glass Fibre-Elium Coating: ALEXIT/471 Dry	5	0.069 (0.003)	38.0 (1.4)	9.6 (0.5)	0.40 (0.03)	0.125 (0.006)	69.4 (3.4)	1.96 (0.21)
3.	Laminate: Glass Fibre-InfuGreen Coating-ALEXIT/411-77	3	0.112 (0.004)	55.7 (1.9)	10.3 (0.4)	0.63 (0.07)	0.129 (0.006)	64.3 (2.6)	1.32 (0.44)
4.	Laminate: Glass Fibre-Elium Coating: ALEXIT/411-77	3	0.094 (0.018)	49.5 (9.8)	10.4 (0.1)	0.55 (0.14)	0.130 (0.001)	68.5 (1.1)	1.87 (0.11)
5.	Laminate-Glass Fibre-InfuGreen Coating-	5	0.111 (0.008)	62.0 (3.5)	10.1 (0.2)	0.61 (0.06)	0.115 (0.003)	64.4 (1.3)	0.69 (0.06)

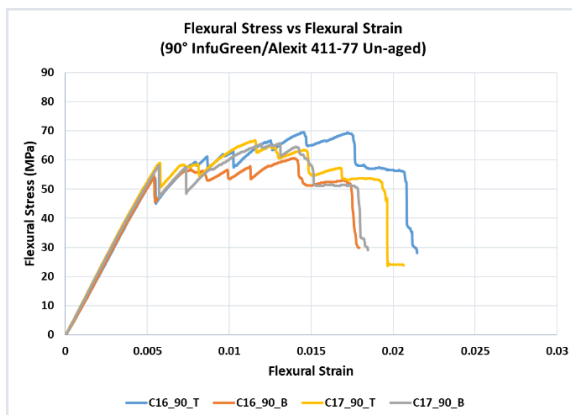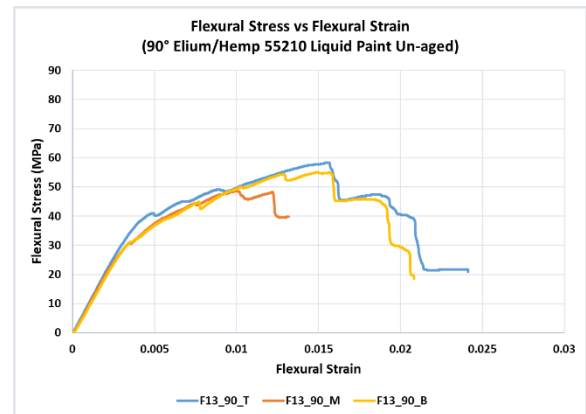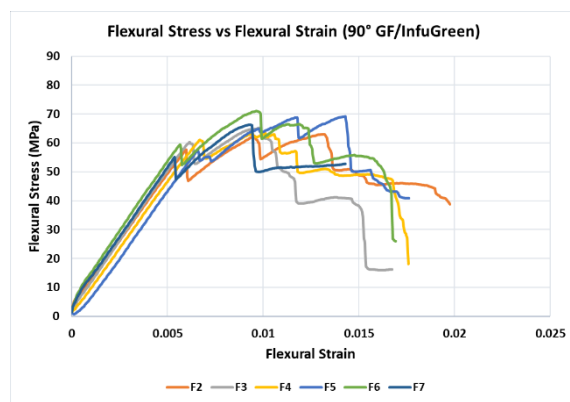|								
	HEMP/55210 Liquid Paint							
6.	Laminate: Glass Fibre-Elium Coating: HEMP/55210 Liquid Paint	5	0.067 (0.008)	40.1 (4.5)	9.6 (0.3)	0.48 (0.07)	0.113 (0.012)	67.3 (6.9)	1.92 (0.19)

Note-Standard deviation in parenthesis;

(i)

(ii)
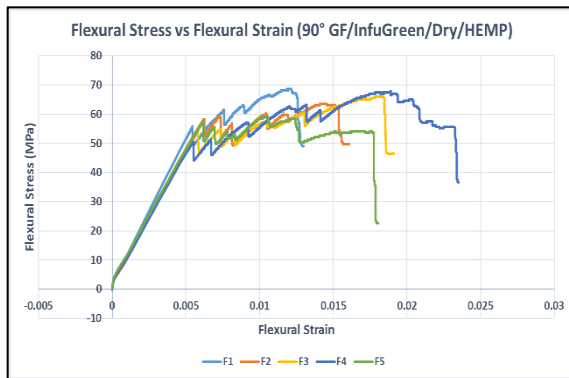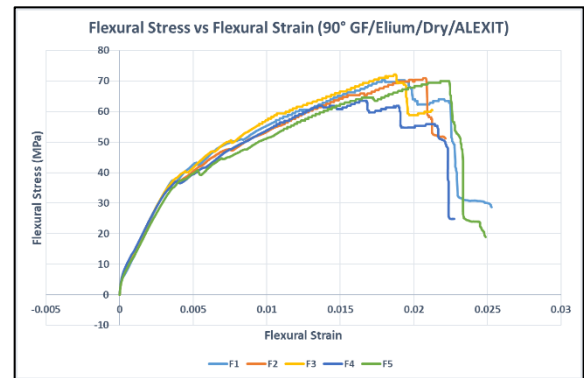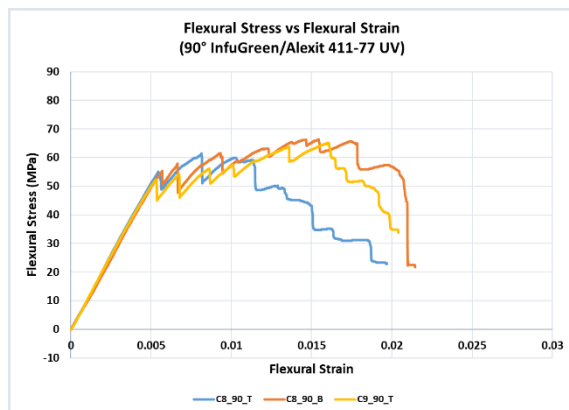
(iii)
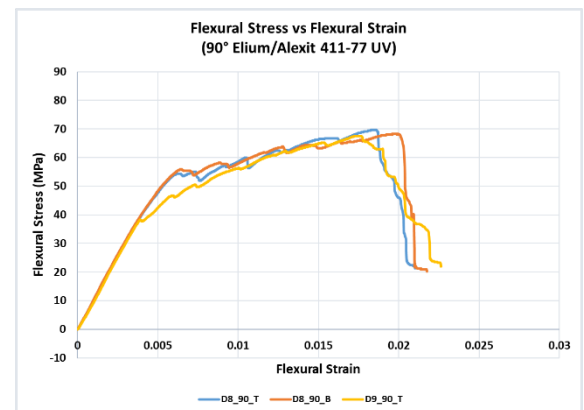
(iv)
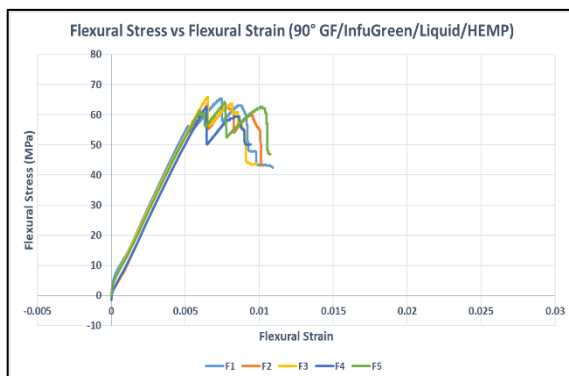
(v)
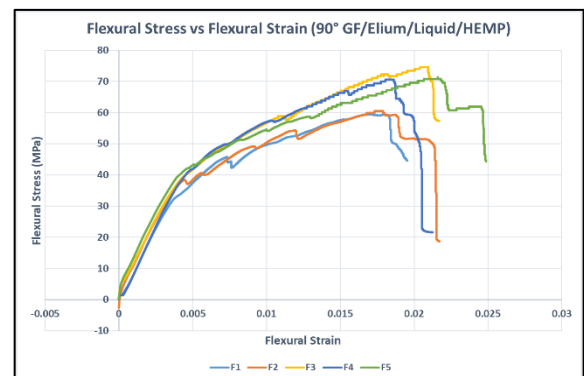
(vi)

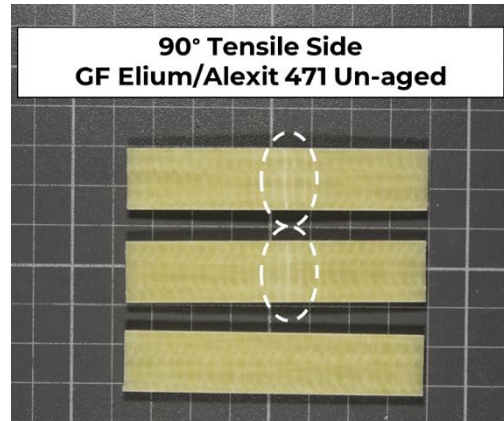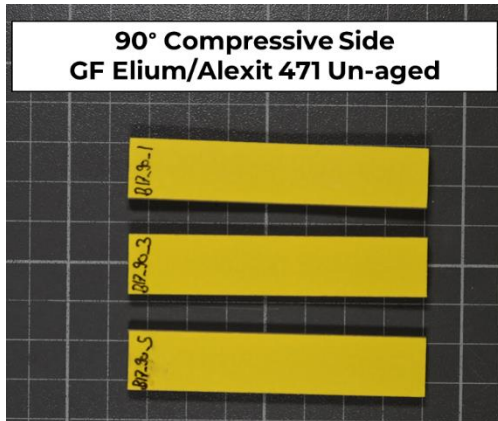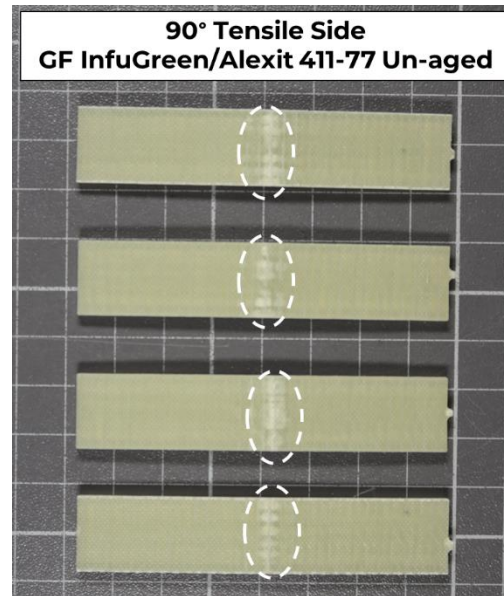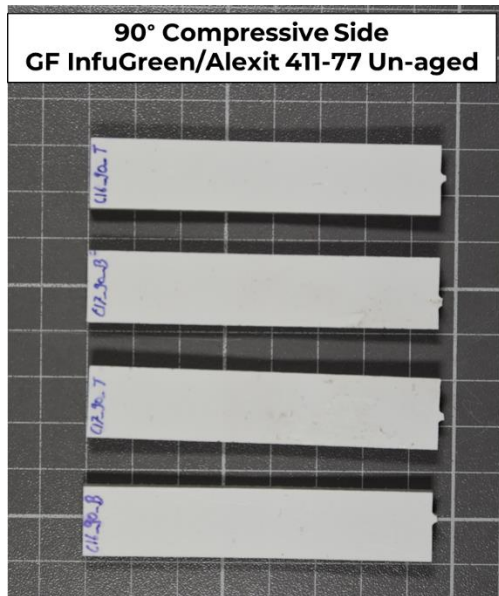Figure 190 - Flexural stress v flexural strain plots for 90° (i) GF/Infugreen/Dry/HEMP (ii) GF/Elium/Dry/ALEXIT (iii) InfuGreen/Alexit 411-77 UV (iv) Elium/Alexit 411-77 UV (v) GF/Infugreen/Liquid/HEMP (vi) GF/Elium/Liquid/HEMP

90° Compressive Side
InfuGreen/Dry/Hemp

Flex 90_I_Hemp_F5
DRY

Flex 90_I_Hemp_F4
DRY

Flex 90_I_Hemp_F3
DRY

Flex 90_I_Hemp_F2
DRY

90° Tensile Side
InfuGreen/Dry/Hemp

(i)

90° Compressive Side
Elium/Dry/ALEXIT

FLEX90-E-DRY-ALEXIT-F6
421

FLEX90-E-DRY-ALEXIT-F4
421

FLEX90-E-DRY-ALEXIT-F3
421

FLEX90-E-DRY-ALEXIT-F2
421

90° Tensile Side
Elium/Dry/ALEXIT

(ii)

90° Compressive Side GF InfuGreen/Alexit 411-77 UV

90° Tensile Side GF InfuGreen/Alexit 411-77 UV

(iii)

90° Compressive Side GF Elium/Alexit 411-77 UV

90° Tensile Side GF Elium/Alexit 411-77 UV

(iv)

90° Compressive Side InfuGreen/Liquid/Hemp

90° Tensile Side InfuGreen/Liquid/Hemp

(v)

(vi)

Figure 191 - Post-test specimen images for 90° (i) GF/Infugreen/Dry/HEMP (ii) GF/Elium/Dry/ALEXIT (iii) InfuGreen/Alexit 411-77 UV (iv) Elium/Alexit 411-77 UV (v) GF/Infugreen/Liquid/HEMP (vi) GF/Elium/Liquid/HEMP

APPENDIX-A: Un-aged Specimens

1. 0° Un-aged Specimen

Table 53 - Flexural 0° test result summary (0° GF InfuGreen/Hemp 55210 Un-aged)

L - SPAN (mm)	60										
SAMPLE	b - WIDTH (mm)	h - THICKNESS (mm)	LOAD (kN) @ Failure	σ_f (MPa)	E_f (GPa)	Strain @ Failure	Span/Thickness	Max Load(kN)	σ_{max} (MPa)	Strain at Max Load (%)
A17_0_1	14.87	3.362	1.999	1070.0	33.0	3.42%	17.85	2.026	1084.3	3.52%
A17_0_2	14.98	3.345	1.936	1039.5	32.3	3.30%	17.94	1.959	1052.2	3.37%
A17_0_3	14.91	3.357	2.030	1088.0	32.0	3.56%	17.87	2.041	1093.8	3.59%
AVERAGE	14.92	3.355	1.988	1065.8	32.4	3.43%	17.89	2.009	1076.8	3.49%
ST DEV	0.06	0.01	0.048	24.5	0.5	0.13%	0.05	0.044	21.8	0.11%
CV (%)	0.38	0.27	2.42	2.30	1.65	3.79	0.27	2.17	2.03	3.15

Table 54 - Flexural 0° test result summary (0° GF Elium/Alexit 471 Un-aged)

L - SPAN (mm)	60										
SAMPLE	b - WIDTH (mm)	h - THICKNESS (mm)	LOAD (kN) @ Failure	σ_f (MPa)	E_f (GPa)	Strain @ Failure	Span/Thickness	Max Load(kN)	σ_{max} (MPa)	Strain at Max Load (%)
B17_0_1	14.83	3.250	2.182	1253.9	35.6	3.93%	18.46	2.184	1255.4	4.01%
B17_0_2	14.88	3.279	2.126	1196.0	33.7	3.72%	18.30	2.129	1197.6	3.73%
B17_0_3	14.89	3.248	2.124	1217.1	34.0	4.02%	18.48	2.139	1225.7	3.93%
AVERAGE	14.87	3.259	2.144	1222.4	34.4	3.89%	18.41	2.150	1226.2	3.89%
ST DEV	0.03	0.017	0.033	29.3	1.0	0.15%	0.10	0.030	28.9	0.15%
CV (%)	0.24	0.53	1.53	2.40	3.05	3.98	0.53	1.38	2.36	3.75

Table 55 - Flexural 0° test result summary (0° GF InfuGreen/Alexit 411-77 Un-aged)

L - SPAN (mm)	60									
SAMPLE	b - WIDTH (mm)	h - THICKNESS (mm)	LOAD (kN) @ Failure	σ_f (MPa)	E_f (GPa)	Strain @ Failure	Span/Thickness	Max Load(kN)	σ_{max} (MPa)	Strain at Max Load (%)
C16_0_L	15.31	3.530	1.931	910.8	29.4	3.07%	17.00	2.004	945.3057	3.27%
C16_0_R	15.33	3.445	1.898	938.8	28.1	3.22%	17.42	1.898	938.7564	3.22%
C17_0_L	15.27	3.465	2.180	1070.1	30.5	3.67%	17.31	2.180	1070.0630	3.67%
AVERAGE	15.31	3.480	2.003	973.2	29.4	3.32%	17.24	2.028	984.7	3.39%
ST DEV	0.03	0.044	0.154	85.0	1.2	0.31%	0.22	0.143	74.0	0.24%
CV (%)	0.20	1.27	7.71	8.74	4.07	9.33	1.27	7.03	7.51	7.22

Table 56 - Flexural 0° test result summary (0° GF Elium/Alexit 411-77 Un-aged)

L - SPAN (mm)	60									
SAMPLE	b - WIDTH (mm)	h - THICKNESS (mm)	LOAD (kN) @ Failure	σ_f (MPa)	E_f (GPa)	Strain @ Failure	Span/Thickness	Max Load(kN)	σ_{max} (MPa)	Strain at Max Load (%)
D16_0_L	15.26	3.373	2.050	1063.3	30.0	3.66%	17.79	2.055	1065.4	3.67%
D16_0_R	15.35	3.342	2.131	1118.7	31.7	3.60%	17.95	2.146	1126.4	3.69%
D17_0_L	15.32	3.380	2.208	1135.8	31.0	3.80%	17.75	2.208	1135.8	3.80%
AVERAGE	15.31	3.365	2.130	1105.9	30.9	3.69%	17.83	2.136	1109.2	3.72%
ST DEV	0.05	0.020	0.079	37.9	0.9	0.11%	0.11	0.077	38.2	0.07%
CV (%)	0.31	0.59	3.70	3.43	2.79	2.88	0.60	3.61	3.45	1.99

Table 57 - Flexural 0° test result summary (0° InfuGreen/Hemp 55210 Liquid Paint Un-aged)

L - SPAN (mm)	60									
SAMPLE	b - WIDTH (mm)	h - THICKNESS (mm)	LOAD (kN) @ Failure	σ_f (MPa)	E_f (GPa)	Strain @ Failure	Span/Thickness	Max Load(kN)	σ_{max} (MPa)	Strain at Max Load (%)
E13_0_M	15.22	3.264	1.810	1005.3	32.5	2.99%	18.39	1.821	1011.5	3.01%
E15_0_L	15.23	3.573	2.016	933.1	30.0	2.91%	16.79	2.019	934.2	2.91%
E15_0_M	15.23	3.589	1.659	761.4	30.0	2.49%	16.72	1.703	781.3	2.64%
E15_0_R	15.28	3.606	1.571	711.7	30.1	2.85%	16.64	1.715	776.7	2.49%
AVERAGE	15.24	3.51	1.764	852.9	30.7	2.81%	17.13	1.814	875.9	2.76%
ST DEV	0.03	0.16	0.195	139.0	1.2	0.22%	0.84	0.146	116.3	0.24%
CV (%)	0.19	4.66	11.04	16.30	4.02	7.92	4.88	8.06	13.27	8.78

Table 58 - Flexural 0° test result summary (0° GF Elium/Hemp 55210 Un-aged)

L - SPAN (mm)	60									
SAMPLE	b - WIDTH (mm)	h - THICKNESS (mm)	LOAD (kN) @ Failure	σ_f (MPa)	E_f (GPa)	Strain @ Failure	Span/Thickness	Max Load(kN)	σ_{max} (MPa)	Strain at Max Load (%)
F15_0_L	15.17	3.199	1.826	1058.3	35.4	3.08%	18.76	1.873	1085.5	3.43%
F15_0_M	15.21	3.214	1.880	1077.2	34.2	3.19%	18.67	1.880	1077.2	3.20%
F15_0_R	15.21	3.279	2.048	1126.5	34.2	3.48%	18.30	2.048	1126.5	3.48%
AVERAGE	15.20	3.23	1.918	1087.3	34.6	3.25%	18.57	1.934	1096.4	3.37%
ST DEV	0.02	0.04	0.116	35.2	0.7	0.21%	0.24	0.099	26.4	0.15%
CV (%)	0.15	1.32	6.03	3.24	2.04	6.41	1.32	5.11	2.41	4.46

2. 90° Un-aged Specimen

Table 59 - Flexural 90° test result summary (90° GF InfuGreen/Hemp 55210 Un-aged)

L - SPAN (mm)	60									
SAMPLE	b - WIDTH (mm)	h - THICKNESS (mm)	LOAD (kN) @ Failure	σ_f (MPa)	E_f (GPa)	Strain @ Failure	Span/Thickness	Max Load(kN)	σ_{max} (MPa)	Strain at Max Load (%)
A17_90_1	15.29	3.366	0.111	57.8	11.5	0.52%	17.83	0.137	71.0	1.54%
A17_90_2	15.30	3.378	0.121	62.2	11.1	0.59%	17.76	0.131	67.7	1.20%
A17_90_3	15.33	3.356	0.120	62.6	10.9	0.62%	17.88	0.132	68.7	1.41%
AVERAGE	**15.30**	**3.37**	**0.117**	**60.8**	**11.2**	**0.58%**	**17.82**	**0.133**	**69.1**	**1.38%**
ST DEV	0.02	0.01	0.005	2.7	0.3	0.05%	0.06	0.003	1.7	0.17%
CV (%)	0.14	0.33	4.53	4.40	3.01	8.66	0.33	2.19	2.43	12.18

Table 60 - Flexural 90° test result summary (90° GF Elium/Alexit 471 Un-aged)

L - SPAN (mm)	60									
SAMPLE	b - WIDTH (mm)	h - THICKNESS (mm)	LOAD (kN) @ Failure	σ_f (MPa)	E_f (GPa)	Strain @ Failure	Span/Thickness	Max Load(kN)	σ_{max} (MPa)	Strain at Max Load (%)
B17_90_1	15.27	3.343	0.088	46.4	10.8	0.49%	17.95	0.139	73.5	1.86%
B17_90_3	15.30	3.320	0.102	54.5	11.3	0.61%	18.07	0.132	70.4	1.56%
B17_90_5	15.24	3.280	0.111	60.9	12.0	0.69%	18.29	0.133	73.0	1.58%
AVERAGE	**15.27**	**3.314**	**0.100**	**53.9**	**11.4**	**0.60%**	**18.10**	**0.135**	**72.3**	**1.67%**
ST DEV	0.03	0.032	0.012	7.3	0.6	0.10%	0.17	0.004	1.6	0.17%
CV (%)	0.19	0.96	11.55	13.47	5.18	16.61	0.96	2.96	2.26	10.27

Table 61 - Flexural 90° test result summary (90° InfuGreen/Alexit 411-77 Un-aged)

L - SPAN (mm)	60									
SAMPLE	b - WIDTH (mm)	h - THICKNESS (mm)	LOAD (kN) @ Failure	σ_f (MPa)	E_f (GPa)	Strain @ Failure	Span/Thickness	Max Load(kN)	σ_{max} (MPa)	Strain at Max Load (%)
C16_90_T	15.22	3.472	0.111	54.4	10.3	0.54%	17.28	0.142	69.6	1.45%
C16_90_B	15.20	3.474	0.111	54.6	10.5	0.54%	17.27	0.123	60.6	1.38%
C17_90_T	15.32	3.458	0.120	59.0	11.0	0.58%	17.35	0.136	66.7	1.16%
C17_90_B	15.30	3.447	0.117	58.1	10.9	0.57%	17.41	0.133	65.8	1.31%
AVERAGE	15.26	3.46	0.115	56.5	10.7	0.56%	17.33	0.133	65.7	1.33%
ST DEV	0.06	0.01	0.005	2.4	0.3	0.02%	0.06	0.008	3.7	0.13%
CV (%)	0.39	0.36	3.96	4.18	3.25	3.57	0.36	5.70	5.69	9.47

Table 62 - Flexural 90° test result summary (90° GF Elium/Alexit 411-77 Un-aged)

L - SPAN (mm)	60									
SAMPLE	b - WIDTH (mm)	h - THICKNESS (mm)	LOAD (kN) @ Failure	σ_f (MPa)	E_f (GPa)	Strain @ Failure	Span/Thickness	Max Load(kN)	σ_{max} (MPa)	Strain at Max Load (%)
D16_90_T	15.26	3.385	0.087	44.8	11.0	0.46%	17.73	0.135	69.6	1.75%
D16_90_B	15.24	3.388	0.092	47.5	10.8	0.48%	17.71	0.140	71.9	1.82%
D17_90_T	15.25	3.411	0.101	51.2	10.7	0.54%	17.59	0.124	63.2	1.67%
D17_90_B	15.25	3.411	0.103	52.5	10.9	0.59%	17.59	0.125	63.4	1.35%
AVERAGE	15.25	3.399	0.096	49.0	10.8	0.52%	17.66	0.131	67.0	1.65%
ST DEV	0.01	0.014	0.008	3.5	0.1	0.06%	0.07	0.008	4.4	0.21%
CV (%)	0.05	0.41	7.96	7.19	1.06	10.96	0.41	5.81	6.59	12.75

Table 63 - Flexural 90° test result summary (90° GF InfuGreen/Hemp 55210 Liquid Paint Un-aged)

L - SPAN (mm)	60									
SAMPLE	b - WIDTH (mm)	h - THICKNESS (mm)	LOAD (kN) @ Failure	σ_f (MPa)	E_f (GPa)	Strain @ Failure	Span/Thickness	Max Load(kN)	σ_{max} (MPa)	Strain at Max Load (%)
E13_90_T	15.28	3.351	0.120	62.9	9.3	0.91%	17.91	0.123	64.3	1.16%
E13_90_B	15.26	3.429	0.134	67.3	10.1	0.74%	17.50	0.136	68.0	0.75%
E14_90_T	15.26	3.284	0.101	55.2	10.3	0.60%	18.27	0.117	63.8	1.06%
E14_90_B	15.22	3.343	0.109	57.7	9.9	0.64%	17.95	0.114	60.5	0.89%
AVERAGE	**15.25**	**3.35**	**0.116**	**60.8**	**9.9**	**0.72%**	**17.91**	**0.122**	**64.1**	**0.96%**
ST DEV	0.03	0.06	0.014	5.4	0.4	0.14%	0.32	0.010	3.1	0.18%
CV (%)	0.17	1.77	12.36	8.86	4.23	18.97	1.76	7.78	4.80	18.92

Table 64 - Flexural 90° test result summary (90° GF Elium/Hemp 55210 Liquid Paint Un-aged)

L - SPAN (mm)	60									
SAMPLE	b - WIDTH (mm)	h - THICKNESS (mm)	LOAD (kN) @ Failure	σ_f (MPa)	E_f (GPa)	Strain @ Failure	Span/Thickness	Max Load(kN)	σ_{max} (MPa)	Strain at Max Load (%)
F13_90_T	15.23	3.291	0.075	41.0	10.3	0.50%	18.23	0.107	58.3	1.54%
F13_90_M	15.24	3.213	0.054	30.9	9.9	0.35%	18.67	0.085	48.6	0.98%
F13_90_B	15.28	3.249	0.081	45.0	9.8	0.77%	18.47	0.099	55.1	1.50%
AVERAGE	**15.25**	**3.251**	**0.070**	**39.0**	**10.0**	**0.54%**	**18.46**	**0.097**	**54.0**	**1.34%**
ST DEV	0.03	0.039	0.014	7.3	0.3	0.21%	0.22	0.011	5.0	0.31%
CV (%)	0.17	1.19	20.07	18.64	2.76	39.54	1.19	11.42	9.18	23.15

APPENDIX-B: Salt-Spray Specimens

1. 0° Salt-Spray Specimen

Table 65 - Flexural 0° test result summary (0° GF InfuGreen/Hemp 55210 Salt Spray)

L - SPAN (mm)	60									
SAMPLE	b - WIDTH (mm)	h - THICKNESS (mm)	LOAD (kN) @ Failure	σ_f (MPa)	E_f (GPa)	Strain @ Failure	Span/Thickness	Max Load(kN)	σ_{max} (MPa)	Strain at Max Load (%)
A4_0_L	14.76	3.522	1.600	786.7	27.2	2.79%	17.04	1.600	786.7	2.79%
A4_0_R	14.80	3.505	1.567	775.9	30.1	2.63%	17.12	1.567	775.9	2.63%
A5_0_L	14.68	3.498	1.718	861.1	29.0	2.85%	17.16	1.722	863.2	2.85%
A5_0_R	14.85	3.483	1.659	829.5	27.7	2.83%	17.23	1.659	829.5	2.83%
AVERAGE	14.77	3.50	1.636	813.3	28.5	2.77%	17.14	1.637	813.9	2.77%
ST DEV	0.07	0.02	0.067	39.4	1.3	0.10%	0.08	0.068	40.2	0.10%
CV (%)	0.47	0.46	4.07	4.84	4.59	3.60	0.46	4.17	4.94	3.63

Table 66 - Flexural 0° test result summary (0° GF Elium/Alexit 471 Salt Spray)

L - SPAN (mm)	60									
SAMPLE	b - WIDTH (mm)	h - THICKNESS (mm)	LOAD (kN) @ Failure	σ_f (MPa)	E_f (GPa)	Strain @ Failure	Span/Thickness	Max Load(kN)	σ_{max} (MPa)	Strain at Max Load (%)
B4_0_R	14.53	3.222	1.779	1062.1	33.2	3.47%	18.62	1.824	1088.6	3.86%
B5_0_L	14.60	3.203	1.797	1079.7	30.5	3.44%	18.73	1.797	1079.8	3.46%
B5_0_R	14.80	3.275	1.845	1046.4	32.4	3.38%	18.32	1.851	1049.9	3.39%
AVERAGE	14.64	3.233	1.807	1062.8	32.0	3.43%	18.558	1.824	1072.8	3.57%
ST DEV	0.14	0.04	0.034	16.7	1.4	0.05%	0.21	0.027	20.3	0.25%
CV (%)	0.97	1.15	1.88	1.57	4.30	1.38	1.14	1.49	1.89	7.07

Table 67 - Flexural 0° test result summary (0° GF InfuGreen/Alexit 411-77 Salt Spray)

L - SPAN (mm)	60									
SAMPLE	b - WIDTH (mm)	h - THICKNESS (mm)	LOAD (kN) @ Failure	σ_f (MPa)	E_f (GPa)	Strain @ Failure	Span/Thickness	Max Load(kN)	σ_{max} (MPa)	Strain at Max Load (%)
C4_0_L	14.68	3.495	1.706	856.7	28.5	2.95%	17.17	1.716	861.9	2.96%
C4_0_R	14.70	3.415	1.864	978.9	30.5	3.29%	17.57	1.878	986.2	3.33%
C5_0_L	14.72	3.445	1.912	984.9	29.5	3.39%	17.42	1.912	984.9	3.39%
AVERAGE	14.70	3.452	1.827	940.1	29.5	3.21%	17.38	1.836	944.3	3.23%
ST DEV	0.02	0.04	0.108	72.4	1.0	0.23%	0.20	0.105	71.4	0.23%
CV (%)	0.15	1.16	5.90	7.70	3.50	7.26	1.16	5.69	7.56	7.20

Table 68 - Flexural 0° test result summary (0° GF Elium/Alexit 411-77 Salt Spray)

L - SPAN (mm)	60									
SAMPLE	b - WIDTH (mm)	h - THICKNESS (mm)	LOAD (kN) @ Failure	σ_f (MPa)	E_f (GPa)	Strain @ Failure	Span/Thickness	Max Load(kN)	σ_{max} (MPa)	Strain at Max Load (%)
D4_0_L	14.69	3.401	1.670	884.3	30.0	2.96%	17.64	1.670	884.3	2.96%
D4_0_R	14.61	3.300	1.613	912.5	27.9	3.15%	18.18	1.724	975.5	3.59%
D5_0_L	14.80	3.381	1.776	945.5	29.5	3.23%	17.75	1.969	1047.8	3.67%
AVERAGE	14.70	3.361	1.686	914.1	29.2	3.11%	17.86	1.788	969.2	3.41%
ST DEV	0.10	0.05	0.083	30.6	1.1	0.14%	0.28	0.159	81.9	0.39%
CV (%)	0.65	1.58	4.92	3.35	3.77	4.37	1.59	8.91	8.45	11.35

Table 69 - Flexural 0° test result summary (0° InfuGreen/Hemp 55210 Liquid Paint Salt Spray)

L - SPAN (mm)	60									
SAMPLE	b - WIDTH (mm)	h - THICKNESS (mm)	LOAD (kN) @ Failure	σ_f (MPa)	E_f (GPa)	Strain @ Failure	Span/Thickness	Max Load(kN)	σ_{max} (MPa)	Strain at Max Load (%)
E4_0_L	14.71	3.492	1.635	820.9	31.1	2.55%	17.18	1.679	842.8	2.67%
E4_0_R	14.75	3.577	1.730	824.9	30.4	2.61%	16.78	1.750	834.6	2.71%
E5_0_L	14.71	3.580	1.823	870.3	27.9	2.88%	16.76	1.838	877.2	2.96%
AVERAGE	14.72	3.549	1.729	838.7	29.8	2.68%	16.91	1.755	851.5	2.78%
ST DEV	0.02	0.05	0.094	27.4	1.7	0.17%	0.24	0.079	22.6	0.16%
CV (%)	0.16	1.41	5.43	3.27	5.69	6.43	1.42	4.53	2.65	5.65

Table 70 - Flexural 0° test result summary (0° GF Elium/Hemp 55210 Salt Spray)

L - SPAN (mm)	60									
SAMPLE	b - WIDTH (mm)	h - THICKNESS (mm)	LOAD (kN) @ Failure	σ_f (MPa)	E_f (GPa)	Strain @ Failure	Span/Thickness	Max Load(kN)	σ_{max} (MPa)	Strain at Max Load (%)
F4_0_L	14.72	3.207	1.644	977.4	35.9	2.87%	18.71	1.766	1049.9	3.26%
F4_0_R	14.64	3.174	1.742	1063.2	36.1	3.05%	18.91	1.859	1134.9	3.43%
F5_0_L	14.63	3.192	1.915	1156.5	35.0	3.67%	18.80	1.920	1159.5	3.73%
F5_0_R	14.65	3.242	1.747	1021.0	35.4	2.98%	18.51	1.838	1074.0	3.22%
AVERAGE	14.66	3.20	1.762	1054.5	35.6	3.14%	18.73	1.846	1104.57	3.41%
ST DEV	0.04	0.03	0.112	76.5	0.5	0.36%	0.17	0.064	51.20	0.23%
CV (%)	0.28	0.90	6.38	7.25	1.34	11.50	0.90	3.44	4.64	6.76

2. 90° Salt-Spray Specimen

Table 71 - Flexural 90° test result summary (90° GF InfuGreen/Hemp 55210 Salt Spray)

L - SPAN (mm)	60									
SAMPLE	b - WIDTH (mm)	h - THICKNESS (mm)	LOAD (kN) @ Failure	σ_f (MPa)	E_f (GPa)	Strain @ Failure	Span/Thickness	Max Load(kN)	σ_{max} (MPa)	Strain at Max Load (%)
A4_90_B	14.75	3.509	0.069	34.3	9.7	0.38%	17.10	0.138	68.6	1.78%
A5_90_T	14.80	3.477	0.070	35.3	9.8	0.38%	17.26	0.138	69.3	1.89%
A5_90_B	14.80	3.507	0.070	34.5	9.7	0.39%	17.11	0.127	63.0	2.15%
AVERAGE	14.78	3.498	0.070	34.7	9.7	0.38%	17.15	0.135	67.0	1.94%
ST DEV	0.03	0.02	0.001	0.5	0.1	0.00%	0.09	0.01	3.5	0.19%
CV (%)	0.21	0.50	0.72	1.52	0.54	0.99	0.51	4.59	5.18	9.89

Table 72 - Flexural 90° test result summary (90° GF Elium/Alexit 471 Salt Spray)

L - SPAN (mm)	60									
SAMPLE	b - WIDTH (mm)	h - THICKNESS (mm)	LOAD (kN) @ Failure	σ_f (MPa)	E_f (GPa)	Strain @ Failure	Span/Thickness	Max Load(kN)	σ_{max} (MPa)	Strain at Max Load (%)
B4_90_T	14.83	3.283	0.044	24.7	8.5	0.33%	18.27	0.104	58.6	2.29%
B4_90_B	14.74	3.271	0.046	26.1	8.1	0.38%	18.34	0.110	62.7	2.51%
B5_90_T	14.70	3.273	0.040	23.0	9.8	0.26%	18.33	0.117	67.1	2.28%
AVERAGE	14.75	3.276	0.043	24.6	8.8	0.32%	18.32	0.110	62.8	2.36%
ST DEV	0.07	0.01	0.003	1.5	0.9	0.06%	0.04	0.007	4.3	0.13%
CV (%)	0.45	0.20	6.44	6.28	9.99	19.60	0.20	6.07	6.81	5.54

Table 73 - Flexural 90° test result summary (90° InfuGreen/Alexit 411-77 Salt Spray)

L - SPAN (mm)	60									
SAMPLE	b - WIDTH (mm)	h - THICKNESS (mm)	LOAD (kN) @ Failure	σ_f (MPa)	E_f (GPa)	Strain @ Failure	Span/Thickness	Max Load(kN)	σ_{max} (MPa)	Strain at Max Load (%)
C4_90_B	14.79	3.426	0.055	28.4	9.5	0.31%	17.51	0.130	67.4	2.03%
C5_90_B	14.70	3.391	0.075	40.1	9.7	0.43%	17.69	0.120	64.1	1.54%
C6_90_V	15.39	3.464	0.068	33.2	10.6	0.33%	17.32	0.123	60.1	1.66%
AVERAGE	14.96	3.427	0.066	33.9	9.9	0.36%	17.51	0.125	63.8	1.74%
ST DEV	0.38	0.04	0.010	5.9	0.6	0.07%	0.19	0.005	3.6	0.25%
CV (%)	2.51	1.06	15.66	17.25	6.31	18.35	1.06	3.94	5.70	14.55

Table 74 - Flexural 90° test result summary (90° GF Elium/Alexit 411-77 Salt Spray)

L - SPAN (mm)	60									
SAMPLE	b - WIDTH (mm)	h - THICKNESS (mm)	LOAD (kN) @ Failure	σ_f (MPa)	E_f (GPa)	Strain @ Failure	Span/Thickness	Max Load(kN)	σ_{max} (MPa)	Strain at Max Load (%)
D4_90_B	14.73	3.390	0.070	37.2	9.9	0.44%	17.70	0.126	67.0	2.19%
D5_90_B	14.64	3.359	0.072	39.3	10.0	0.41%	17.86	0.119	64.8	2.20%
D6_90_V	15.43	3.328	0.073	38.3	10.1	0.47%	18.03	0.123	64.8	1.76%
AVERAGE	14.93	3.359	0.072	38.3	10.0	0.44%	17.86	0.123	65.5	2.05%
ST DEV	0.43	0.03	0.001	1.1	0.1	0.03%	0.16	0.00	1.29	0.25%
CV (%)	2.89	0.92	2.04	2.78	0.69	5.97	0.92	2.90	1.97	12.32

Table 75 - Flexural 90° test result summary (90° GF InfuGreen/Hemp 55210 Liquid Paint Salt Spray)

L - SPAN (mm)	60									
SAMPLE	b - WIDTH (mm)	h - THICKNESS (mm)	LOAD (kN) @ Failure	σ_f (MPa)	E_f (GPa)	Strain @ Failure	Span/Thickness	Max Load(kN)	σ_{max} (MPa)	Strain at Max Load (%)
E4_90_B	14.70	3.586	0.080	38.1	9.2	0.42%	16.73	0.136	64.6	1.64%
E5_90_B	14.78	3.686	0.081	36.4	9.4	0.41%	16.28	0.122	54.7	1.12%
E6_90_V	14.94	3.310	0.065	35.7	9.9	0.39%	18.13	0.117	64.5	1.38%
AVERAGE	14.81	3.527	0.075	36.7	9.5	0.41%	17.05	0.125	61.3	1.38%
ST DEV	0.12	0.19	0.009	1.3	0.4	0.02%	0.96	0.010	5.7	0.26%
CV (%)	0.80	5.53	12.12	3.45	4.20	3.88	5.66	7.71	9.29	18.85

Table 76 - Flexural 90° test result summary (90° GF Elium/Hemp 55210 Liquid Paint Salt Spray)

L - SPAN (mm)	60									
SAMPLE	b - WIDTH (mm)	h - THICKNESS (mm)	LOAD (kN) @ Failure	σ_f (MPa)	E_f (GPa)	Strain @ Failure	Span/Thickness	Max Load(kN)	σ_{max} (MPa)	Strain at Max Load (%)
F4_90_B	14.70	3.166	0.069	42.1	10.0	0.53%	18.95	0.103	62.9	1.68%
F5_90_B	14.65	3.191	0.059	35.9	8.9	0.55%	18.81	0.088	53.3	1.52%
F6_90_V	15.37	3.144	0.081	47.7	11.3	0.46%	19.09	0.115	68.0	1.59%
AVERAGE	14.91	3.167	0.070	41.9	10.1	0.52%	18.95	0.102	61.4	1.60%
ST DEV	0.40	0.02	0.011	5.9	1.2	0.05%	0.14	0.013	7.5	0.08%
CV (%)	2.69	0.74	15.19	14.16	11.60	8.75	0.74	12.99	12.18	5.04

APPENDIX-C: UV-aged Specimens

1. 0° UV-aged Specimen

Table 77 - Flexural 0° test result summary (GF/Infugreen/Dry/HEMP 0° UV)

L - SPAN (mm)	60						
SAMPLE	b - WIDTH (mm)	h - THICKNESS (mm)	LOAD (kN) @ Failure	σ_f (MPa)	E_f (GPa)	Strain at Failure (%)	Span/Thickness
F1	15.02	3.458	1.845	924.6	26.8	3.22%	17.35
F2	14.96	3.503	1.941	951.4	23.7	3.54%	17.13
F3	14.85	3.468	1.717	865.3	27.3	3.25%	17.30
F4	15.11	3.577	1.606	747.6	25.8	3.06%	16.77
AVERAGE	14.98	3.50	1.777	872.2	25.9	3.27%	17.14
ST DEV	0.11	0.05	0.146	90.5	1.6	0.20%	0.26
CV (%)	0.73	1.53	8.24	10.38	6.14	6.20	1.52

Table 78 - Flexural 0° test result summary (GF/Elium/Dry/ALEXIT 0° UV)

L - SPAN (mm)	60						
SAMPLE	b - WIDTH (mm)	h - THICKNESS (mm)	LOAD (kN) @ Failure	σ_f (MPa)	E_f (GPa)	Strain at Failure (%)	Span/Thickness
F1	14.94	3.235	1.771	1019.5	28.3	3.34%	18.55
F2	14.77	3.193	1.822	1089.1	30.8	3.66%	18.79
F3	15.06	3.261	1.960	1101.5	31.5	3.51%	18.40
F4	15.04	3.292	2.013	1111.9	27.3	3.92%	18.23
AVERAGE	14.95	3.245	1.892	1080.5	29.5	3.61%	18.49
ST DEV	0.13	0.042	0.114	41.7	2.0	0.24%	0.24
CV (%)	0.88	1.29	6.01	3.86	6.8	6.75	1.29

Table 79 - Flexural 0° test result summary (0° GF InfuGreen/Alexit 411-77 UV)

L - SPAN (mm)	60									
SAMPLE	b - WIDTH (mm)	h - THICKNESS (mm)	LOAD (kN) @ Failure	σ_f (MPa)	E_f (GPa)	Strain @ Failure	Span/Thickness	Max Load(kN)	σ_{max} (MPa)	Strain at Max Load (%)
C8_0_1	14.91	3.440	1.868	953.1	29.9	3.27%	17.44	1.868	953.1	3.27%
C8_0_2	14.91	3.407	1.896	986.0	30.9	3.31%	17.61	1.896	986.0	3.31%
C8_0_3	14.94	3.484	1.740	863.8	29.8	2.87%	17.22	1.747	867.3	3.33%
AVERAGE	14.92	3.444	1.835	934.3	30.2	3.15%	17.42	1.837	935.5	3.30%
ST DEV	0.02	0.04	0.08	63.2	0.6	0.24%	0.19	0.079	61.3	0.03%
CV (%)	0.13	1.11	4.53	6.77	2.02	7.77	1.11	4.30	6.55	0.97

Table 80 - Flexural 0° test result summary (0° GF Elium/Alexit 411-77 UV)

L - SPAN (mm)	60									
SAMPLE	b - WIDTH (mm)	h - THICKNESS (mm)	LOAD (kN) @ Failure	σ_f (MPa)	E_f (GPa)	Strain @ Failure	Span/Thickness	Max Load(kN)	σ_{max} (MPa)	Strain at Max Load (%)
D8_0_1	14.89	3.450	1.736	881.5	27.5	3.11%	17.39	1.736	881.5	3.11%
D8_0_2	14.86	3.397	1.814	951.9	19.2	3.45%	17.66	1.814	951.9	3.45%
D8_0_3	14.85	3.335	1.769	964.1	29.5	3.20%	17.99	1.995	1087.3	3.91%
D8_0_4	14.94	3.385	2.127	1118.1	30.2	3.92%	17.73	2.127	1118.1	3.92%
AVERAGE	14.89	3.39	1.861	978.9	26.6	3.42%	17.69	1.918	1009.7	3.60%
ST DEV	0.04	0.05	0.180	99.7	5.1	0.36%	0.25	0.176	111.9	0.39%
CV (%)	0.27	1.39	9.65	10.18	19.17	10.61	1.39	9.20	11.08	10.94

Table 81 - Flexural 0° test result summary (GF/Infugreen/Liquid/HEMP 0° UV)

L - SPAN (mm)	60						
SAMPLE	b - WIDTH (mm)	h - THICKNESS (mm)	LOAD (kN) @ Failure	σ_f (MPa)	E_f (GPa)	Strain at Failure (%)	Span/Thickness
F1	14.55	3.330	1.549	864.1	28.6	2.82%	18.02
F2	14.89	3.288	1.703	952.3	30.1	2.97%	18.25
F3	15.19	3.330	1.734	926.8	30.0	2.98%	18.02
F4	14.73	3.287	1.724	974.8	26.6	3.10%	18.25
AVERAGE	14.84	3.31	1.678	929.5	28.8	2.97%	18.13
ST DEV	0.27	0.02	0.087	47.8	1.6	0.11%	0.13
CV (%)	1.81	0.74	5.16	5.14	5.72	3.80	0.74

Table 82 - Flexural 0° test result summary (GF/Elium/Liquid/HEMP 0° UV)

L - SPAN (mm)	60						
SAMPLE	b - WIDTH (mm)	h - THICKNESS (mm)	LOAD (kN) @ Failure	σ_f (MPa)	E_f (GPa)	Strain at Failure (%)	Span/Thickness
F1	14.78	3.134	1.764	1093.4	34.3	3.13%	19.14
F2	14.88	3.162	1.884	1139.5	31.3	3.49%	18.98
F3	14.85	3.152	1.936	1181.0	32.3	3.65%	19.03
F4	15.01	3.153	1.916	1155.3	31.1	3.75%	19.03
AVERAGE	14.88	3.15	1.875	1142.3	32.2	3.51%	19.05
ST DEV	0.10	0.01	0.077	36.8	1.5	0.27%	0.07
CV (%)	0.65	0.37	4.11	3.22	4.57	7.66	0.37

2. 90° UV-aged Specimen

Table 83 - Flexural 90° test result summary (GF/Infugreen/Dry/HEMP 90° UV)

L - SPAN (mm)	60									
SAMPLE	b - WIDTH (mm)	h - THICKNESS (mm)	LOAD (kN) @ Failure	σ_f (MPa)	E_f (GPa)	Strain @ Failure	Span/Thickness	Max Load(kN)	σ_{max} (MPa)	Strain at Max Load (%)
F1	15.16	3.403	0.120	61.5	9.9	0.76%	17.63	0.134	68.7	1.19%
F2	15.30	3.508	0.122	58.3	9.4	0.63%	17.10	0.133	63.6	1.46%
F3	15.06	3.496	0.110	53.8	8.9	0.58%	17.16	0.135	66.0	1.84%
F4	15.28	3.533	0.107	50.5	8.8	0.55%	16.98	0.144	67.9	1.89%
F5	15.30	3.504	0.120	57.5	8.9	0.62%	17.12	0.123	58.9	1.06%
AVERAGE	15.22	3.489	0.116	56.3	9.2	0.63%	17.20	0.134	65.0	1.49%
ST DEV	0.11	0.050	0.007	4.3	0.5	0.08%	0.25	0.007	3.9	0.38%
CV (%)	0.70	1.44	5.87	7.58	4.94	12.67	1.46	5.58	6.07	25.29

Table 84 - Flexural 90° test result summary (GF/Elium/Dry/ALEXIT 90° UV)

L - SPAN (mm)	60									
SAMPLE	b - WIDTH (mm)	h - THICKNESS (mm)	LOAD (kN) @ Failure	σ_f (MPa)	E_f (GPa)	Strain @ Failure	Span/Thickness	Max Load(kN)	σ_{max} (MPa)	Strain at Max Load (%)
F1	15.31	3.219	0.066	37.5	10.3	0.36%	18.64	0.124	70.3	1.94%
F2	15.26	3.249	0.066	37.1	10.0	0.39%	18.47	0.127	70.9	2.08%
F3	15.33	3.253	0.073	40.5	9.6	0.45%	18.44	0.130	72.1	1.88%
F4	15.29	3.279	0.068	37.2	9.3	0.39%	18.30	0.116	63.5	1.68%
F5	15.35	3.302	0.070	37.4	9.0	0.41%	18.17	0.130	69.9	2.24%
AVERAGE	15.31	3.26	0.069	38.0	9.6	0.40%	18.40	0.125	69.4	1.96%
ST DEV	0.03	0.03	0.003	1.4	0.5	0.03%	0.18	0.006	3.4	0.21%
CV (%)	0.21	0.96	4.08	3.77	5.54	7.62	0.96	4.64	4.87	10.81

Table 85 - Flexural 90° test result summary (90° GF InfuGreen/Alexit 411-77 UV)

L - SPAN (mm)	60									
SAMPLE	b - WIDTH (mm)	h - THICKNESS (mm)	LOAD (kN) @ Failure	σ_f (MPa)	E_f (GPa)	Strain @ Failure	Span/Thickness	Max Load(kN)	σ_{max} (MPa)	Strain at Max Load (%)
C8_90_T	15.07	3.450	0.110	55.1	10.5	0.55%	17.39	0.122	61.5	0.81%
C8_90_B	15.13	3.457	0.116	57.9	9.8	0.66%	17.36	0.133	66.4	1.54%
C9_90_T	15.08	3.473	0.110	54.2	10.6	0.67%	17.28	0.132	65.1	1.61%
AVERAGE	15.10	3.460	0.112	55.7	10.3	0.63%	17.34	0.129	64.3	1.32%
ST DEV	0.03	0.01	0.004	1.9	0.4	0.07%	0.06	0.006	2.6	0.44%
CV (%)	0.20	0.34	3.40	3.41	4.04	11.47	0.34	4.53	3.99	33.37

Table 86 - Flexural 90° test result summary (90° GF Elium/Alexit 411-77 UV)

L - SPAN (mm)	60									
SAMPLE	b - WIDTH (mm)	h - THICKNESS (mm)	LOAD (kN) @ Failure	σ_f (MPa)	E_f (GPa)	Strain @ Failure	Span/Thickness	Max Load(kN)	σ_{max} (MPa)	Strain at Max Load (%)
D8_90_T	15.13	3.341	0.102	54.3	10.4	0.61%	17.96	0.131	69.7	1.86%
D8_90_B	15.06	3.365	0.106	55.9	10.5	0.64%	17.83	0.129	68.3	1.99%
D9_90_T	15.07	3.389	0.074	38.3	10.4	0.39%	17.71	0.130	67.6	1.77%
AVERAGE	15.09	3.365	0.094	49.5	10.4	0.55%	17.83	0.130	68.5	1.87%
ST DEV	0.04	0.02	0.018	9.8	0.1	0.14%	0.13	0.001	1.1	0.11%
CV (%)	0.25	0.71	18.75	19.68	0.89	25.21	0.71	0.49	1.56	5.91

Table 87 - Flexural 90° test result summary (GF/Infugreen/Liquid/HEMP 90° UV)

L - SPAN (mm)	60									
SAMPLE	b - WIDTH (mm)	h - THICKNESS (mm)	LOAD (kN) @ Failure	σ_f (MPa)	E_f (GPa)	Strain @ Failure	Span/Thickness	Max Load(kN)	σ_{max} (MPa)	Strain at Max Load (%)
F1	15.07	3.228	0.098	56.3	10.0	0.52%	18.59	0.114	65.3	0.75%
F2	15.29	3.264	0.115	63.5	10.3	0.65%	18.38	0.115	63.5	0.65%
F3	15.24	3.266	0.119	65.9	10.3	0.65%	18.37	0.119	65.9	0.65%
F4	15.25	3.247	0.112	62.7	10.0	0.64%	18.48	0.112	62.7	0.64%
F5	15.27	3.260	0.111	61.6	10.0	0.60%	18.40	0.116	64.3	0.77%
AVERAGE	15.22	3.25	0.111	62.0	10.1	0.61%	18.45	0.115	64.4	0.69%
ST DEV	0.09	0.02	0.008	3.5	0.2	0.06%	0.09	0.003	1.3	0.06%

Table 88 - Flexural 90° test result summary (GF/Elium/Liquid/HEMP 90° UV)

L - SPAN (mm)	60									
SAMPLE	b - WIDTH (mm)	h - THICKNESS (mm)	LOAD (kN) @ Failure	σ_f (MPa)	E_f (GPa)	Strain @ Failure	Span/Thickness	Max Load(kN)	σ_{max} (MPa)	Strain at Max Load (%)
F1	15.27	3.150	0.056	33.0	9.6	0.39%	19.05	0.100	59.4	1.72%
F2	15.31	3.148	0.065	38.4	9.5	0.45%	19.06	0.102	60.5	1.79%
F3	15.33	3.174	0.075	43.9	9.2	0.56%	18.91	0.128	74.6	2.09%
F4	15.31	3.095	0.071	43.3	10.1	0.53%	19.39	0.115	70.6	1.86%
F5	15.26	3.162	0.071	41.8	9.7	0.45%	18.98	0.121	71.4	2.16%
AVERAGE	15.30	3.15	0.067	40.1	9.6	0.48%	19.08	0.113	67.3	1.92%
ST DEV	0.03	0.03	0.008	4.5	0.3	0.07%	0.19	0.012	6.9	0.19%
CV (%)	0.19	0.96	11.27	11.19	3.43	14.15	0.97	10.66	10.22	10.07
CV (%)	0.58	0.49	7.01	5.71	1.61	9.44	0.49	2.25	2.02	8.52

Annex 3 – Technical drawings

Ø16 - F8 THRU
R10
50
50
25
25
25
25
85
10
Ø36

15
R10
35
M30x2.0 L.H.
30

ESCALA: 1:3	TOLERANCIAMENTO: ISO 8015 TOLERANCIAS GERAIS: ISO 2768 - m K	MATERIAL: Aço F10		
	NOME	DATA	QUANTIDADE: 1	inegi driving science & innovation
DESENHOU	João Cardoso	03/11/2022		Fitting de baixo
VERIFICOU	Jorge Silva	15/12/2022	ACABAMENTO:	
APROVOU	Jorge Silva	15/12/2022		Fitting_baixo_rosca_LH
UNIDADE DE MATERIAIS E ESTRUTURAS COMPOSTAS			INDICE REVISAO: 1	FOLHA 1/1

M30x2.0 R.H. ↧ 34
50
50
25
25
25
A
R10
25
25
115
A
15
R10
65
Ø16 - F8 THRU
34
SECTION A-A

ESCALA: 1:3	TOLERANCIAMENTO: ISO 8015 TOLERANCIAS GERAIS: ISO 2768 - m K	MATERIAL: Aço F10		
	NOME	DATA	QUANTIDADE: 1	inegi driving science & innovation
DESENHOU	João Cardoso	03/11/2022		Fitting de cima
VERIFICOU	Jorge Silva	15/12/2022	ACABAMENTO:	
APROVOU	Jorge Silva	15/12/2022		Fitting_cima_rosca_RH
UNIDADE DE MATERIAIS E ESTRUTURAS COMPOSTAS			INDICE REVISAO: 0	FOLHA 1/1

Flange de baixo — Flange_baixo

Ø 228
Ø 180

8 X Ø 18
EQUALLY SPACED
THRU HOLES

Nota: Flange pode ser constituída por
duas peças soldadas(disco+peça central)
conforme proposto a 07/11/2022.

0.5

15
50
104.2
19.6

20
25
50
Ø 16 - F8 THRU

MATERIAL : Aço
QUANTIDADE : 1

	NOME	DATA
DESENHOU	João Cardoso	03/11/2022
VERIFICOU	Jorge Silva	15/12/2022
APROVOU	Jorge Silva	15/12/2022

ESCALA: 1:2
TOLERANCIAMENTO: ISO 8015
TOLERÂNCIAS GERAIS: ISO 2768 - m K
UNIDADE DE MATERIAIS E ESTRUTURAS COMPOSTAS
ÍNDICE REVISÃO: 0

Flange de baixo
Flange_baixo

Flange de cima — Flange_cima

Ø 254
Ø 210

8 X Ø 18
EQUALLY SPACED
THRU HOLES

Nota: Flange pode ser constituída por
duas peças soldadas(disco+peça central)
conforme proposto a 07/11/2022.

0.5

15
50
117.2
19.6

20
25
50
Ø 16 - F8 THRU

MATERIAL : Aço
QUANTIDADE : 1

	NOME	DATA
DESENHOU	João Cardoso	03/11/2022
VERIFICOU	Jorge Silva	15/12/2022
APROVOU	Jorge Silva	15/12/2022

ESCALA: 1:2
TOLERANCIAMENTO: ISO 8015
TOLERÂNCIAS GERAIS: ISO 2768 - m K
UNIDADE DE MATERIAIS E ESTRUTURAS COMPOSTAS
ÍNDICE REVISÃO: 0

Flange de cima
Flange_cima

FIBREGY

This project has received funding from the European
Union's Horizon 2020 research and innovation
programme under grant agreement No 952966.

146

FIBREGY

Subcomponent_Assy (Sheet 1)

DETAIL B
SCALE 1 : 1

0.5 ±0.5

Ø 254
Ø 228

SECTION A-A

Ø 18
Ø 125
Ø 100
Ø 18

480
80
27
25
300
260
6
6
6

ITEM NO.	PART NUMBER	DESCRIPTION	QTY.
1	GFRP Tubulated Flange 100	Rotec TFS-100-300(3)	1
2	GFRP Tubulated Flange 125	Rotec TFS-125-300(3)	1
3	Exterior Sleeve	Steel sleeve 1,5 mm w/ pre-drilled holes	1
4	Overlaminated GFRP	Overlaminated GFRP 5,5 mm thick	1
5	Interior Sleeve	Steel sleeve 1,5 mm w/ pre-drilled holes	1
6	Hexagon nut M3	Hexagon nut DIN 934 - M3	48
7	Hexagon bolt M3	Hexagon bolt DIN 933 - M3x25	48

ESCALA 1:5
TOLERANCIAMENTO: ISO 8015
TOLERANCIAS GERAIS: ISO 2768 - m K
MATERIAL: Various
QUANTIDADE: 4

	NOME	DATA
DESENHOU	João Cardoso	11/11/2022
VERIFICOU	jmcardoso	20/04/2023
APROVOU	jmcardoso	20/04/2023

UNIDADE DE MATERIAIS E ESTRUTURAS COMPOSTAS
INDICE REVISAO: 2

inegi driving science & innovation

DES. No.
ACABAMENTO:
TITULO: **Subcomponent_Assy**
FOLHA 1/1

GFRP Tubulated Flange 100 (Sheet 2)

The tube should be cut from 300 mm heigh to 260 mm heigh after the overlamination

3 ROWS OF 16 X Ø 3.5 EQDS. THRU HOLES

SECTION A-A

260
60
40
20
6
24
25
R10
Ø 18

Ø 228
Ø 100

8 x Ø 18 THRU EQUIDISTANT HOLES

ESCALA 1:3
TOLERANCIAMENTO: ISO 8015
TOLERANCIAS GERAIS: ISO 2768 - m K
MATERIAL: GFRP
QUANTIDADE: 4

	NOME	DATA
DESENHOU	João Cardoso	14/11/2022
VERIFICOU	jmcardoso	15/11/2022
APROVOU	jmcardoso	15/11/2022

UNIDADE DE MATERIAIS E ESTRUTURAS COMPOSTAS
INDICE REVISAO: 2

inegi driving science & innovation

DES. No.
ACABAMENTO:
TITULO: **Rotec TFS-100-300(3)**
GFRP Tubulated Flange 100
FOLHA 1/1

Technical drawing sheet: GFRP Tubulated Flange 125

- A dimension 300
- R10
- 27
- SECTION A-A
- 3 ROWS OF 16 X ⌀3.5 EQDS. THRU HOLES
- 60, 40, 20
- 6
- 22
- ⌀18
- ⌀254
- ⌀125
- 8 x ⌀18 THRU EQUIDISTANT HOLES

Technical drawing sheet: Exterior Sleeve

- ⌀137
- ⌀134
- (0.02)
- 3 ROWS OF 16 X ⌀3.5 EQDS. THRU HOLES
- 80
- Flat pattern
- 8.575
- 8.575
- 60, 40, 20
- 27.19
- 425

Drawing 1 — Overlaminated GFRP

3 ROWS OF 16 X ⌀3.50 EQDS. THRU HOLES

190

60 40 20

SECTION A-A

30°

Taper angle can be higher than 30°

DETAIL B
SCALE 1 : 1

⌀124 +1 −1
⌀112

ESCALA 1:3	TOLERANCIAMENTO: ISO 8015 TOLERANCIAS GERAIS: ISO 2768 - m K	MATERIAL: GFRP	
	NOME	DATA	QUANTIDADE: 4
DESENHOU	João Cardoso	15/11/2022	
VERIFICOU	jmcardoso	20/04/2023	ACABAMENTO:
APROVOU	jmcardoso	20/04/2023	
UNIDADE DE MATERIAIS E ESTRUTURAS COMPOSTAS			INDICE REVISAO: 2

Overlaminated GFRP 5,5 mm thick

TÍTULO: Overlaminated GFRP

FOLHA 1/1

Drawing 2 — Interior Sleeve

⌀102
⌀99

7.0

3 ROWS OF 16 X ⌀3.5 EQDS. THRU HOLES

80

Flat pattern

9.625

60 40 20

19.25

308

ESCALA 1:2	TOLERANCIAMENTO: ISO 8015 TOLERANCIAS GERAIS: ISO 2768 - m K	MATERIAL: Stainless Steel	
	NOME	DATA	QUANTIDADE: 4
DESENHOU	João Cardoso	15/11/2022	
VERIFICOU	jmcardoso	01/02/2023	ACABAMENTO:
APROVOU	jmcardoso	01/02/2023	
UNIDADE DE MATERIAIS E ESTRUTURAS COMPOSTAS			INDICE REVISAO: 2

Steel sleeve 1,5 mm w/ pre-drilled holes

TÍTULO: Interior Sleeve

FOLHA 1/1

149